Faculty of Science and Engineering

Department of Petroleum Engineering

Microwave Heating Effects on Formation Damages in Tight Gas Sands

Hongcai Wang

This thesis is presented for the Degree of

Doctor of Philosophy

of

Curtin University

May 2016

Declaration

To the best of my knowledge and belief, this thesis contains no material previously published by any other person, except where due acknowledgment has been made.

This thesis contains no material which has been accepted for the award of any other degrees or diplomas in any university.

Signature:

Date:

Abstract

The tight gas sand reservoir is problematic due to its intrinsically low permeability and high capillary pressure. Formation damages, such as water blocking and clay swelling, will further bring down the effective permeability of gas phase. In order to eliminate such formation damages, thermal methods have been applied to tight gas reservoirs. The traditional heat treatment used the electrical heater as a heat source. Although traditional heat treatment has been proven to be an effective method, its disadvantages, such as a long duration and low energy efficiency, cannot be ignored. In this study, the microwave heating method is proposed as an alternative heat source. This research investigates how microwave heating influences the petrographic and petrophysical properties of tight sandstone samples by using various experimental techniques. Besides numerical modeling was used to assess how microwave heating impacts the relative permeability to gas and gas production rate.

The petrophysical and petrographic properties of the sandstone samples are investigated utilizing several experimental methods including: porosity and permeability measurements, Nuclear Magnetic Resonance (NMR) analysis, X-ray Computed Tomography scanning (CT), relative permittivity measurement, thin section examinations, X-ray Diffraction (XRD) analysis and Scanning Electronic Microscope (SEM) examinations. Both traditional and microwave heating methods have been examined. The same properties are measured by identical procedures after traditional and microwave heating experiments have been conducted. Then,

comparisons are made between the samples. The porosity and permeability of the samples studied increased greatly after the heat treatments, which is caused by clay decomposition and fracture generation. Microwave heating has similar effects on permeability as traditional heating, although the former brings about less increase in porosity than the latter.

The numerical simulation indicates the positive effects of microwave heating on reservoir quality and gas production rate. The heating depth of the microwave proves to be sufficient to treat the formation damage with an invasion depth of around 1 m in the near wellbore region. The production rate of gas also obtains a two-fold increase after the microwave heat treatment.

Based on the changes of the petrophysical properties of the tight sandstone before and after the heating treatment, this thesis demonstrates the feasibility of microwave heating in removing formation damage and enhancing reservoir quality in the near wellbore region.

Acknowledgements

First of all, I would like to express my great appreciation to Professor Reza Rezaee and Dr. Ali Saeedi for being my supervisor and co-supervisor and for providing me sufficient support and guidance in my studies and life in general.

In addition, I owe my gratitude to Professor Brian Evans and Associate Professor Mofazzal Hossain for being the chair of my supervisory panel. Special appreciation and thanks for organizing the panel meeting and providing me the necessary feedback and assistance for the progress of my research.

Special thanks also goes to Dr. Nguyen Tran (Microwave Power Components), Dr. Matthew Josh, Dr. Lionel Esteban, Prof. Keyu Liu, Derek Winchester, Jeremie Dautriat from CSIRO, Ms Elain Miller, as well as Veronica from John de Laeter Centre, who contributed to my research.

I am grateful to my colleagues, Adnan Saif Hamed Al Hinai, Hanieh Jafary Dargahi, and Mohammad Mehdi Labani, who helped me a lot at the beginning of my research.

Thanks also to the Unconventional Gas Research Group and Department of Petroleum Engineering of Curtin University for providing the necessary research facilities and technical support. Special mention to the China Scholarship Council and Australia-China Natural Gas Technology Partnership Fund for providing the funding for this research.

Last but not least, I would like to express my thanks to my wife and our parents, without whom the journey would have been difficult and meaningless.

Parts of this thesis have been published in the following conference articles and journals:

Wang, H., Rezaee, R., & Saeedi, A. (2016). Preliminary study of improving reservoir quality of tight gas sands in the near wellbore region by microwave heating. Journal of Natural Gas Science and Engineering, 32, 395-406.

Wang, H., Rezaee, R., & Saeedi, A. (2015, October). The High Temperature Effects on Pore Size Distribution of Tight Sandstone: An Application of Microwave Heating in Enhanced Gas Recovery (EGR). In SPE/IATMI Asia Pacific Oil & Gas Conference and Exhibition. Society of Petroleum Engineers.

Wang, H., Rezaee, R., & Saeedi, A. (2015, November). Evaluation of Microwave Heating on Fluid Invasion and Phase Trapping in Tight Gas Reservoirs. In SPE Asia Pacific Unconventional Resources Conference and Exhibition. Society of Petroleum Engineers.

Wang, H., Rezaee, R., & Saeedi, A. (2015). Evaporation Process and Pore Size Distribution in Tight Sandstones: A Study Using NMR and MICP. Procedia Earth and Planetary Science, 15, 767-773.

Wang, H., Rezaee, R., & Saeedi, A. (2015). The Interaction of Reservoir Properties and Microwave Heating–An Experimental and Numerical Modeling Study of Enhanced Gas Recovery (EGR). Procedia Earth and Planetary Science, 15, 542-548.

Table of Contents

List of Figures

List of Tables

To my beloved mother (Ms. Huixian Du), father (Mr. Mingde Wang) and my wife (Ms. Qin Du). Thank you for always supporting me with your unconditional love.

To my forthcoming child who brings me great hope and strength.

1.INTRODUCTION

1.1 Tight Gas Sands

Tight gas sands are reservoirs with permeability less than 0.1mD, or those need well stimulations such as hydraulic fracturing or drilling a horizontal or multilateral wellbores, in order to produce at economic flow rates or to recover economic volumes of natural gas (Holditch, 2006).

The initial water saturation of tight gas reservoirs can be lower than the irreducible water saturation. This state is named as "subirreducibly saturated" (Bennion, et al., 1996A) or "sub capillary-equilibrium water saturation distribution"/ "sub-irreducible water saturation". (Newsham and Rushing, 2002). Bennion, el al. (1996B) indicated that this state is established by dehydration, desiccation, compaction and diagenesis. Bennion, et al. (2002) further explained three mechanisms: 1) hydratable shales contact with formation extract water; 2) diagenesis related processes reduce reservoir quality and the formation is disconnected from water source; 3) formation water is evaporated. Newsham, et al. (2002) supported the third mechanism and claimed that the evaporated water becomes gaseous and dissolves in the hydrocarbon gas.

In the tight gas reservoir, the formation is sensitive to all kinds of fluids. In highly permeable zones, a strong mud cake will be formed around the borehole so that further invasion of fluids can be prevented. However, for tight formations, only a weak mud cake is formed, so the invasion time of fluids will be longer and the penetration depth will be deeper. This is due to the low matrix permeability and strong capillary pressure (Bahrami et al., 2011). Capillary pressure (P_c) is the difference between the non-wetting and wetting phase pressures. In the gas-liquid system, the capillary is given as below (Washburn, 1921):

$$P_c = \frac{2\sigma_{gw}\cos\theta}{r}$$

Equation 1

Where σ_{gw} is the gas water surface tension, in dynes/cm; r is the capillary radius, in cm; θ is the contact angle. The capillary pressure is exceedingly high in tight sandstones and is not the direct cause of the movement of the fluid, but gives rise to potential gradients which leads to fluid movement (Evans and Guerrero, 1979). Newsham (2004) reviewed and used different methods, including high-speed centrifuge, high-pressure mercury injection, high pressure porous plate and vapor desorption techniques, to measure capillary pressure. The high-pressure mercury injection test is used in the measurement of pore size distribution, but MICP test may underestimate the water saturation in the low saturation range.

High capillary pressure is a result of the small pore throat radius in sandstones. Based on the study conducted by Nelson (2009), in the conventional reservoir, the pore size is greater than 2μm; in tight gas sandstones, it ranges from 2 to 0.03μm; whereas in shale, it varies from 0.1 to 0.05μm.

The high capillary pressure also results in a higher irreducible water saturation and smaller gas relative permeability. With elevated temperatures, the relative permeability of the non-wetting phase was found to increase, while that of the wetting phase decreases (Sinnokrot et al., 1971).

In tight gas reservoirs, the main damage mechanisms are mechanical damage, mud solid particles invasion and plugging, relative permeability reduction due to filtrate invasion, liquid leak off in the process of fracturing, water trapping, wellbore breakout and damage caused by perforation (Bahrami et al., 2011).

Bennion et al. (1998) summarized the processes in the development of the wells which caused uneconomic production rates of tight gas formation in 6 categories:

1 Inherently poor reservoir quality
2 Disadvantageous initial saturation conditions
3 Formation damage due to drilling and completion
4 Formation damage due to hydraulic or acid fracturing
5 Formation damage due to work-over treatments
6 Formation damage due to production

From another point of view, Civan (2011) summarized the adverse physical, chemical and biological causes as follows:

1 Fluid/fluid incompatibility and rock/fluid incompatibility

2 Solid invasion

3 Phase trapping or phase blocking

4 Chemical adsorption/ wettability change

5 Fine migration

6 Biological activity

In this thesis, we will focus on the formation skin damage in the near wellbore area that can be alleviated by microwave heating. As such, the main formation damages focused on are rock-fluid incompatibilities, such as clay swelling due to contact with incompatible water and phase trapping/ blocking. The mechanisms of these formation damages will be introduced in the following sections.

1.2 Formation Skin Damages in Tight Gas Sands

1.2.1 Phase Trapping

Water blocking is one of the main damage mechanisms in tight gas sands because of the effects of relative permeability and capillary pressure (Bahrami et al., 2011). It is a process related to the combined effects of adverse capillary pressure and relative permeability effects (Bennion, 2002). Figure 1-1 illustrates the evolution of water trapping in a tight gas reservoir. Sub-irreducible water saturation condition is the key reason for the establishment of phase trapping (Bennion et al., 1996). Once water invades the formation, water saturation increases dramatically and a reduction of gas relative permeability takes place. Jamin effect indicated that the presence of bubbles will resist the liquid flow in the capillary tubes (Jamin, 1860), as a result, water or oil drop will be trapped in the formation and difficult to be removed. The formation will remain at a higher water saturation than the initial level.

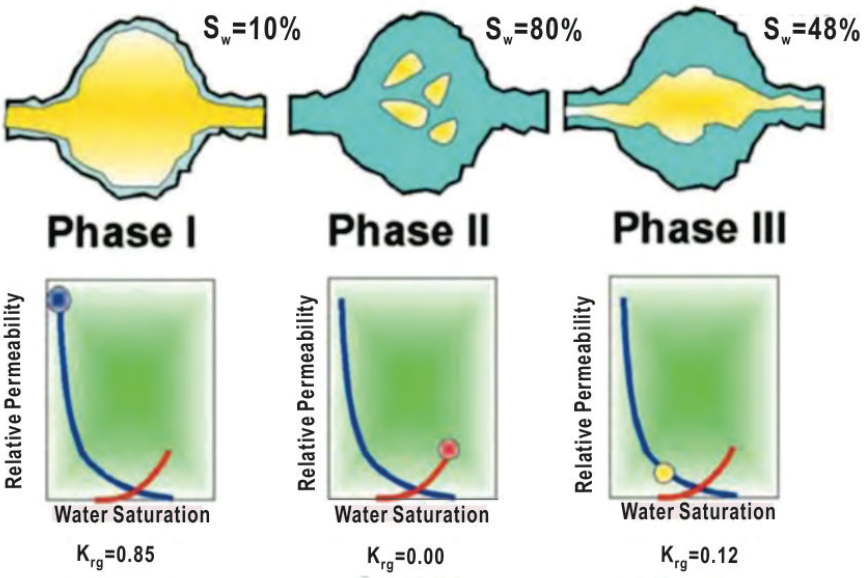

Figure 1-1 Illustration of water based phase trapping effects in a low permeability gas reservoir (Bennion, 2002). In Phase I, the gas relative permeability is high at 0.85 when water saturation is 10%; after the water invasion in Phase II, the gas relative permeability reduced to 0; in Phase III, the relative permeability to gas remained low at 0.12 due to the effect of moisture phase trapping.

The reason for the difficulty to remove the water phase in the reservoir is the high capillary pressure in tight sandstones, as discussed before. In tight gas reservoirs, the pore sizes are smaller, most of which are micro-pore (pore width less than 2nm) and meso-pore (pore width between 2 and 50 nm). According to the capillary equation, this will bring about a high capillary pressure. Thus, water blocking plays a more negative role in tight gas sands. If the interconnected mesopores, macropores or fractures are dominant, this pore geometry is probably less susceptible to water trapping. However, when the micropores are dominant in the pore system, the gas relative permeability and ability of gas flowing within the tight reservoir will be impaired because of a slight increase in water saturation (Bennion and Thomas, 2005).

Furthermore, according to the Equation 1, the wettability of the reservoir rocks needs to be taken into consideration in the study of capillary pressure. Anderson (1987) discussed the impacts of wettability on capillary pressure; the drainage capillary pressure is not sensitive to the wettability in the case of the contact angle being less

than 50°, while the spontaneous imbibition capillary pressure curve is not sensitive to wettability in the case of the contact angle being less than 20°.

In gas reservoirs, gas and water exist together and the sum of gas and water saturations equals to one. The gas relative permeability, which directly controls the flow rate and production, reduces while the water saturation increases (Figure 1-2).

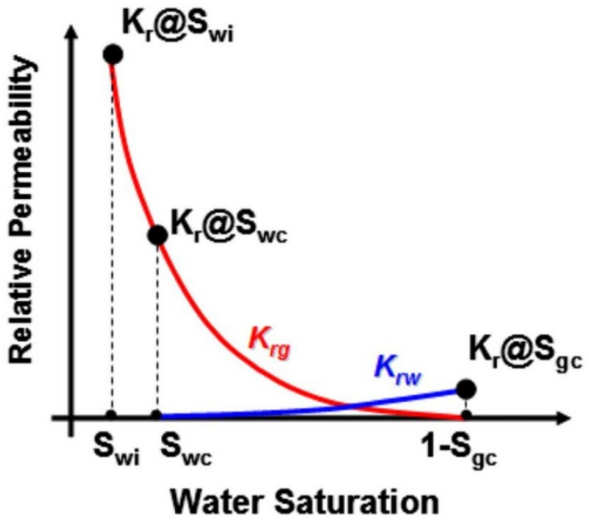

Figure 1-2 The relationship between gas relative permeability and water saturation. The relative permeability to gas is high when the water saturation is S_{wi}, but dropped significantly to $K_r@S_{gc}$ when the water saturation increased (Revised from Bahrami, Rezaee, & Clennell, 2012**).**

Moore and Slobod (1955), Rose and Witherspoon (1956), Stegemeier (1974) and Doscher (1981) discussed the Pore-Doublet Model, which consists of doublet interconnected capillaries with different radii, to approximate the flow behavior and predicted that water velocity is higher in smaller capillary. Due to the different flow rate, one of the tube will be trapped. The trapping extent is determined by the viscosity ratio and capillary pressure (Ehrlich and Crane, 1969).

The five factors that control the severity of water blocking as suggested by Bennion (1996) are:

(1) The difference between S_{wi} and S_{wirr}; (2) the features of gas phase relative permeability curves; (3) the physical invasion depth; (4) enough reservoir pressure to mobilize the entrapped fluids and (5) wettability.

1.2.2 Formation Damage Due to Alteration and Migration of Clays

Krueger (1986) reported that much of the formation damages, which could occur during drilling, completion, stimulation, work-over and Enhanced Oil Recovery (EOR), are related to clays. When in contact with foreign fluids, such as the fluids from drilling, completion and stimulation, clay minerals may swell and the pores can be blocked (Zhou and Law, 1998), leading to the reduction of absolute permeability.

In terms of the mineralogy characteristics of problematic clays, they are layered minerals, classified as phyllosilicates. They constitute stacks of two-dimensional negatively charged aluminosilicate layers (Wyckoff, 1968). In expandable clays, for example in montmorillonite, the negative charge of the clay layers is balanced by the positive charge of the cations that exist in the interlayer spaces (Civan, 2011). Cation substitution causes the structure layers to be deficient in positive charges; thus, in order to balance the negative charge, interlayer cations are necessary. The process of exchange of interlayer cations is reversible for simple cations. Water molecules can get into the space between the structural layers if the exchangeable cations are hydrated. Also, thick films will form over the clay platelets. As a result, the distance between the two structure layers expands and the clay swells (Zhou and Law, 1998).

There are two swelling mechanisms observed in swelling clays, crystalline swelling and osmotic swelling (Madsen and Müller, 1989). Crystalline swelling results from the hydration of the exchangeable cations of the dry clay which occurs within the crystalline. For the individual clay layer, it is negatively charge because of the cation substitution, which causes the formation of an electrical double layer in the interlayer zone. These cations can be exchanged with other cations and hydrated with water, thus leading to the entry of water and subsequent expansion of the interlayer space.

Osmotic swelling results from the large difference in the ion concentrations between the clay surfaces and formation water (Madsen and Müller 1989). This occurs between the crystalline. Furthermore, the magnitude of clay swelling relies heavily on the composition of its contacted solution (Figure 1-3). As indicated in the figure, in

the case of clay swelling damage, fresh water is the most harmful fluid. Figure 1-3 demonstrates the mechanisms of permeability decrease because of clay swelling.

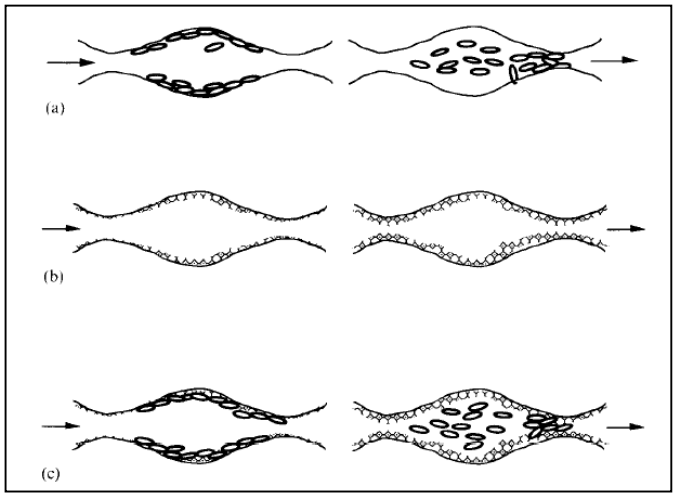

Figure 1-3 Mechanisms of permeability reduction caused by clays in porous media: (a) Migration; (b) Swelling; (c) Swelling-induced Migration (Mohan et al., 1993).

X-ray Diffraction (XRD) is a powerful tool used to predict the water sensitivity of clay minerals. The samples show that moderate or greater intensities of the glycerol-expanded peak have serious water sensitivity, while large concentrations of non-expendable clay minerals do not exhibit serious water sensitivity effects (Dodd et al., 1955).

Civan and Knapp (1987) proposed a phenomenological model for clay swelling and fines migration, as well as their effects on permeability. The flow behavior and permeability reduction during the particle suspension flow through the swelling porous media is given below:

$$-k\frac{\partial^2 P}{\partial x^2}-\frac{\partial k}{\partial x}\frac{\partial P}{\partial x}=\mu\left(\frac{1}{\rho_P}\frac{d\sigma_{SW}}{dt}-\frac{S}{\rho l}\right)$$

Where k is the permeability, P is the fluid pressure, x is the distance, S is the mass rate of liquid absorption per unit volume of porous medium, ρl is the density of the incompressible liquid, ρ_P is the mass concentration of the fine particles and σ_{SW} is the change of pore volume per unit bulk volume due to swelling expressed as equivalent particle mass.

The rate of porosity change due to clay swelling is proportional to two factors: 1) the difference between the instantaneous and terminal porosities and 2) the water absorption rate (Civan, 1996):

$$\Delta\emptyset_{SW} = \emptyset - \emptyset_o = (\emptyset_t - \emptyset_o)[1 - \exp(-k_\emptyset S)]$$

Where $\emptyset$ is the instantaneous porosity, $\emptyset_t$ is the terminal porosities, $k_\emptyset$ is the constant of formation swelling rate and t is the actual time of water contact.

1.2.3 Other Problems

Water blocking and clay swelling are caused by the reservoir's sensitivity to the water and solution concentration. However, because of the acid, velocity and salts, there could be other problems with the tight gas production. For example, kaolinite may break apart and migrate towards the pore throat. The concentration of kaolinite around the narrow pore throat leads to the blockage of the pore throat. Other migrating and blocking minerals include illite, which may be altered by the swelling clay via the leaching of potassium ions; chlorite, which will precipitate $Fe(OH)_3$ once the acid and oxygenated water encounters each other and lastly, mixed-layer clays, which may break apart and bridge across pores (Civan, 2011). The sensitivity of a formation is determined by the following factors: mineralogy or chemical composition (Table 1-1), mineral richness, morphology, size and location of minerals in the pore system (Amaerule et al., 1988). The petrographic studies can identify potential sensitivity problems in the reservoir. Thereafter, measures can be taken to reduce the influence of potential formation damages.

Table 1-1 Mineralogical sensitivity to potential formation damage (Kersey, 1986)

Water Sensitive	Chlorite/ Smectite Illite	Illite/Smectite Smectite (Montmorillonite)
Acid Sensitive (HCL)	Chamosite Chlorite (Iron rich) Chlorite/Smectite Dolomite (Iron rich)	Glauconite Hematite Pyrite Siderite
Acid Sensitive (HF)	Calcite Dolomite	Silicate Minerals
Scale	Anhydrite Barite Brucite Calcite Celestite Gypsum	Halite Hamitite Magnetite Siderite Trolite
Migration of fines	Illite Kaolinite	Silicate Minerals
Sand production	Rock-forming minerals	

1.2.4 Depth of Skin Damage

Water blocking is one of the formation skin damages, which occurs in the near wellbore area with the depth of invasion ranging from several centimeters to about 2 meters. The Depth of Invasion (DI), which is defined as the distance from the borehole wall, is a function of several parameters including temperature, pore pressure, type of mud, invasion time, porosity and permeability. Miesch and Albright (1967) and Rider (2002) mentioned the relationship between porosity, ratio of DI and diameter of the borehole (Table 1-2).

Table 1-2 Depth of invasion versus porosity (Miesch and Albright, 1967 and Rider, 2002)

Hole size (in)	**17.5**	**12.25**	**8.5**	**Ratio of Invasion Diameter to Hole Diameter**
Porosity (%)	**Depth of Invasion (cm)**			
1-8	200.0	140.0	97.0	10
8-20	90.0	62.0	43.0	5
20-30	22.5	15.5	11.0	2
30+	3.0	2.0	1.7	<2

By the regression study of experimental data, Yan et al. (1997) revealed the empirical equation to calculate the invasion depth:

$$d = 1.612\Delta p^{0.521}(\frac{V_f}{\emptyset})^{0.271}e^{0.043K}$$

Equation 2

Where d is the invasion depth in cm, Δp is the pressure differential in MPa, V_f is the cumulative filtrate loss in cm^3, $\emptyset$ is porosity in % and K is permeability in μm^2.

1.3 Methods to Remove Formation Damages in Tight Gas Reservoirs

In order to recover the gas production of the well with formation damages, different methods have been attempted to stimulate the well. These include acidizing, hydraulic fracturing and thermal methods.

1.3.1 Acidizing Treatment

Acidizing is a method to remove the near wellbore permeability damage by pumping acid into the wellbore, which can enhance the production by increasing the effective well radius. The acidizing is different between the gas well, the oil well and the water injection well, due to the two-phase gas-liquid flow and viscosity differences between the acid and gas (Fadele et al., 2000). There are two types of acidizing operations: acid fracturing and matrix acidizing. However, as acid fracturing is more effective to carbonate formation (Schmidt et al., 2015), we will not discuss it further here.

In the treatment of matrix acidizing, the acid plays the role of dissolving the invasion solids within the pores (which block the flow path and impair the permeability of the rock). As a result, the production of hydrocarbons can be enhanced.

1.3.2 Hydraulic Fracturing

Hydraulic fracturing creates fractures in the pay zone and enhances the hydrocarbon flow into the wellbore. Fluids are injected into the reservoir at high pressures, which is greater than the fracture pressure. After the fractures are created, the proppant is pumped into the fractures in order to keep the fractures open (Jennings Jr, 1990).

Therefore, the created fractures can bypass the formation damage in the near wellbore area and improve the gas production. During the design of the treatment, it is important to select the suitable fracture and propping agent. With the purpose of optimizing the hydraulic fracturing, the volume of the fractured reservoir rock needs to be maximized. The interaction of hydraulic fracturing fluids with shale affects the performance of fractures. The inorganic and organic particles may dissolve and agglomerate, leading to the block of fractures (Ali and Hascakir, 2016). The adsorption of polymer in the water-based fracturing fluids might harm the production as well (Abdulsattar, 2015). However, its impacts on health and environment are issues that need to be taken into consideration.

1.3.3 Formation Heat Treatment (FHT)

The concept of FHT was raised by Jamaluddin et al. (1999) and has proven to be effective in the treatment of water blockage and clay swelling in water sensitive formations. Formation Heat Treatment (FHT) is the method of raising the temperature of the target formation using a downhole heater. Electrical heating was used in the FHT, which has advantages when compared with steam due to the depth, formation incompatibility, low incipient injection, excessive heat losses or existence of thief zones (Sierra et al., 2001). Permeability was observed to increase to 150% after heating water sensitive sandstone cores at 600°C. A 750% and 1000% increase of the permeability of the gas and oil formation was found at 800°C. The process involved intense heat to the near wellbore area and the increased temperature was the result of the following:

1 Vaporization of trapped moisture;

2 Dehydration of the clay minerals;

3 Partial destruction of the clay minerals;

4 Possible presence of micro-fracture.

Jamaluddin et al. (1998) revealed the change in clay minerals when heated. Kaolinite peaks disappeared at 550°C, which means that kaolinite is collapsed at this temperature. Up to 300°C, the progressive vaporization of water in smectite was

observed as peaks shifted to the right. Up to 800℃, the crystallinity of smectite collapsed and it became an amorphous structure.

High temperature is the most important factor in the technique of FHT due to the temperature sensitivity of the minerals found in sedimentary rocks. The impact of temperature on clay minerals has been studied by many researchers (Atomic Energy of Canada Limited Research Company, 1990; Grim and Bradley, 1940; Hajpál and Török, 2004; Hoekstra, 1976; Jamaluddin et al., 1998; Li et al., 2006; Li, 2007; Mubiayi, 2013; McGill et al., 1995; Sanmiguel et al., 2001; Wu et al., 2011;). Listed in Table 1-3 is the temperature effects on clay minerals.

Table 1-3 Effect of temperature on clay minerals (Carroll, 1970)

Mineral	Temperature, 1 hour	Effect
Kaolinite, well-crystallized	575-625°C	Replaced by amorphous meta-kaolin; no diffraction pattern was found
Kaolinite, disordered	550-562°C	Replaced by amorphous meta-kaolin; no diffraction pattern was found
Dickite	665-700°C	Replaced by amorphous meta-kaolin; no diffraction pattern was found
Mica, well-crystallized	700°C	Gradual weight loss, but does not break down below 700°C; (001) spacing remains in diffractograms below 700°C and up to 1000°C
Illite, and clay micas	125-250°C	Loss of hydroscopic water
	350-550°C	Reverts to mica structures
	700°C	Similar to mica
Glauconite	58-650°C	Loss of interlayer water; reverts to mica structure
Biotite	700°C	Phlogopite is similar to muscovite Biotite, which breaks down between 700-1000°C
Montmorillonite Group	300°C	Original 15Å spacing disappears; 9Å spacing develops
Chlorite Group	600-800°C	Shows gradual weight loss without structural change
Mg-chlorite	650°C	14Å spacing is intensified while (004) at 3.54 not affected
Fe-chlorite	500°C	14Å spacing is less intense and may become broad and diffuse
Mixed-layer clays	<600°C	Varies with different types and amounts of minerals present

Besides the degradation or decomposition of the clay minerals, the high temperature caused the evaporation of the free water and partial clay-bound water in the pore spaces, which increased the effective and relative permeability of gas. The thermally induced stress in the heated zone may exceed the yield strength of the grains and cements and create inter-grain and intra-grain fractures (Jamaluddin et al., 1999).

A transient two-dimensional mathematical model, which studied fluid flow and heat transfer in the reservoir has been proposed by Jamaluddin et al. (1997). In their

model, the momentum and energy balance equations were coupled to solve the problem of gas in the borehole and adjacent reservoir. It is found that the temperature in the near wellbore region can be manipulated by: 1) controlling the quantity of gas injected through the tube and annulus, as well as 2) controlling the input power of the down-hole heater (Jamaluddin et al., 1997).

The field test of the FHT has been described and conducted by Jamaluddin et al. (1999), where an electrical heater was lowered to the target formation, used to heat the formation and then retrieved to the surface. Pressure transient analysis, using type curve matching techniques, was carried out after heating. Permeability and skin values were estimated from the pressure analysis. The post-heat treatment permeability improved dramatically from the pre-heat treatment. The well test indicated that the near wellbore region dehydrated at 382°C, while the permeability of the studied zone increased to 700% after heating. However, heating the sandstones to a temperature of 700°C will cause irreversible changes to the clay minerals' structures (Jamaluddin et al., 1999).

1.3.4 Eliminating Water Loading in the Wellbore

Gases are mixed with the evaporated water when they enter the wellbore. After reaching the evaporated water limit, any temperature decrease or pressure increase will cause a condensation of the water vapor. The condensed water will accumulate and this will lead to a cease of the gas flow. The solution to this problem is heating the wellbore to the reservoir temperature so that the fluid condensation is prevented and the pressure problem can be eliminated. The additional benefit is that the abandonment pressures are lower while the production rates are higher (Pigott et al., 2002).

Electromagnetic heating is used in gas well deliquification (Osman et al., 2010). A liquid loading problem arises once the velocity of the produced gas drops lower than the critical velocity. The experimental results indicate that it is effective to evaporate the moderately-saline water with microwave heating, while it requires a longer time to

produce high salinity water. Moreover, the fine sands produced with the gas can assist in the process of well deliquification.

1.4 Thermally induced Fracture

During the process of heating the core samples in the laboratory, some issues such as thermal fractures can occur and cause problems. These fractures can enhance the reservoir quality during FHT. The thermally induced fractures are the results of difference in thermal expansion of reservoir rock material.

White and Moss (1965) reported that sharp temperature gradients in the reservoir were due to the combustion, which could cause thermal fractures in formations. This brings about trouble in an open-hole completion in which case, the formation tends to cave into the wellbore. Li (2007) established that there were three mechanisms for the presence of micro-fractures: volumetric shrinkage due to the water loss of hydrated clay mineral aggregation, inter-grain fractures due to the grains' non-uniform swelling and non-uniform swelling inside a grain.

Zhang et al. (2005) heated fine sandstones and reported that micro flaws formed inside the minerals, while on the boundaries of the grains, big cracks formed after heating the samples up to 900°C. They also found the threshold temperature for the cracking of fine sandstone to be 150 - 200°C.

1.5 Electromagnetic Wave Heating

Electromagnetic heating has been increasingly popular because of its time and cost efficiency. Radio Frequency (RF) has a frequency range from 3MHz to 300GHz whereas Microwave (MW), which has larger frequencies of electromagnetic waves in heating, has a frequency range from 300MHz to 3GHz. These heating methods are also known as Induction Heating. The heat is generated via the polarization of the charges in the material by the electric field and this polarization is unable to follow extremely rapid reversals of the electric field (Metaxas and Meredith, 1983). Materials can be penetrated by microwaves and get heated; heat can be generated volumetrically and the energy transfer is not heavily dependent on the thermal

conductivity. Thus, the rapid and uniform heating of thick materials can be achieved and heating time can be reduced (Thostenson and Chou, 1999).

Studies of microwave heating on food, chemical, ceramic and textile industries have been widely conducted and their experiences can be useful in the application of microwave heating in geoscience. Microwave drying of food requires removing water from them without impacting their compositions and structures. To describe microwave propagation and absorption, Lambert's law and Maxwell's field equations are used. As the dielectric properties of the food samples depend significantly on temperature, the coupling of wave and energy equations is crucial to the prediction of temperature distributions (Chandrasekaran et al., 2013). Ni et al. (1999) developed a multiphase porous media model to describe water transport when heating biomaterials using the microwave and found that the transport properties varied with structure, moisture and temperature. From their modeling results, the internal pressure boosted more moisture flow to the surface than that which can be evaporated from the surface.

The applications of microwave heating in Environmental Engineering include contaminated soil remediation, waste processing, mineral processing, activated carbon regeneration (Jones, et al., 2002) and removing oil from drill cuttings. Robinson et al. (2008) introduced and studied the application of microwave heating on the stripping process of drill cuttings contaminated by oil. Since the microwave can deliver heat energy into the pore structure but not on the surface, it can cause thermal desorption and enhanced diffusion. The dielectric loss factor of the sample is increased due to the remaining water in the sample. However, the water on the surface of the sample increases the surface loss of the microwave and reduces the penetration depth. The distribution of moisture plays an important role in microwave heating.

Microwave technology is able to remove n-paraffin as required by the environmental legislation and the processing is influenced by the initial fluid, cutting mass and the specific energy (Naufel et al., 2013).

Microwave energy has also been used as a method to remove toxic metal in contaminated soils. Abramovitch (2003) inserted a graphite or an iron rod into the

contaminated soil. The rod gets heated by the microwave and conducts the energy all the way to the end of the rod evenly. The temperature was observed to be almost the same at all depths.

However, the researches of microwave heating in the oil and gas industry are limited. In the oil and gas industry, electromagnetic heating has been used in removing water loading in gas wells, drying drill cuttings, reducing heavy oil viscosities, recovery of oil shales and water-oil emulsion breaking (Kar and Hascakir, 2015). Oil recovery from shales depends on both the pyrolysis temperature and the time maintained for the temperature (Hascakir and Serhat, 2010). In the process of water-oil emulsion breaking, the asphaltenes and resins are the controlling factors of microwave heating effectiveness (Kar and Hascakir, 2015). Studies on microwave heating focused on the interaction of the microwave and the material: Firstly, the permittivity of the material affects the heating; secondly, as some properties of the materials are temperature and frequency dependent, they will vary with the changing temperatures and different microwave devices. The geological materials we are concerned with are sandstones - which are composed of minerals such as quartz, feldspar and clay; formation water with different salinity; as well as hydrocarbons (gas or oil). The research conducted by Hascakir et al. (2009) indicated that high salinity water can improve oil production when producing with microwave heating and high water saturation will enhance production whether the oil viscosity is high or low.

Microwave heating is a process of electromagnetic energy converting to heat. The dielectric properties of target material play the most important role in microwave heating. The propagation of electromagnetic wave was described by the Maxwell's equations:

Gauss's law

$$\nabla \cdot E = \frac{\rho}{\epsilon_0}$$

Equation 3

Gauss's law for magnetism

$$\nabla \cdot B = 0$$

Equation 4

Maxwell-Faraday Equation

$$\nabla \times \mathrm{E} = -\frac{\partial B}{\partial t}$$

Equation 5

Ampere's Circuital Law

$$\boldsymbol{\nabla \times B = \mu_0 (J + \epsilon_0 \frac{\partial E}{\partial t})}$$

Equation 6

The absorbed power per unit volume, P, and penetration depth, D, can be calculated respectively as (Sutton, 1989) and (Clark, 1996):

$$\boldsymbol{P = 2\pi f \epsilon_0 \epsilon''_{eff} |E|^2}$$

Equation 7

$$\boldsymbol{D = \frac{\lambda_0}{2\pi(2\epsilon')^{1/2}} [(1 + ((\frac{\epsilon''_{eff}}{\epsilon'})^2)^{1/2} - 1]^{-1/2}}$$

Equation 8

1.5.1 Microwave Absorbing Minerals and Microwave Transparent Minerals

Microwave heating of samples has been conducted by researchers in different areas for different purposes. The experiments mentioned in previous papers provided valuable information for the laboratory study of microwave heating (Kawala and Atamanczuk, 1998; Li et al., 2006; Hascakir et al., 2009; Asghari and Sheidaei, 2011; Anwar et al., 2015; Kar and Hascakir, 2015; Wang et al., 2016).

In terms of the ability to absorb microwave, minerals can be divided into microwave transparent minerals and microwave absorbing minerals (McGill et al., 1995). Microwave absorbing minerals can transform microwave energy into heat, so that the attenuation of microwave energy is high. On the contrary, microwave transparent minerals do not absorb microwave energy, thus the attenuation of microwave energy

is negligible. Chen et al. (1984) summarized the minerals that are transparent to microwave in Table 1-4.

Table 1-4 Minerals transparent to microwave irradiation (Frequency=2.45GHz; Power=150W; Time=5 min) (Chen et al., 1984)

Mineral Class	Minerals/Compounds
Carbonates	Aragonite, calcite, dolomite, siderite
Jarosite-type compounds	Argentojarosite, synthetic natrojarosite (zinc plant residue, Kidd Creek Mines Ltd), synthetic plumbojarosite (zinc plant residue, Cominco Ltd)
Silicates	Almandine, allanite, anorthite, gadolinite, muscovite, potassium feldspar, quartz, titanate, zircon
Sulphates	Barite, gypsum
Others	Fergusonite, monazite, sphalerite (low Fe), stibnite

1.5.2 The Cut-off Temperature

Ford and Pei (1967) reported that the heating curves have a similar pattern, as shown in Figure 1-4. The temperature of the heated object increases at the beginning of the microwave heating. After reaching the maximum temperature, the temperature curve becomes flat. In their study, the maximum temperatures of some compounds have been recorded in Table 1-5. McGill et al. (1995) gave a similar table indicating the maximum temperatures of different minerals in Table 1-6.

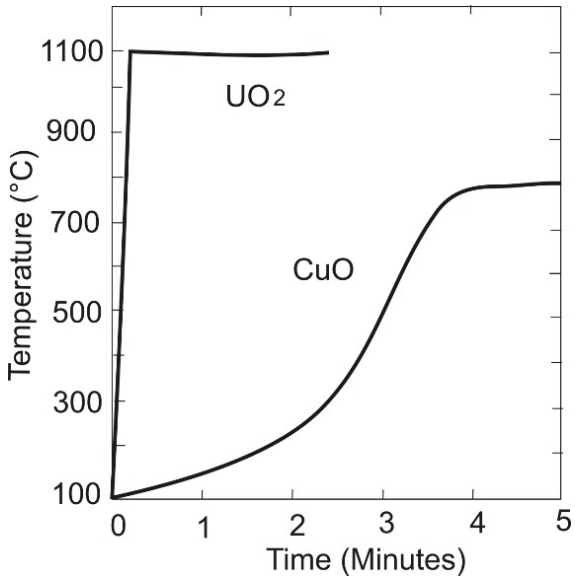

Figure 1-4 Typical MW heating curves of CuO and UO_2 (There is a maximum temperature value for the object heated by the microwave. after reaching the maximum temperature, the temperature curve becomes flat) (Ford and Pei, 1967).

Table 1-5 Heating times and maximum temperatures for some compounds (Ford and Pei, 1967)

Compound	Colour	Heating Time (min.)	Max Temperature (°C)
Al_2O_3	White	24	1900
C	Black	0.2	1000
CaO	White	40	200
Co_2O_3	Black	3	900
CuO	Black	4	800
CuS	Dark Blue	5	600
Fe_2O_3	Red	6	1000
Fe_3O_4	Black	0.5	500
FeS	Black	6	800
MgO	White	40	1300
MoO_3	Pale green	46	750
MoS_2	Black	0.1	900
Ni_2O_3	Black	3	1300
PbO	Yellow	13	900
UO_2	Dark green	0.1	1100
ZnO	White	4	1100

Table 1-6 Effect of fixed power microwave heating on the temperature of natural minerals (McGill et al., 1995)

Mineral	Chemical composition	Temp, °C at 1 min	Maximum temp, °C	Time, min
Albite	NaAlSi3O8	53	82	7
Arizonite	$Fe_2O_3 \cdot 3TiO_2$	84	290	10
Chalcocite	Cu_2S	506	746	7
Chalcopyrite	$CuFeS_2$	920	920	1
Chromite	$FeCr_2O_4$	89	155	7
Cinnabar	HgS	83	144	8
Galena	PbS	755	956	7
Hematite	Fe_2O_3	102	182	7
Magnetite	Fe_3O_4	861	1258	2.75
Marble	$CaCO_3$	50	74	4.25
Molybdenite	MoS_2	108	192	7
Orpiment	As_2S_3	71	92	4.5
Orthoclase	$KAlSi_3O_8$	49	67	7
Pyrite	FeS_2	816	1019	6.75
Pyrrhotite	$Fe_{1-x}S$	730	886	1.75

Quartz	SiO_2	52	79	7
Sphalerite	ZnS	65	87	7
Tetrahedrite	$Cu_{12}Sb_4S_{13}$	64	151	7
Zircon	$ZrSiO_4$	41	52	7

Atomic Energy of Canada Limited Research Company and Voss Associates Engineering Ltd (1990) considered the reason for the cut-off temperature to be the surface reflection limiting the heating process. The dielectric constant plays a vital role in this phenomenon. The fraction of reflected power is expressed as:

$$\boldsymbol{R = \frac{1-\sqrt{2\varepsilon'[1+\sqrt{1+(tan\delta)^2}]}+\varepsilon'\sqrt{1+(tan\,\delta)^2}}{1+\sqrt{2\varepsilon'[1+\sqrt{1+(tan\delta)^2}]}+\varepsilon'\sqrt{1+(tan\,\delta)^2}}}$$

Equation 9

The fraction of absorbed power is estimated as (Bykov et al., 2001):

$$\mathbf{1 - R \approx 2\sqrt{\frac{2}{\varepsilon' \tan \delta}}}$$

Equation 10

The dielectric constant of minerals increases with temperature in the manner of Figure 1-5. This leads to the fraction of the absorbed power being reduced to 0, whereas the fraction of the reflected power rose close to 1.

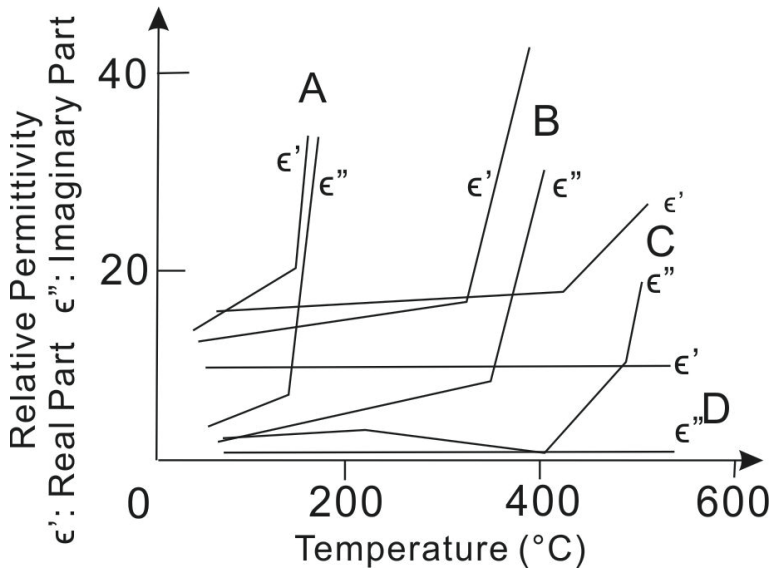

Figure 1-5 Dielectric data for four sulphide minerals and ores at 2375MHz (A: pyrrhotite, $Fe_{1-x}S$, where x lies between 0 and 0.2; B: chalcopyrite, $CuFeS_2$, C: pyrite, FeS_2 and D: sphalerite, ZnS (Atomic Energy of Canada Limited Research Company and Voss Associates Engineering Ltd, 1990).

The penetration depth, D_p, of the microwave, which is approximated as $D_p = \frac{\lambda_0'(\epsilon')^{1/2}}{2\pi\epsilon_{eff}^{"}}$, is also dependent on the relative permittivity, where λ_0' is the wavelength, ϵ' is the dielectric constant, and $\epsilon_{eff}^{"}$ is the effective loss factor; thus, it is dependent on temperature. The dramatic decrease of the penetration depth inhibits the heating process and it is another reason for the cut-off temperature.

2.Methodology

2.1 Thin Section Analysis

Thin sections were prepared in CSIRO for each sample in order to investigate the texture, composition and structures of samples. As this study focused on the effects of microwave heating on tight sandstone samples, the major properties to investigate are the mineralogy (composition, shape and color change of minerals before and after heating), change of matrix and cement, structure of the sample, as well as presence of any micro-fractures.

Thin sections were prepared by cutting slices of the sandstone samples from the core plugs and grinding them to less than 30μm. The microscopy, Nikon polarizing microscope Eclipse LV100POL (Figure 2-1), was provided by the Department of Applied Geology of Curtin University. Thin sections have been prepared both before and after heating.

Figure 2-1 Nikon polarizing microscope Eclipse LV100POL.

2.2 Scanning Electron Microscopy (SEM)

Scanning Electron Microscopy (SEM) produces images by recording various signals resulting from the interactions of an electron beam with the sample. SEM focuses on the small pieces of samples and provides relatively high-resolution images, namely

information about the grains' relationships, the intergranular pore structures (Welton, 1984) and the occurrence of micro-fractures. With a high resolution, the morphology and structures of the minerals and micro-fractures are able to be clearly observed by SEM.

The samples were prepared using relatively small and flat samples carefully with disposable gloves and lab tools. It is important to note that the surface of the sample should not be prepared by cutting but by breaking. Then, the specimens were coated with carbon. Finally, a 4nm platinum coating was carefully applied on the sample. After vacuuming for one week it was ready for SEM imaging. Observations were made in the Department of Physics of Curtin University (Now the John de Laeter Centre) with the equipment of Zeiss Neon 40EsB FIBSEM (Figure 2-2).

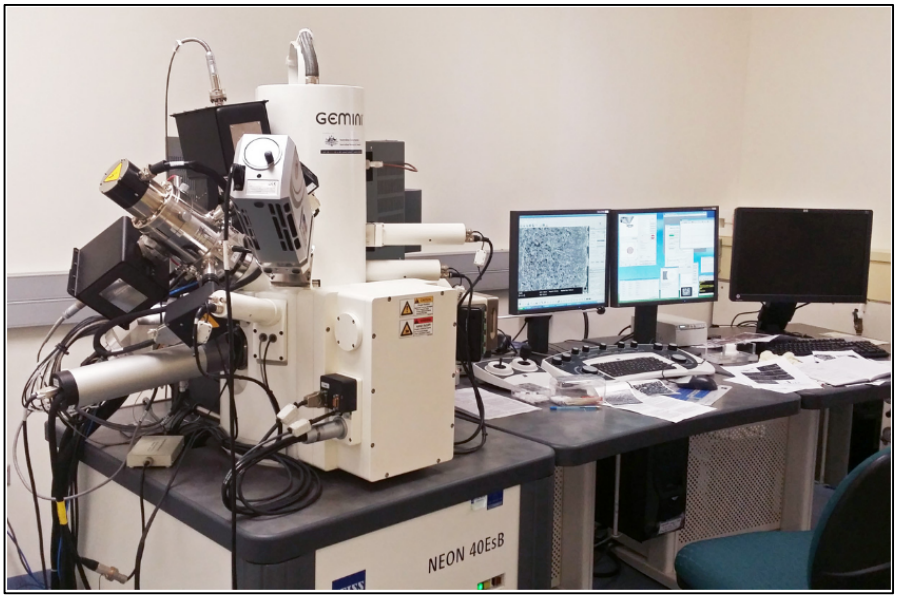

Figure 2-2 The equipment used to acquire SEM images: the Zeiss Neon 40EsB FIBSEM in John de Laeter center of Curtin University

2.3 X-ray Diffraction (XRD)

XRD (X-ray Diffraction) is used for the composition analysis. The fundamental basis for determining the characteristic peaks of known minerals and compounds is Bragg's Law. The combined diffraction analysis of the bulk powder and oriented mounts was used to obtain the bulk rock mineralogy. Quantitative Phase Abundance Analysis by XRD was conducted in the Centre for Materials Research of Curtin University (Now

the John de Laeter Centre). In particular, the samples had to be grounded into powder before the XRD analysis.

Our experimental work revealed the changes in the composition and microstructure of sandstones. In the XRD patterns, there are several important components: peak position, peak shape, peak height (maximum intensity), peak area (integral intensity) and peak width. The peak position reflects the *d* spacing and the lattice parameters. The peak area is related to the crystal structure and phase quantity. The peak width and peak shape are determined by the crystallite size and defects (Sharon and Javier, 2012).

2.4 X-ray Computed Tomography (CT) Imaging

Besides SEM, X-ray CT scanning, has also been used in this study to visualize the sample. X-ray CT scanning is a non-destructive method used to study the internal structure of sandstones. The X-ray CT image stacks provide the visualization of 3D information of the microwave heated samples in a relative low resolution, which shows the position and dimension of the fractures. The density/ porosity changes of core plugs along the sample length proved to correlate with the CT number, which can be calculated in the software conveniently. The CT number obtained from these stacked images indicates the profile of porosity variations along the length of each sample (Akin and Kovscek, 2003).

CT attenuation data are presented in Hounsfield Unit (*HU*), which is given by the CT number of air at -1000 *HU* and of water at 0 *HU* (Wellington and Vinegar, 1987). The CT numbers are important parameters yielded from X-ray CT scanning, which directly correlate to grain density (Perez, 1993). For sandstone CT scanning experiments, a change of $\pm 1\,HU$ is equivalent to a fractional density change of $\pm 0.5\times10^{-3}(\Delta\rho/\rho)$ (Wellington and Vinegar, 1987). However, the disadvantage is that the resolution of X-ray CT scanning is not sufficient to investigate details of the microstructures, so the Scanning Electron Microscope (SEM) has to be employed to

obtain the information of minerals and microstructures of rock samples as a complement of X-ray CT scanning.

Tight sandstone core plugs (Diameter=1.5inch) were examined with medical X-ray CT in CSIRO. The software Image-J was used to analyze the X-ray CT data in order to investigate the structure and texture characteristics of the sandstone samples.

2.5 Porosity and Permeability

Porosity is defined as the ratio of void space in the rock to the bulk volume of the rock, which indicates the storage ability of sandstone; permeability indicates the ability of sandstone to let fluids pass through. These two properties are two of the most important petrophysical properties of reservoir rock and most of the measures taken in the production of hydrocarbon are relevant to them directly or indirectly.

By combining pore volume compressibility and the effect of brine saturation on stress dependence of the relative permeability of gas, relevant information on reservoir quality can be obtained (Randolph, 1984). Petrography studies found that the pore geometry of tight sandstones falls into three general types: grain supported primary pores, secondary solution pores connected by narrow inter-granular slots and matrix supported grains (Figure 2-3) (Soeder and Randolph, 1987). Amongst them, matrix supported grains have lowest porosity and very low permeability.

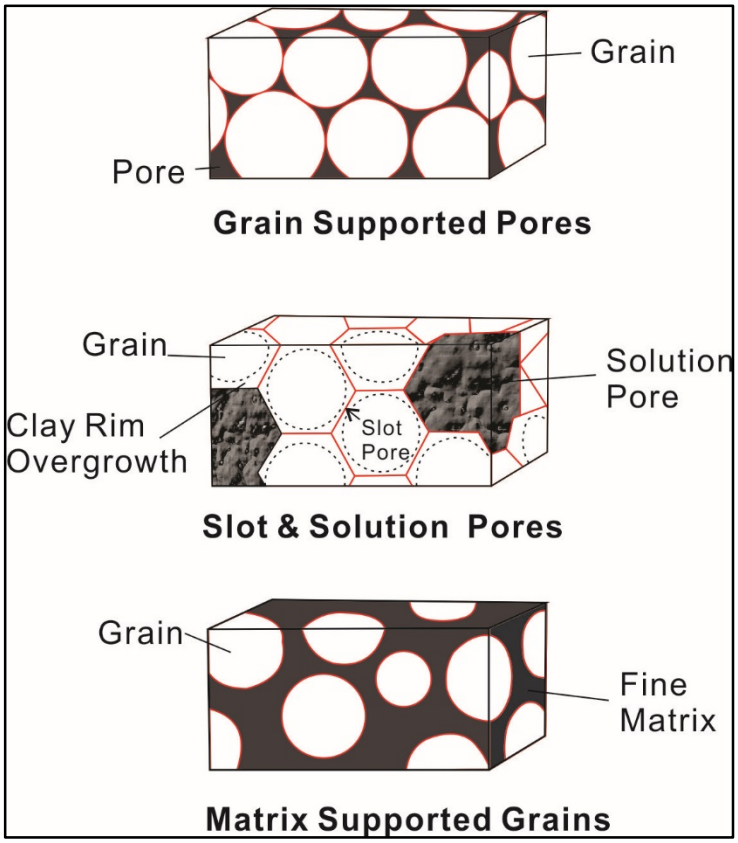

Figure 2-3 Pore geometry in tight gas sandstones. Grain supported pores, which are high porosity and permeability; slot and solution pores, which are moderate porosity and narrow permeability and matrix-supported grains, which are low porosity and permeability. (Soeder and Randolph, 1987).

Porosity and permeability are measured in the lab by the Automated Porosimeter and Permeameter (Figure 2-4), which uses helium/ nitrogen to measure the porosity and permeability under overburden pressure. It accommodates core plugs with 1.5-inch diameter. The inputs include dimensional information and the outputs are the porosity, pore volume, permeability and klinkenberg-corrected permeability.

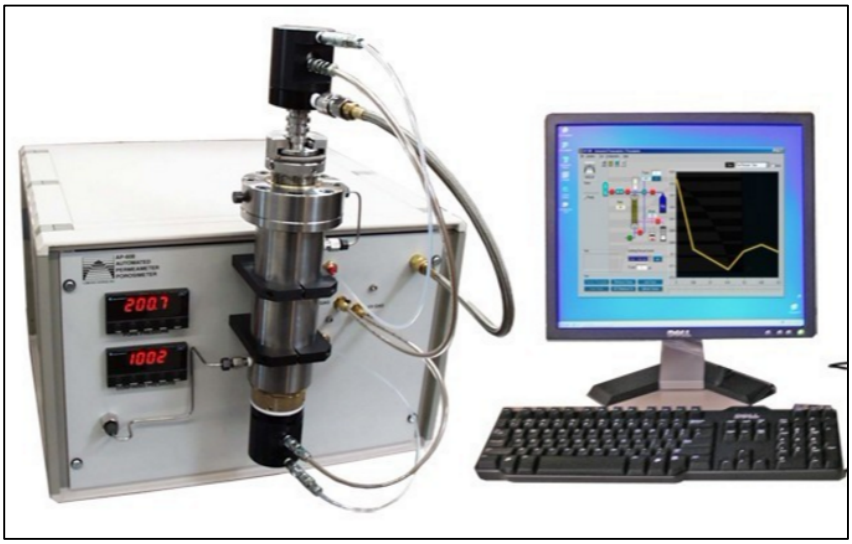

Figure 2-4 The automated porosimeter and permeameter (AP-608).

Nuclear Magnetic Resonance (NMR) is also used in studies of porosity and permeability in the porous medium. In general, porosity can be measured by conducting the NMR relaxation test after fully saturating the sample with brine.

To predict permeability, there are two models, the Free Fluid (or Coates) Model and the Mean T2 (or SDR) Model (Figure 2-5).

The Free Fluid Model is given below:

$$k = [\left(\frac{\emptyset}{C}\right)^2 (\frac{FFI}{BVI})]^2$$

Where k is the permeability, $\emptyset$ is the porosity, FFI is the free fluid volume, BVI is the bound water volume, C is a variable dependent on the formation and $FFI=\phi-BVI$. BVI can be determined by Cutoff BVI method or Spectral BVI. In unflushed gas zones, the estimation will be too low due to a lack of the hydrogen index (Coates, 1999).

The Mean T_2 Model takes the following form:

$$k = a{T_{2gm}}^2\emptyset^4$$

Where T_{2gm} is the geometric mean of the T2 distribution and a is a coefficient dependent on the formation type. This model works well in zones containing only water (Coates, 1999).

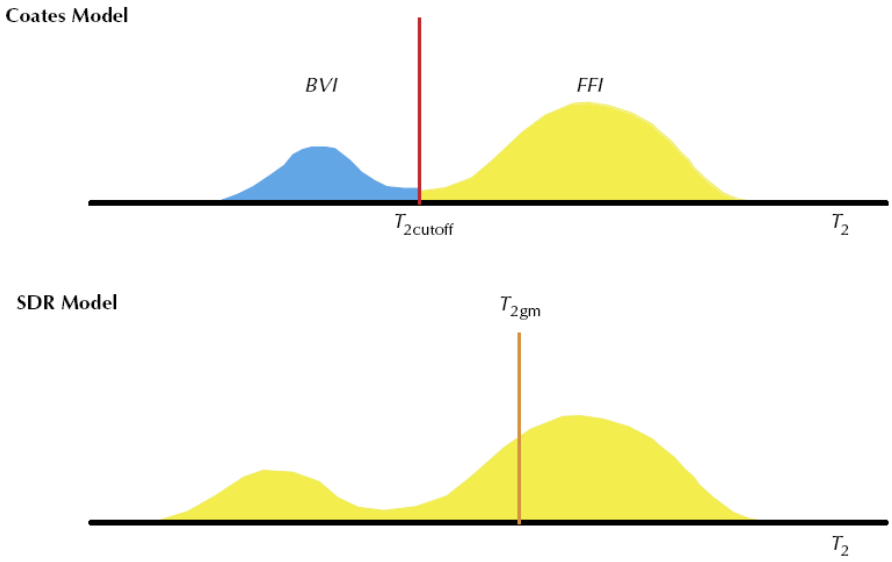

Figure 2-5 The Coates permeability model (top) uses the FFI/ BVI ratio to describe the changes in the surface-to-volume ratio and the SDR permeability model (bottom) uses an average T_2 value instead (Coates, 1999).

2.6 Pore Size Distribution

In addition to its application in porosity measurement and permeability estimation, NMR can also be applied in the measurements of pore size distribution. There are two types of relaxation: Longitudinal Relaxation (T1) and Transverse Relaxation (T2). T2 is always less than or equal to T1. T2 distribution curves reflect the pore size distribution after shift is being applied (Coates, 1999).

NMR Longitudinal Relaxation (T1) curves measured in the laboratory can be converted to sums of exponentials. The exponential decomposition can be interpreted as a pore size distribution. The results of NMR and digital analysis of thin sections match well (Kenyon, 1989). Each pore type represents a sub-distribution of pores with a characteristic size and shape. The relationship between mean T1 and the size of pore types is linear. The constant of their proportionality is the surface relaxivity, which represents the enhancement of relaxation induced by the pore wall (Bowers et al., 1995).

The NMR measurements were conducted using the Magritek 2 MHz NMR Rock Core Analyzer (Figure 2-6) in the Department of Petroleum Engineering of Curtin

University. The core plugs were all saturated with 20000 brine made of NaCl and distilled water using a high-pressure saturator (2000psi) (Figure 2-7) which provided a high confining pressure. After weighing the sample, they were put into the saturator and vacuumed for at least 12 hours due to low porosity and permeability. Then, the samples were saturated with the de-aerated brine for another 12 hours. Once the pressure stabilized, the samples were taken out and weighed.

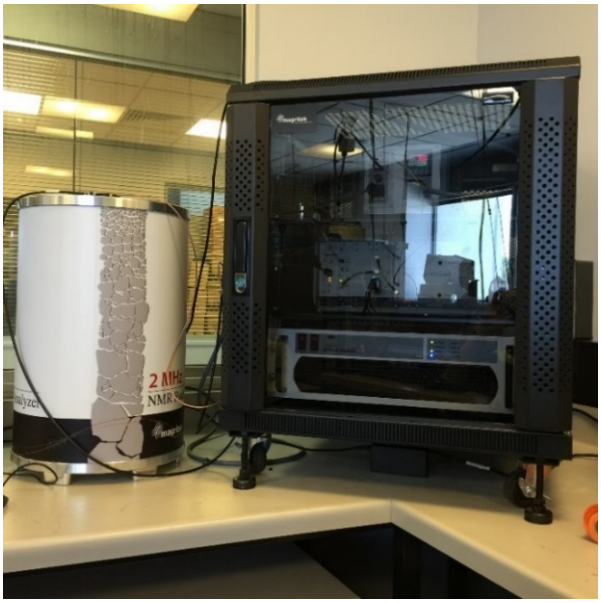

Figure 2-6 2MHz NMR core analyzer in Department of Petroleum Engineering of Curtin University.

Figure 2-7 High-pressure saturator in the Department of Petroleum Engineering of Curtin University.

The samples were wrapped with cling wrap and measured in the NMR Core Analyzer. The parameters of the T_2 experiments are listed in Table 2-1.

Table 2-1 Parameters of NMR T_2 experiments

Inter-Expt Delay (ms)	Dummy Scans	No. of Echoes	Tau
10000	1	10000	50
Minimum SNR	**Points Per Echo**	**Echo Shift (us)**	**Dwell Time (us)**
200	32	15	0.5

The T_2 distribution of fully saturated sandstone is a measure of the pore size distribution of the sample (Coates, 1999). The longer T_2 represents the larger pores, while the shorter T_2 represents the smaller pores. The amplitude represents the population of corresponding pore size.

2.7 Experimental Setup

Two types of heating methods have been conducted in this study: conventional heating with muffle furnace and laboratory microwave heating. The muffle furnace heated tight sandstones by thermal radiation, thermal conduction and thermal convection, and the temperature was monitored by the furnace controller. The microwave heated tight sandstone samples via high frequency induction and the temperatures of the samples were measured by an infrared thermometer. The heated core plugs were fully studied with laboratory tests such as the Automated Permeameter, NMR, SEM, XRD, X-ray CT and thin sections. More importantly, the experiment results were comparable with those before heating.

2.7.1 Tight Sandstone Samples

The tight sandstones are collected from the Perth Basin, Western Australia. In accordance with the locations, where the samples are collected from, and experiments, which are planned to be conducted on these samples, 12 samples are divided into 2 groups: Group 1 and Group 2. Group 1 are samples from Northern Perth Basin, including West-Erregulla, GinGin-3, Erregulla-1 and Erregulla-2, and Group 2 are those from Southern Perth Basin, including Whicher Range-01, Whicher

Ranger-05, Whicher Range-06, Whicher Range-08, Whicher Range-09, Whicher Range-11, Whicher Range-12 and Whicher Range-14. Samples of Group 2 are further divided into two subgroups. Table 2-2 summarised the grouping information and experiment types of each sample. Their properties are listed in Table 2-3.

Table 2-2 Summary of Sample Grouping and Experimental Information.

Group No.	Subgroup	Sample ID	Porosity	Permeability	X-ray CT	Permittivity	SEM	XRD	Thin Section	Furnace Heating	MW Heating
Group 1	**N/A**	North-Erregulla	✔	✔	✔	✔	✔	✔	✔		
		West-Erregulla	✔	✔	✔	✔	✔	✔	✔		✔
		GinGin-3	✔	✔	✔	✔	✔	✔	✔		Backup
		Erregulla-1	✔	✔	✔	✔	✔	✔	✔		Backup
		Erregulla-2	✔	✔	✔		✔	✔	✔		✔
Group 2	**Subgroup A**	Whicher Range-01	✔	✔	✔	✔	✔	✔	✔		✔
		Whicher Range-05	✔	✔	✔	✔	✔	✔			Damaged
		Whicher Range-06	✔	✔	✔	✔	✔	✔	✔	✔	
		Whicher Range-08	✔	✔	✔	✔	✔	✔		✔	
	Subgroup B	Whicher Range-09	✔	✔	✔	✔	✔	✔		✔	
		Whicher Range-11	✔	✔	✔	✔	✔	✔			✔
		Whicher Range-12	✔	✔	✔	✔	✔	✔		✔	
		Whicher Range-14	✔	✔	✔	✔	✔	✔			✔

Table 2-2 Summary of Sample Grouping and Experimental Information.

Group No.	Subgroup	Sample ID	Porosity	Permeability	X-ray CT	Permittivity	SEM	XRD	Thin Section	Furnace Heating	MW Heating
Group 1	**N/A**	North-Erregulla	✔	✔	✔	✔	✔	✔	✔		
		West-Erregulla	✔	✔	✔	✔	✔	✔	✔		✔
		GinGin-3	✔	✔	✔	✔	✔	✔	✔		Backup
		Erregulla-1	✔	✔	✔	✔	✔	✔	✔		Backup
		Erregulla-2	✔	✔	✔		✔	✔	✔		✔
Group 2	**Subgroup A**	Whicher Range-01	✔	✔	✔	✔	✔	✔	✔		✔
		Whicher Range-05	✔	✔	✔	✔	✔	✔			Damaged
		Whicher Range-06	✔	✔	✔	✔	✔	✔	✔	✔	
		Whicher Range-08	✔	✔	✔	✔	✔	✔		✔	
	Subgroup B	Whicher Range-09	✔	✔	✔	✔	✔	✔		✔	
		Whicher Range-11	✔	✔	✔	✔	✔	✔			✔
		Whicher Range-12	✔	✔	✔	✔	✔	✔		✔	
		Whicher Range-14	✔	✔	✔	✔	✔	✔			✔

Table 2-3 Physical Properties of Tight Sandstone Samples Used in the Study.

Sample ID	***West-Erregulla***	***GinGin-3***	***Erregulla-1***	***Erregulla-2***
Location	Northern Perth Basin	Northern Perth Basin	Northern Perth Basin	Northern Perth Basin
Well Name	West-Erregulla	GinGin-3	Erregulla-1	Erregulla-2
Length (cm)	4.769	4.993	6.232	4.933
Diameter (cm)	3.869	3.869	3.872	3.875
V bulk (cm3)	56.068	58.701	73.382	58.176
Porosity (500psi, %)	6.328	8.365	2.788	3.362
Permeability (500psi, mD)	0.058	0.263	0.021	0.013
Mass (dry, g)	138.8	142.1	188.7	149.2
Sample ID	**Whicher Range-01**	**Whicher Range-05**	**Whicher Range-06**	**Whicher Range-08**
Location	Southern Perth Basin	Southern Perth Basin	Southern Perth Basin	Southern Perth Basin
Well Name	Whicher Range-4	Whicher Range-4	Whicher Range-4	Whicher Range-4
Length (cm)	4.851	4.558	4.966	4.831
Diameter (cm)	3.788	3.781	3.786	3.782
V bulk (cm3)	54.669	51.177	55.906	54.271
Porosity (500psi, %)	3.745	3.169	9.122	7.977
Permeability (500psi, mD)	0.028	0.201	0.887	0.608
Mass (dry, g)	140.4	130.3	135.6	131.5

Table 2-3 Physical Properties of Tight Sandstone Samples Used in the Study (Continued).

Sample ID	***Whicher Range-09***	***Whicher Range-11***	***Whicher Range-12***	***Whicher Range-14***
Location	Southern Perth Basin	Southern Perth Basin	Southern Perth Basin	Southern Perth Basin
Well Name	Whicher Range-4	Whicher Range-4	Whicher Range-4	Whicher Range-4
Length (cm)	6.49	4.98	4.945	4.478
Diameter (cm)	3.787	3.786	3.782	3.782
V bulk (cm3)	73.101	56.064	55.552	50.407
Porosity (500psi, %)	7.993	9.711	3.34	3.58
Permeability (500psi, mD)	0.259	0.149	0.109	0.054
Mass (dry, g)	179	136.1	141.5	128.4

2.7.2 Dielectric Properties Measurement

Dielectric properties decide the heat generation rate of the sandstone heated by microwave. There are many methods and probes for investigating dielectric properties in the lab including: the Perturbation Technique (the cavity perturbation technique and the resonant cavities), as well as the Waveguide and Coaxial Transmission Line Method (transmission line technique), resonators and transmission line, open ended probe, time domain spectroscopy (TDR) methods, free space transmission techniques, microstrip transmission line, six port reflectometer using an open-ended coaxial probe and colloid dielectric probe) (Venkatesh and Raghavan, 2005). Some of them are only suitable for measurements at low frequency; for example, the parallel plate cell, while others are designed for high frequency.

In this study, relative permittivity and dielectric loss have been measured using End Loaded Transmission lines. The reason for choosing this technique is that this probe is suitable for the 1.5-inch sandstone sample and its working frequency range is from 1MHz to 3GHz, which includes the frequency of microwave heating. As required by the measurement, the tight sandstone plugs were all prepared on a flat surface so as to minimize the effect of air between the sample and the probe. The properties have been measured against different water saturations and salinities at the frequencies from 300 KHz to 3GHz. The large loaded coaxial transmission line is one of the useful tools. This probe can measure the dielectric properties from 1MHz to 3GHz with a high precision, when used together with the Agilent E5070B network analyzer (Figure 2-8).

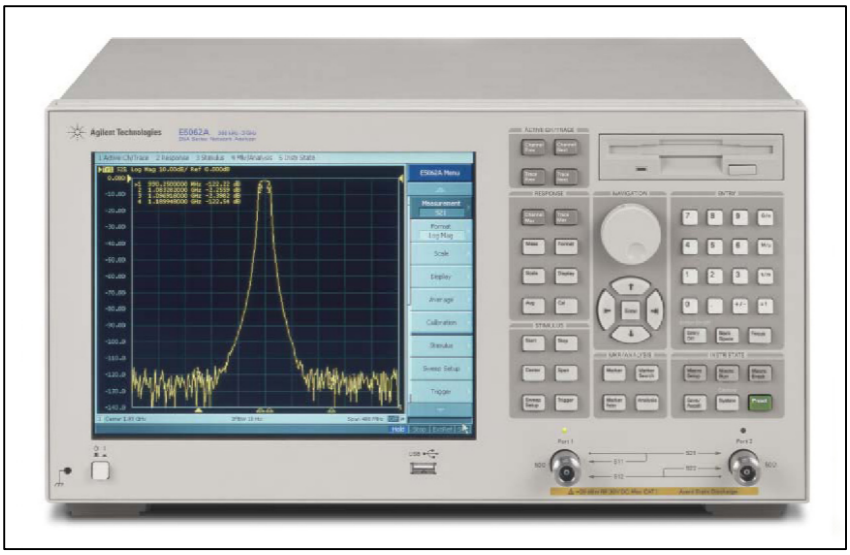

Figure 2-8 Agilent E5070B network analyzer.

The dielectric loss factor and permittivity are not only a function of frequency but also a function of water saturation. Metaxas and Meredith (1983) reported that the change of loss factor with moisture content, *M*, of a typical wet solid is as shown in Figure 2-9. The two distinct regions, I & II, are related to the different water states - bound water and free water respectively. The bound water (region I) can be reflected from gradual slope at a low moisture content, while the free water (region II) can be reflected from the steeper slope at increased moistures. The change of slope occurs at the point of critical moisture content, *Mc*. (Hasted, 1973; De Loor, 1968; Tinga, 1969; Stuchly, 1970; Kraszewski, 1977; Metaxas and Meredith, 1983)

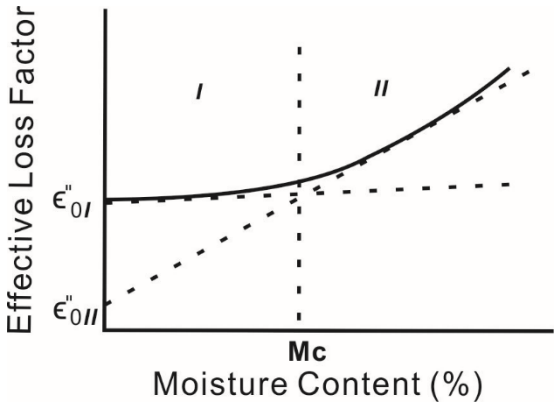

Figure 2-9 The effective loss factor as a function of the moisture content, the curve in region I has a gradual slope due to the bound water, while region II has a steeper slope due to free water (Metaxas and Meredith, 1983).

A total of 12 sandstone plugs of standard size (diameter = 1.5 inch) were prepared and saturated with 20000ppm brine. There are 4 samples in Group 1 (Northern Perth Basin): North Erregulla, West Erregulla, Erregulla-1 and GinGin-3, which are saturated with brine of 20000ppm. In Group 2 (Southern Perth Basin), 8 samples are divided into two subgroups: subgroup A, including sample Whicher Range-01, Whicher Range-05, Whicher Range-06 and Whicher Range-08, was saturated with 20000ppm brine; subgroup B, including Whicher Range-09, Whicher Range-11, Whicher Range-12 and Whicher Range-14, was dried in the oven at 45℃ for 48 hours.

2.7.3 High Temperature Furnace Heating

High temperature muffle furnace has been used to heat 4 samples, Whicher Range-6, Whicher Range-8, Whicher Range-9, and Whicher Range-12. The temperature has been set to 600 ℃ and heating time is 1 hour After the sample had been cooled down to the room temperature, the required experiments are conducted.

A series of systematic methods regarding the heating process and property investigation have been designed and conducted in the lab. The measurements conducted with automated porosimeter and permeameter before and after heating are used to provide the information related to pore volume, porosity and permeability improvement quantitatively. After heating, these measurements are conducted at 500psi only to avoid any mechanical damages. NMR is an alternative method used to obtain the porosity of the samples. The incremental porosity curve is a reflection of pore size distribution while the cumulative porosity curve is the porosity of the sample. The dry samples after heating and cooling down have been measured with NMR equipment before re-saturating them for the other NMR measurements. Then, the samples 100% saturated and the NMR tests were carried out on them. Finally, the samples were put into the centrifuge for 24 hours to produce the free fluid in the sample and were measured with NMR.

The microstructures of the samples are of great interest in the present study. X-ray CT scanning and SEM again are used to observe the texture and structure changes in two different magnifications.

2.7.4 Laboratory Microwave Heating

The most common frequency band for microwave processing is between 915 and 2450MHz. Two processes are involved in the interaction of the microwave and sandstone: polarization, which is the short-range charge displacement, and conduction, which is the long-range charge transport. At low electromagnetic wave frequencies, the ionic conduction losses overwhelm the polarization, while the reverse takes place at higher frequencies (Clark and Sutton, 1996). The dielectric losses are decided by both properties of microwave radiation, namely frequency and power level, and the properties of the porous medium, such as porosity, water saturation and mineralogy.

The characteristics of microwave propagation are of great importance to the application of microwave heating in FHT. The electromagnetic wave can penetrate the formation for a certain distance and heat it up without relying on thermal conduction. From Equation 8, the penetration depth is proportional to the wavelength, which is inversely proportional to the frequency. Field measurements of the penetration depth showed that it reached 1.33m at 2.45GHz, while at 915MHz, it reached 2.62m (Carrizales, 2010). Wacker et al. (2011) claimed that microwave heating could penetrate 1m if the water saturation is 10% and the penetration depth of inductive heating ranges from 10 to 100m. In addition, the conversion of microwave to heat can be completed in a short time, so the heating time is minimal.

The operating frequency of commercial microwave oven is 2450MHz and there are different levels of heating power, with the maximum level being 1050W. The oven was equipped with high temperature insulation in order to suit the requirements of high temperature heating. The samples were tightly wrapped with an aluminum tube, which is transparent to the microwave, in order to provide the confining pressure and reduce the samples' contact with air (Figure 2-10). The temperature was measured

with an infrared thermometer with measurement ranging from -60 to 1000°C (-76° to 1832°F) and an accuracy of the greater one between ±2% of reading and 2°C. The response time is 1 second, so as to attain the best reading within the shortest time frame.

The surface temperature of sandstone during heating is measured through the bottom. The effect of the aluminum tubes is obvious when compared with samples heated without the aluminum tube in the test stage of the microwave heating experiment. Those samples without the confining aluminum broke into pieces after microwave heating for tens of second and their petrophysical properties could not be measured in equipment like the NMR or Porosimeter which requires the sample to be in a good shape. After conducting the microwave heating and temperature measurements, the aluminum tube was removed with care.

Figure 2-10 A sandstone sample confined by an aluminum tube in order to provide the confining pressure on the sample and reduce the sample's contact with air.

The similar experimental procedures were adopted before and after heating the sandstone samples:

- Separate the small pieces of samples from the core plugs before any experiments.
- Dry the sample in the lab oven at a lower temperature (50°C) for 24 hours and then measure their porosity and permeability with an Automated Permeameter.
- Subject the whole core plugs to X-ray CT scanning with a medical X-ray CT.

- Saturate the sample with 20000ppm brine in a high-pressure (2000psi) saturator and then conduct the NMR test.
- Measure the dry sample with the NMR and then measure the porosity and permeability after heating and cooling the samples to room temperature.
- Break up the samples for SEM and other experiments after X-ray CT scanning, full saturation, and NMR analysis.

All our samples were prepared in the same way, with the same equipment and the imaging settings were kept the same, in order to minimize experimental errors caused by the equipment or procedures.

2.7.5 Factors Affecting the Microwave Heating of Sandstones

The experiments were conducted with a modified microwave oven operating at 2.45GHz. The output power level can be changed according to the requirements of heating. The waveguide used is WR-340 with a dimension of 86.36 × 43.18mm. The temperature was measured with an infrared thermometer. The samples used in this study were Berea Sandstone, with the purpose of reducing the influences of porosity and permeability.

In order to investigate the effects of salinities on microwave heating, samples were saturated in sodium chloride solutions with different salinities: distilled water, 20000ppm, 30000ppm and 40000ppm. The temperature was measured every minute for a duration of 2 minutes. For this test, the initial temperature is the room temperature of 24°C.

The effects of water saturation on microwave heating were studied by saturating samples with different amount of brine (20000ppm). Specifically, the weight of the 100% saturated sample and dry sample were recorded as water saturation of 1 and 0 respectively. Then, the mass of sample was converted to water saturation that fall between 0 and 1. The temperature variations with time were recorded for different water saturation.

Finally, the samples were saturated with different types of salt and heated with the microwave. The salts used were NaCl, KCl, $MgCl_2$ and $CaCl_2$. The salinity of these solutions was the same, specifically at 20000ppm. The temperatures were measured every minute for a total duration of 4 minutes.

2.8 Numerical Simulation

Numerical simulation is a significant method to study the feasibility of removing formation damage in tight gas reservoir with microwave heating technique. The concept of heating reservoir with microwave and related simulation works are being introduced. The modeling work has been conducted at two scales: laboratory and

reservoir. ANSYS Multiphysics and CMG-STARS have been used for different simulation objectives.

The main reservoir interval of Whicher Range tight gas field is the Permian Willespie Formation located in the depth from 3800m to 4600m approximately. Reservoir quality is poor, with average total porosity and effective as low as 9.7% and 2% respectively and the in-situ permeability is less than 0.3mD. Relative permeability measurements show high irreducible water saturation leading to a low gas relative permeability for the sand intervals (WA: ERA et al., 2012). According to the Well Completion Report of WR4, the temperature gradient is 3.26°C/100m to 1006m, 2.26°C/100m to 2472m and 2.06 °C/100m to 4575m. Temperatures recorded at different depths are: 47.80°C at 1006m, 71.00°C at 2472m and 109.00°C at 4575m. The hydrostatic pressure from 3800m to 4600m can be calculated as 380 kg/cm^2 (37.27MPa) to 460 kg/cm^2 (45.11MPa). The water boiling point can be determined by using the Water Phase Diagram (Henry Greenside, 2011). As seen in the diagram, the water boiling temperature from 37.27MPa to 45.11MPa is 690-700K (417-427℃). For a reliable model, the input data are of great importance. Based on the previous study (Birchak, 1974; Rodriguez, 1990; Seleznev, 2004) the dielectric properties of the rock and reservoir are predicted using available petrophysical data and mixing formulas.

2.8.1 Microwave Heating in the Lab

Two-dimensional model has been constructed to simulate the heating of core plugs by microwave. Details of the simulation will be described below. The microwave oven runs at 2.45GHz with power 1000 Watt.

In terms of model geometry, there are two important components: waveguide and cavity. In TE Mode waveguide, the dimension of waveguide determines the cutoff wavelength λ_{cutoff}, larger than which electromagnetic wave cannot propagate in the waveguide, by the following equation:

$$(\frac{2}{\lambda_{cutoff}})^2 = (\frac{m}{a})^2 + (\frac{n}{b})^2$$

Equation 11

For TE10 mode, m=1, n=0. The length and height of the waveguide cross section are a and b respectively. The equation used to determine the cutoff wavelength is:

$$\lambda_{cutoff} = \frac{2\sqrt{ab}}{\sqrt{m^2\frac{b}{a}+n^2\frac{a}{b}}}$$

Equation 12

In this model, the dimension of waveguide used 86mm*43mm. The dimension of microwave oven plays a critical role in the distribution of electric field. For rectangular oven, one or more dimensions are several half wavelengths long at the excitation wavelength (Meredith, 1998).

The input properties of sandstone, including thermal properties, electrical properties and petrophysical properties, are listed in Table 2-4 and Table 2-5.

Table 2-4 Petrophysical parameters for numerical simulation

Property	Value	Unit
Thermal Conductivity	2	W/(m*K)
Density	2650	Kg/m3
Relative Permeability	1	1
Heat Capacity	900	J/(kg*K)
Permeability	9.87e-17	m2
Porosity	0.1	1

Table 2-5 Electrical properties at 2.45GHz of tight sandstone samples

Property	Value	Unit
WR-1 Relative Permittivity	7.19-0.49i	1
WR-1 Electrical Conductivity	0.21	S/m
WR-11 Relative Permittivity	5.18-0.20i	1
WR-11 Electrical Conductivity	0.027	S/m
W-ERREG Relative Permittivity	6.93-0.665i	1
W-ERREG Electrical Conductivity	0.084	S/m

2.8.2 Reservoir Microwave Heating

In the reservoir heating simulation, the microwave device is lowered to the target formation and heats up the reservoir rock and interstitial fluids (Figure 2-11). The microwave device is operating at 2.45GHz and the power of 1000 Watt, which could

be adjusted according to the heating requirements, and the microwave is directed to the formation through a TE_{10} mode rectangular waveguide.

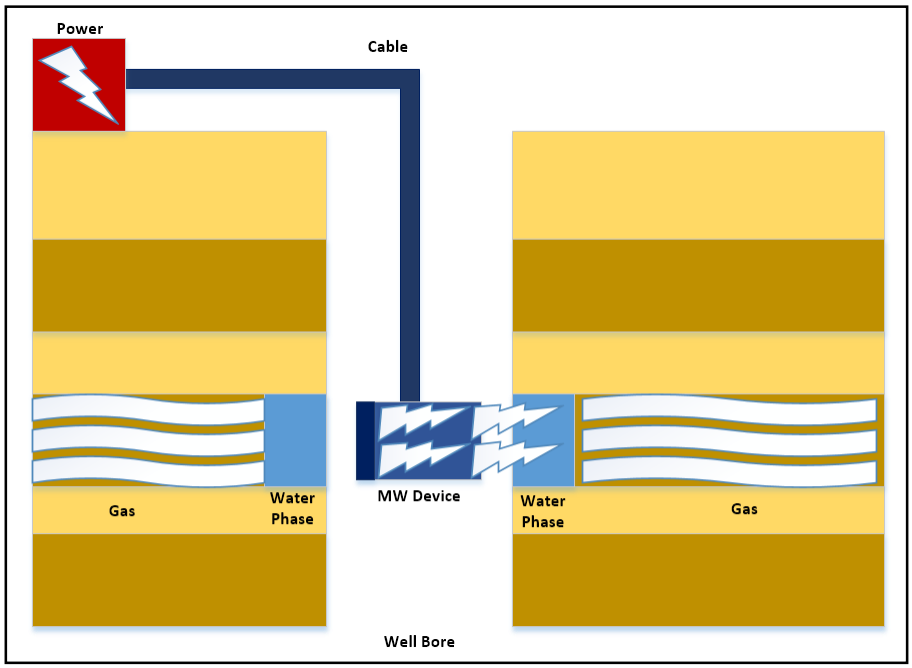

Figure 2-11 Concept Figure of Heating Formation with Microwave

In this study, we conducted our numerical simulation in two steps. The first step is to simulate the process of microwave heating in the reservoir in ANSYS. Electromagnetic and thermal field were coupled in this step to compute the distribution of power dissipation and temperature distribution. The second step is to simulate the process of reservoir property change. The results from the first step were used as a parameter to compute the reservoir properties and gas production.

2.8.2.1 Numerical Simulation with ANSYS

The reservoir properties used in this simulation are listed in Table 2-6. The power dissipation rate was also one of the important outputs from the simulation and will be a critical input in the subsequent reservoir simulation. The power dissipation rate was also one of the important outputs from the simulation and will be a critical input in the subsequent reservoir simulation. After applying microwave to the reservoir, the electric field distribution and then the temperature distribution in the reservoir can be computed in this model. The power dissipation rate was also one of the important outputs from the simulation and will be a critical input in the subsequent reservoir simulation.

Table 2-6 Reservoir Properties Used in the Simulation

Parameter	Value
Reservoir Temperature (°C)	139
Reservoir Porosity (1)	0.1
Reservoir Permeability (mD)	0.1
Initial Water Saturation (1)	0.3
Critical Water Saturation (1)	0.6
Reservoir Depth (m)	4000
Thermal Gradient (°C/100m)	2.8
Surface Temperature (°C)	27
Thermal Conductivity (J/ (m· day·°C))	1.73×10^{5}
Heat Capacity (J/ (cm^{3} ·°C))	2.385
Microwave Frequency (MHz)	2450
Operation Power (Watt)	10000

The numerical model was built in ANSYS with the geometry illustrated in Figure 2-12. The excitation method is rectangular waveguide (TE10) mode. The excited electromagnetic wave (2.45GHz) propagates through the reservoir sandstone and generated heat.

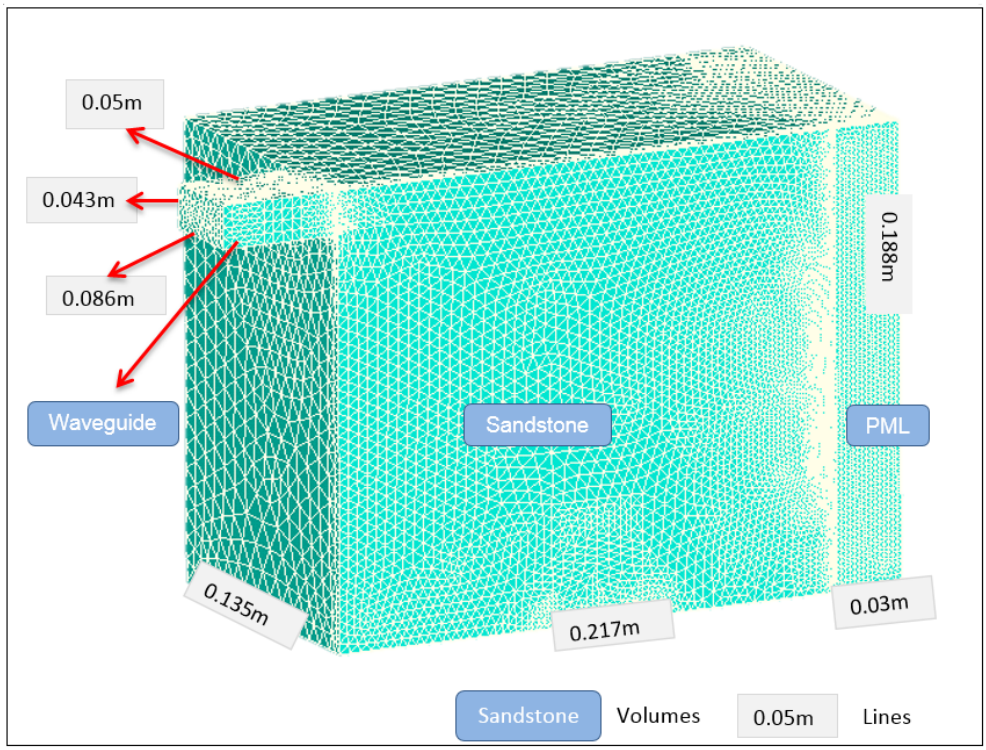

Figure 2-12 The Geometry Dimensions and Meshing of Numerical Model (Waveguide simulates the microwave device which is lowered to the target depth in the wellbore and radiates microwave to the reservoir; sandstone is the target formation; PML is the layer absorbing microwave, so that the microwave will not be reflected by the boundary.

2.8.2.2 Numerical Simulation with CMG

To simulate water invasion, the well was injected with water for 3 days with a daily injection rate of $5m^3$. After that, the well was heated with microwave for 1 day. Microwave heating in four different directions (-X, +X, -Y, +Y) in the wellbore was simulated simultaneously. The dimensions for the simulated area are 3.5m (length) x 3.5m (width) x 10m (thickness). Two scenarios were considered in this study: the first is the well producing without the microwave heater, the second is with the heater. To simplify the problem, the reservoir properties, which have been listed in Table 2-6, were set to be temperature independent.

3.Experimental and Simulation Results

3.1Dielectric Properties

Data from the dielectric property, porosity and NMR measurements indicate that for the saturated samples, both the real and imaginary parts of the permittivity correlate well with the permeability; for the dry samples, the permittivity correlates with the bound water and porosity (Figure 3-1). The saturated samples with higher permeability tend to have a higher conductivity, dielectric loss and permittivity at all frequencies from 1MHz to 3GHz. The dry samples, with higher bound water tend to have higher conductivity, dielectric loss and permittivity at all the frequencies as above, except sample Whicher Range-11. The probable reason could be the high porosity, as the air would take a higher percentage in the mixing of materials and contribute to the decrease of permittivity.

The measured complex permittivity and loss tangent of the samples were plotted in Figure 3-1 and Figure 3-3. The real and imaginary parts of permittivity tend to decrease with frequency. Interestingly, the exception is that the dielectric loss factor of the dry sample presented a peak at 3MHz and dropped to less than 1 at 3GHz. The brine saturated in the samples played an important role in permittivity. It significantly increased the dielectric loss, which is important to electromagnetic heating.

The permittivity of the measured samples was closely dependent on frequency. The dielectric constant increased slightly from 1 to 2.5MHz and then dropped to around 20 at frequency 10MHz and kept almost constant until 3GHZ. The dielectric loss decreased all the way to less than 10 and the sharpest drop was between 1 and 10MHz. The loss tangent is defined as the ratio of dielectric loss and dielectric constant. From the measurement result, the loss tangent dropped to about 3.5 at the frequency 3MHz and rose by 3-5.5 at the frequency around 10MHz and then decreased to less than 1 (greater than 0) at the frequency 3GHz.

Besides, when analyzing the dielectric data with the porosity data (Table 2-3) in addition to the permittivity data (Figure 3-1and Figure 3-3), we find that the greater the porosity, the greater the dielectric constant and dielectric loss.

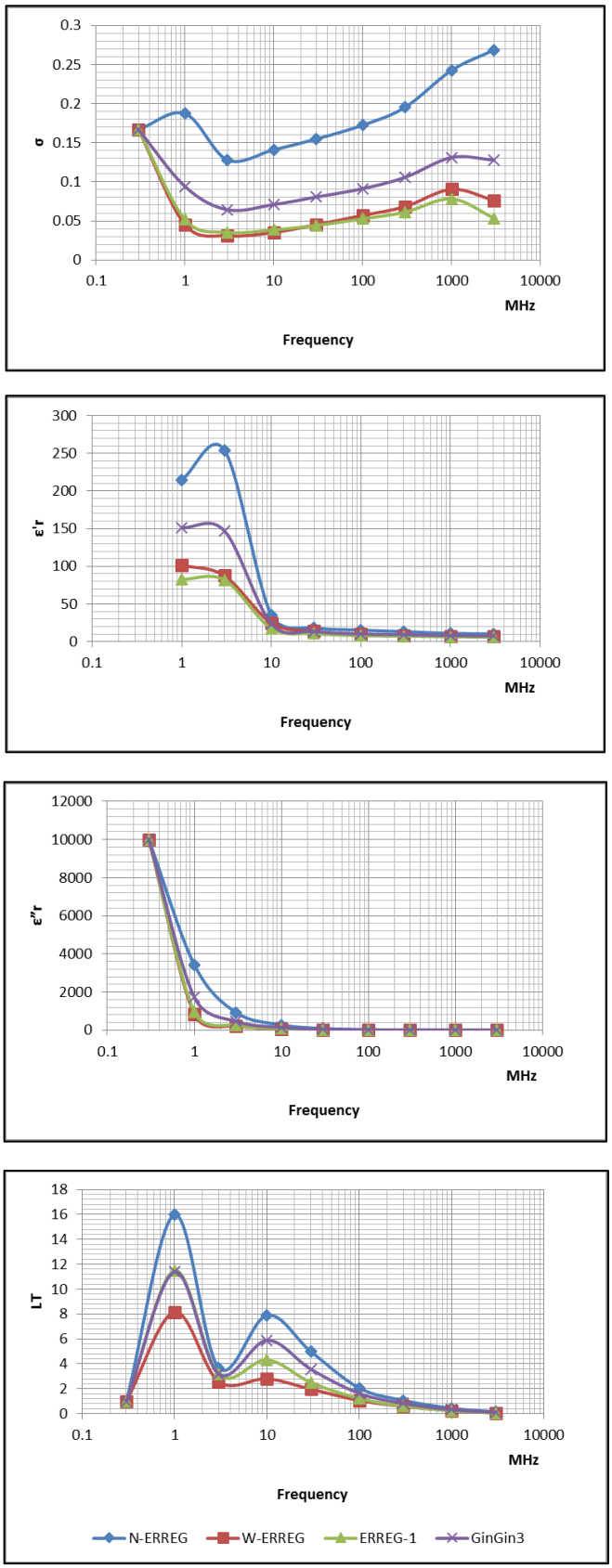

Figure 3-1 Dielectric properties of tight sandstone samples (Group 1). The electrical conductivity (σ), the real parts (ε'_r) and imaginary (ε''_r) of permittivity, and loss tangent (LT) are measured against different electromagnetic wave frequencies for the four samples.

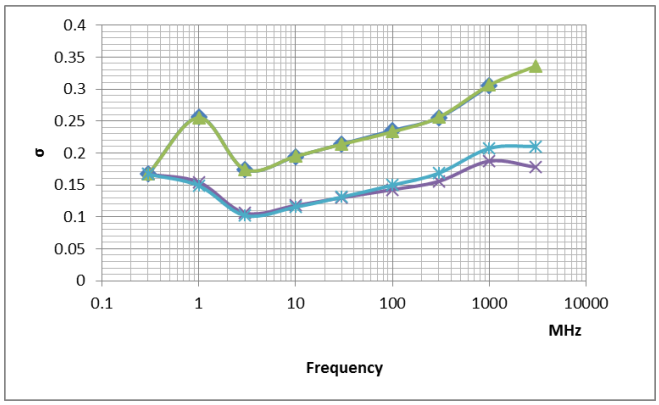

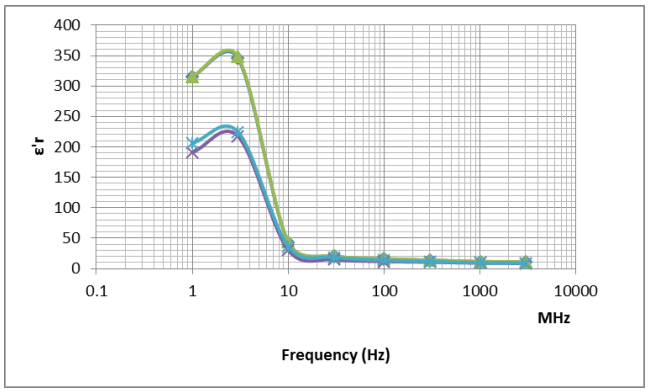

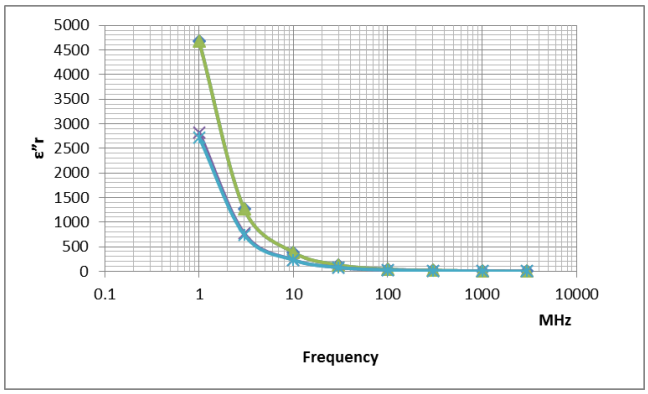

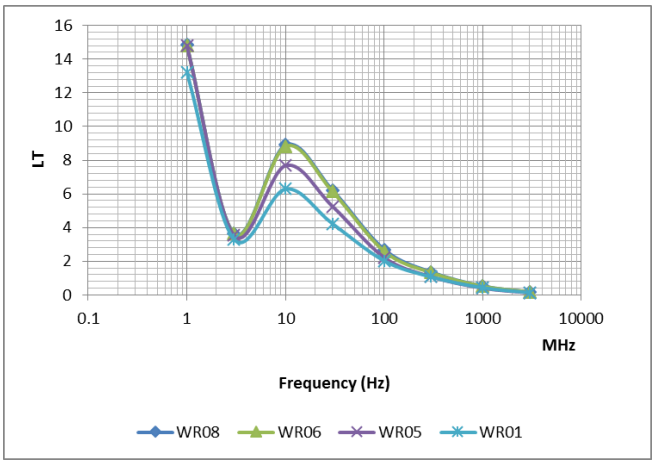

Figure 3-2 Dielectric properties of tight sandstone samples (Group 2, Subgroup A, Saturated with 20000ppm brine). The electrical conductivity (σ), the real parts (ε'r) and imaginary (ε”r) of permittivity, and loss tangent (LT) are measured against different electromagnetic wave frequencies for this subgroup.

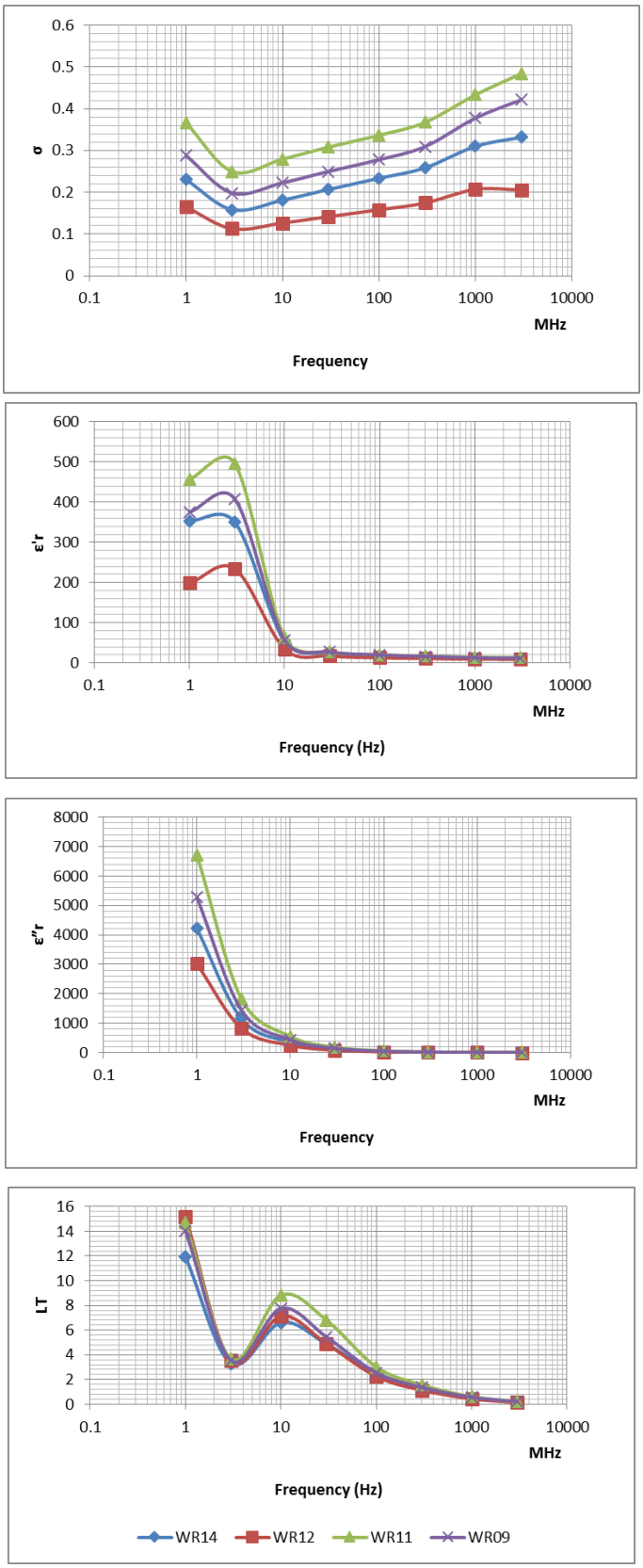

Figure 3-3 Dielectric properties of tight sandstone samples (Group 2, Subgroup B, dried at 45°C for 48 hours). The electrical conductivity (σ), the real parts (ε'r) and imaginary (ε”r) of permittivity, and loss tangent (LT) are measured against different electromagnetic wave frequencies for this subgroup.

3.2 High Temperature Furnace Heating

3.2.1 Reservoir Quality and Pore Size Distribution

The bulk volume, pore volume, porosity and permeability were measured before and after heating in the muffle furnace.

Figure 3-4 compare porosity and permeability alterations before and after furnace heating.

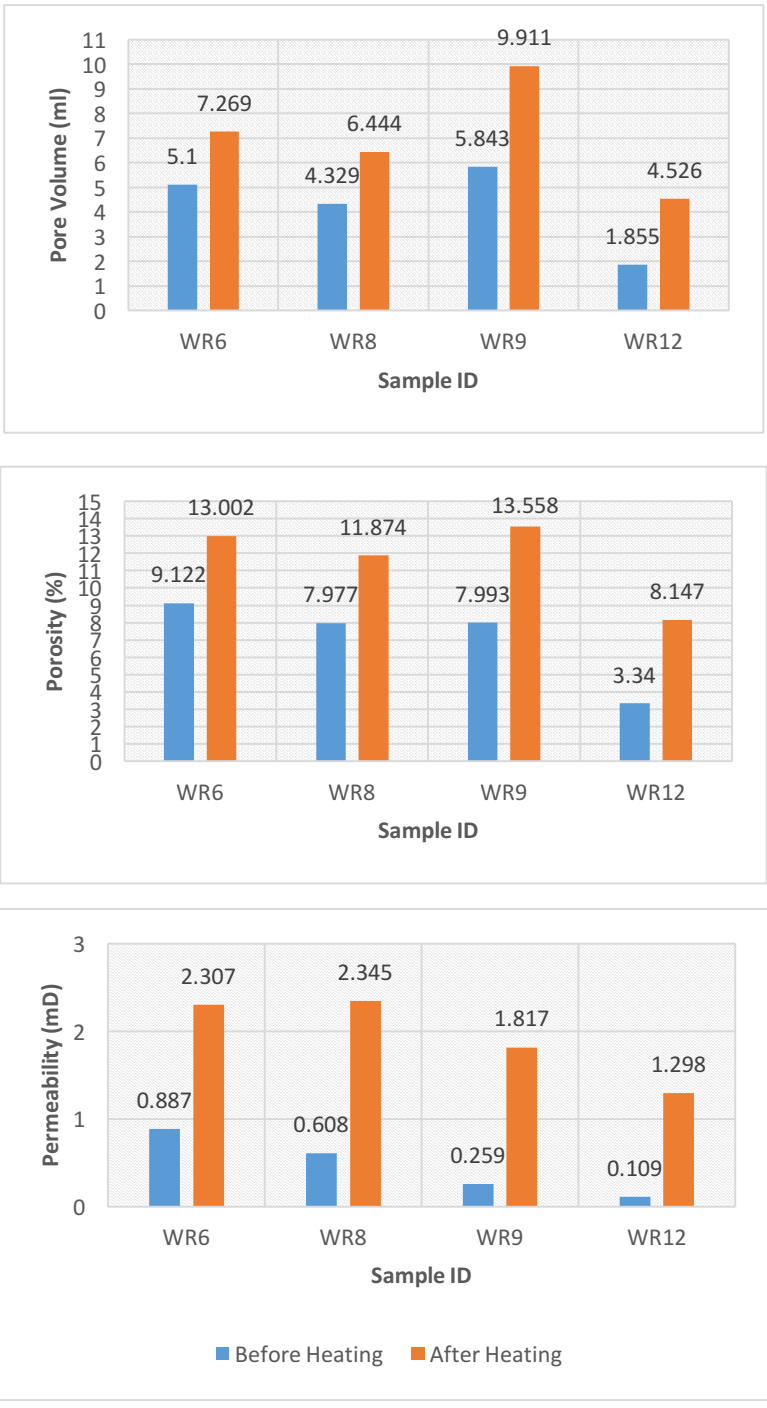

Figure 3-4 Comparison of pore volume, porosity and permeability before and after heating at 600°C. The pore volume and porosity have a moderate increase while the increase of permeability is larger.

The bulk volume of these samples keeps unchanged after heating. Pore volume, porosity and permeability increase after heating, and amongst them, permeability has the most dramatic increase. Permeability of the samples Whicher Range-6, Whicher Range-8, Whicher Range-9 and Whicher Range-12 increased about 260%, 390%, 700% and 1190% respectively. Jamaluddin et al. (1995) illustrated that the clay

degradation and micro-fractures due to thermal stress are the reasons for the increase of permeability. Porosity has increased (143%, 149%, 170% and 244% respectively for the same samples), but, as it can be seen, not as much as permeability increase.

Similarly, the NMR experiments show obvious increases of porosity after heating.

In this study, the pore sizes were divided into three levels according to their transverse relaxation time: relative small pores (less than 0.1ms), medium pores (0.1 to 10ms) and relative large pores (greater than 10ms).

It is observed that in Figure 3-5, in addition to the increase of porosity of the samples, the quantity of relatively large pores increased in all the samples. On the contrary, the relative small pores on the left end of the T2 distribution decreased or disappeared. The possible reasons could be: the small pores or fractures expanded (grew) after exposing to intensive heating, some of these fractures may join together to create a larger void space. This process transformed some smaller pore spaces into larger ones, which was reflected by the NMR pore size distribution. Hajpál and Török (2004) indicated that the micro-fractures will develop at grain boundaries at temperatures over 600℃ and the higher temperature of 750℃ is necessary for the fractures within the crystals.

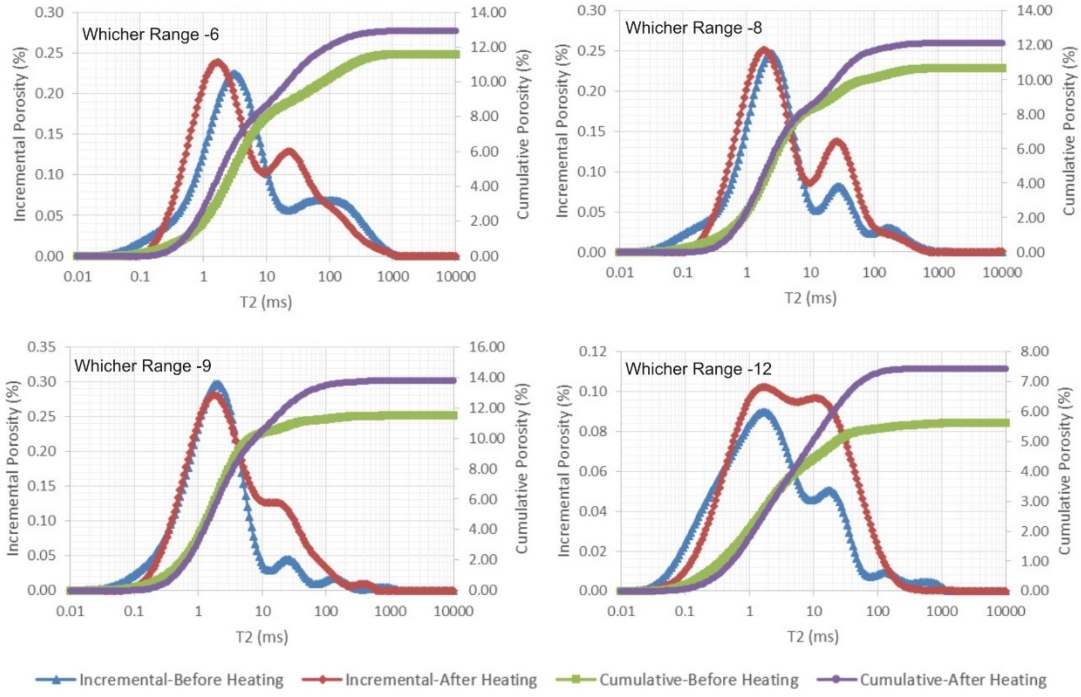

Figure 3-5 Comparisons of the NMR experiments results of 4 tight sandstone samples. The cumulative porosity shows the increase of total porosity, while the incremental porosity indicates the changes of pore size distributions. The portion of relative small pores (less than 0.1ms) decrease while the relative large pores (greater than 10ms) increase.

As shown in Figure 3-6, the cumulative porosity of Whicher Range-9 increased from 12% to 14% approximately and that of Whicher Range-12 increased from 5.8% to 7.5% approximately. The quantity of small pores remains steady in total but varies in the incremental T2 distributions. The heat changed minerals and caused thermal stress in samples, so more space, in the form of fractures, were created. The NMR cumulative porosity increased as a result of the additional space. There is an obvious difference in the results of the dry samples. The water in the samples (both irreducible and free water) reduced significantly after heating at 600℃. In other words, by heating the tight sandstone, almost all the water (even the clay bound water) in the rock can be evaporated. As a result, the water blocking damage and clay swelling can be eliminated and the gas relative permeability will increase.

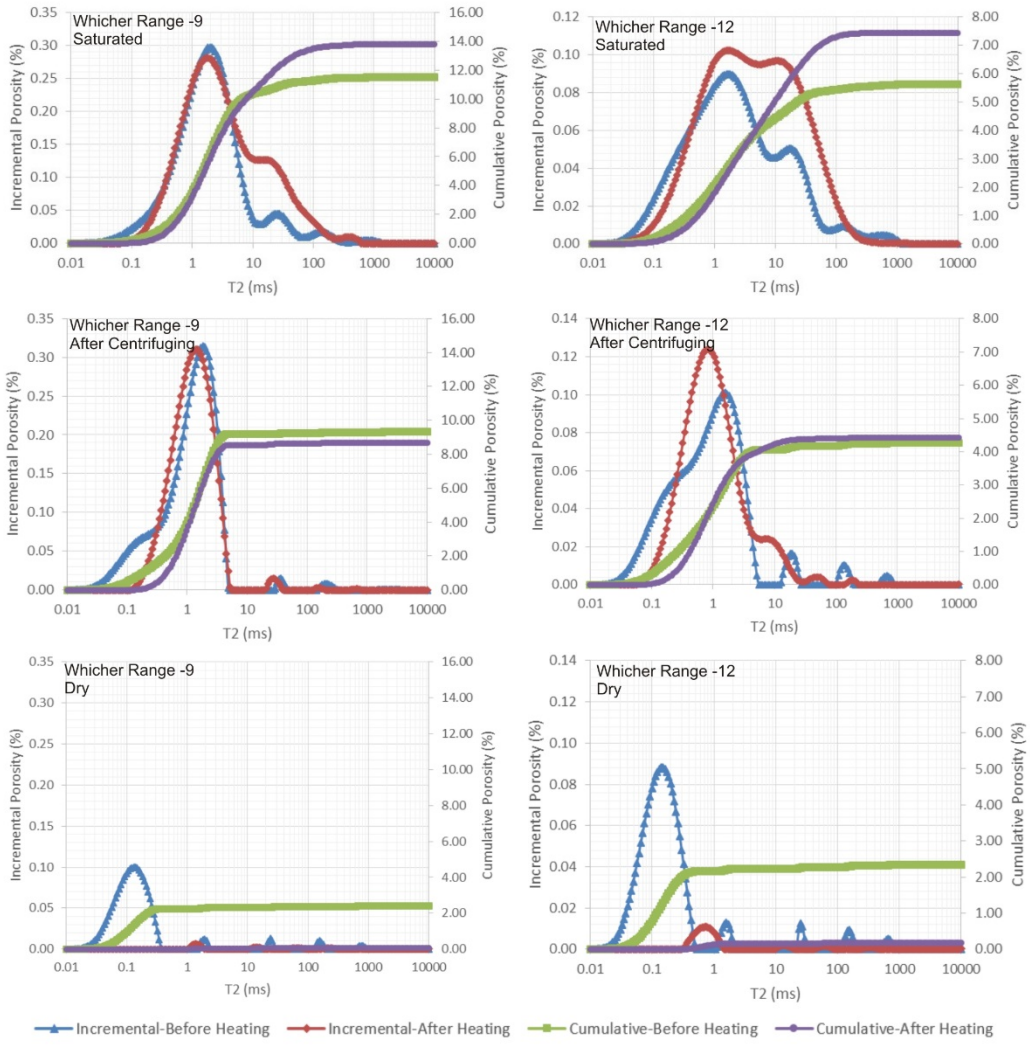

Figure 3-6 Whicher Range-09 and Whicher Range-12 NMR spectrums in three different saturations. Due to high capillary pressure, the centrifuge failed to remove much water from the samples. The NMR test on the dry samples indicates that the water in the samples, both free water and bound water, can be effectively removed by heating (disappearance and reduction of the peaks).

3.2.2 Texture and Structure

Micro-fractures, which are induced by differential stresses, are small cracks with high aspect ratio (Anders et al., 2014). In this study, the micro-fractures are generated from thermal stress due to various thermal expansions of minerals and uneven temperature distribution. The grains in the tight sandstones have different thermos-elastic moduli and thermal conductivities. As a result, when exposed to high temperature, these grains have different thermal expansions resulting in the intergranular micro-fractures (Kranz, 1983).

Sandstones are composed of grains, which are mainly quartz and feldspar, cements, which mainly consist of clay and pores filled with air when running CT scanning. In CT images, pores are identified by low CT numbers, while minerals are identified by high CT numbers (Yao et al., 2009).

As shown in Figure 3-7, the CT numbers of the samples studied decreased after heating but the degrees of decrease are different; from large to small: Whicher Range-12, Whicher Range-09, Whicher Range-08 and Whicher Range-06. This correlates with the increase tendency of porosity for these 4 samples.

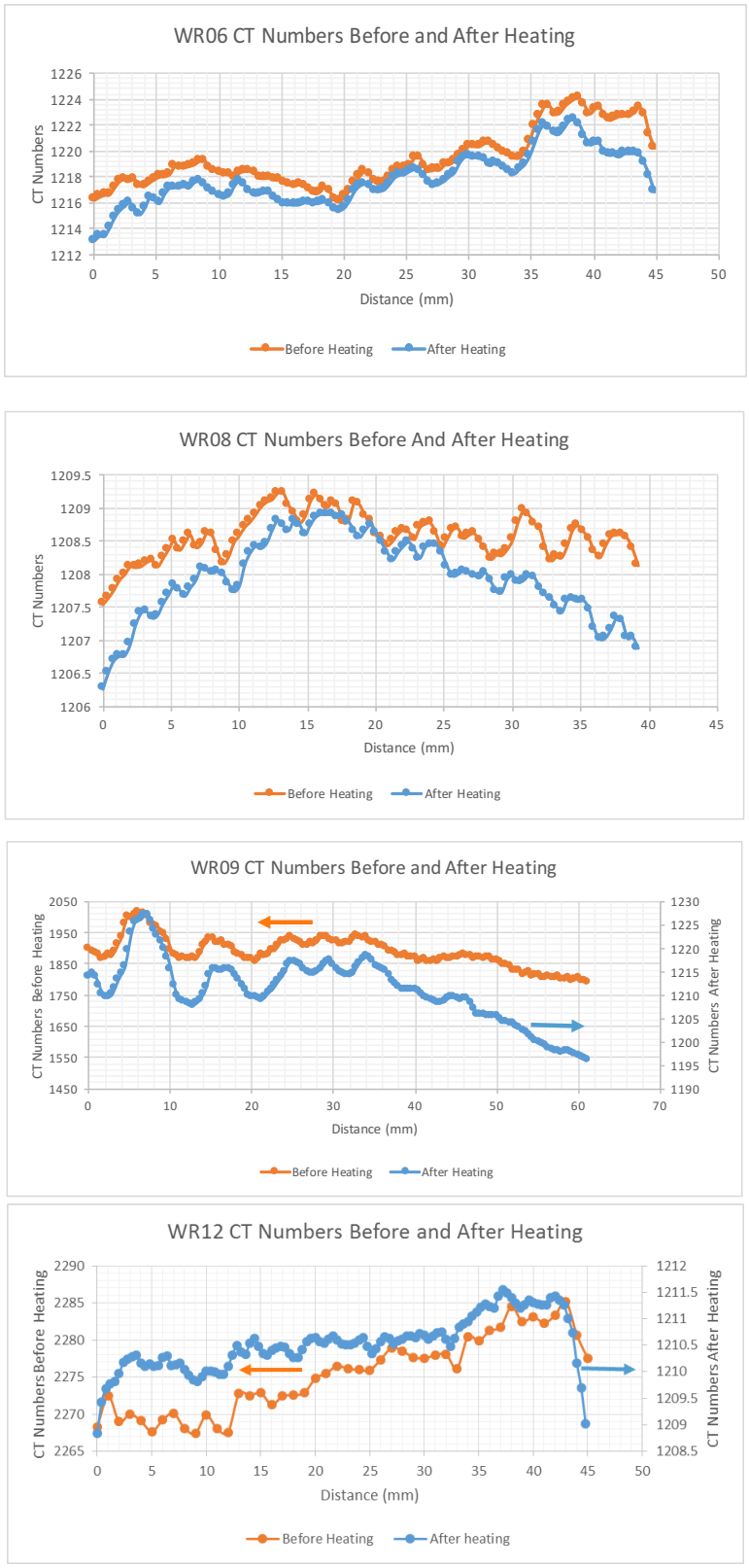

Figure 3-7 Comparisons of CT numbers before and after heating. High CT numbers represent low porosity, while low CT numbers represent high porosity. The distance is the measurement from one end of the core plug to another. The comparisons between the plugs before heating and after heating are made from the same scanning direction. The distances are smaller than the real sample length due to removal of low quality CT images.

In sample Whicher Range-12, for example, the porosity increased from 3.34% to 8.147% after heating; as such, it is ranked first in terms of porosity increase among four samples. The CT numbers decreased dramatically after heating, from around 2275 to 1210, especially the part close to the end of the sample.

Tight sandstone samples, Whicher Range-6 (Figure 3-8a), Whicher Range-8 (Figure 3-8), Whicher Range-9 (Figure 3-9a) are highly cemented and no fractures are observed in these samples with a magnification of 100. Small fractures along the grain boundaries appear in sample Whicher Range-12 (Figure 3-9i). The highly cemented grains are the major reasons for low porosity and permeability. Figure 3-8c, d and p show the micro-pores in the smectite cementation, while Figure 3-9i shows the micro-pores in the pore-filling kaolinite booklets.

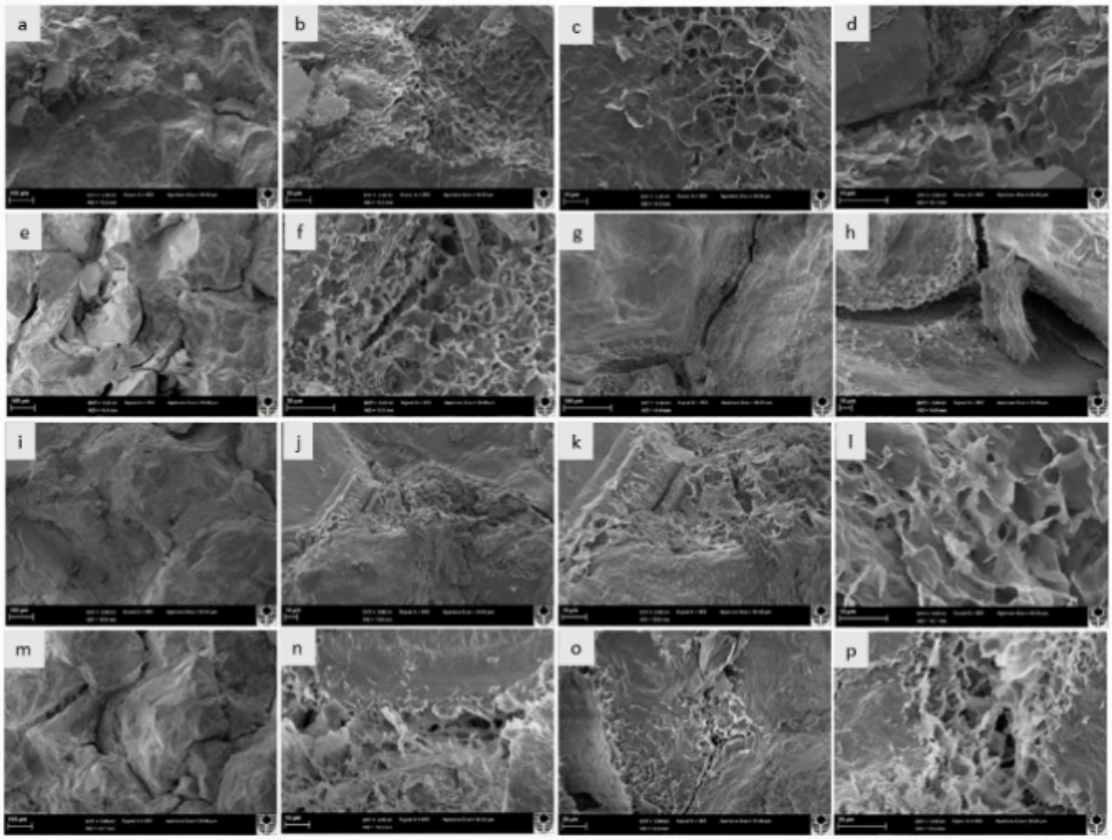

Figure 3-8 SEM images of samples Whicher Range-6 and Whicher Range-8 before and after heating (Figures a – d are from sample Whicher Range-6 before heating; Figures e – h are from sample Whicher Range-6 after heating at 600℃; Figures i – l are from Whicher Range--8 before heating; Figures m – p are from Whicher Range--8 after heating at 600℃).

After heating, fractures in all the samples are widely observed in low and high magnifications. In Figure 3-8e, m and Figure 3-9e, m, at a relatively low magnification, grains attach to each other loosely due to the creation of fractures. Besides, the numbers and widths of the fractures have increased when compared to the samples before heating, which leads to the rise of porosity and permeability.

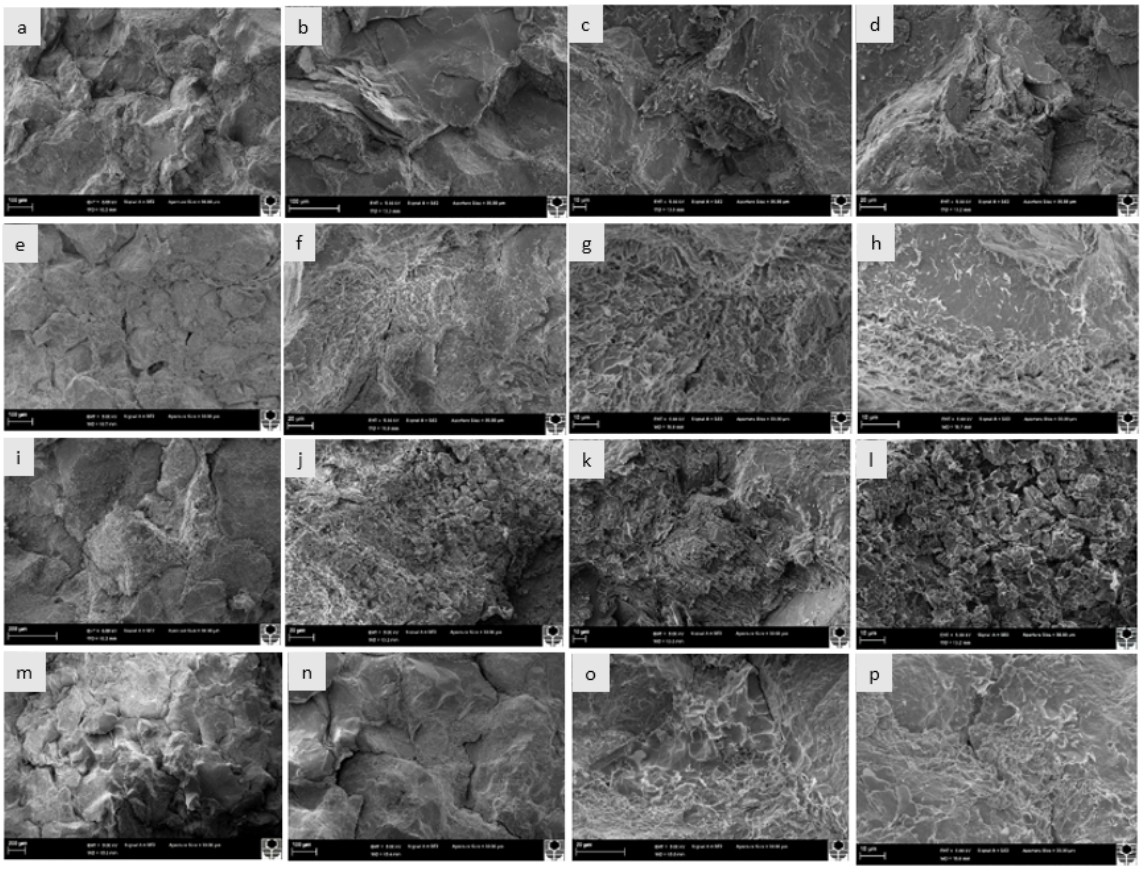

Figure 3-9 SEM images of samples Whicher Range-9 and Whicher Range-12 before and after heating (Figures a – d are from sample Whicher Range-9 before heating; Figures e – h are from sample Whicher Range-9 after heating at 600℃; Figures i – l are from Whicher Range--12 before heating; Figures m – p are from Whicher Range--12 after heating at 600℃).

The investigation of the thin sections of these heated samples indicates that the grains are fractured due to high temperature heating. As shown in Figure 3-10, sample Whicher Range-1 is sub-mature siltstone with angular grains. Majority of the grains are quartz and mica flakes; most of which are biotite, which can be observed between quartz grains. A handful of feldspar is present in the visual field, while the clay minerals cannot be identified. According to this sample, the reservoir quality is poor. Sample Whicher Range--6 shows a higher maturity with sub-rounded to rounded

grains and poor sorting. In terms of mineralogy, Quartz dominates in the sample and microcline, orthoclase and plagioclase are observed as well. It is worth to note that the microcline has a typical crosshatched twinning and the plagioclase shows simple carlsbad twinning or multiple twinning, while the orthoclase has no twinning but is cloudy and brownish. In addition to the single crystals of quartz, there are also polycrystalline quartz grains.

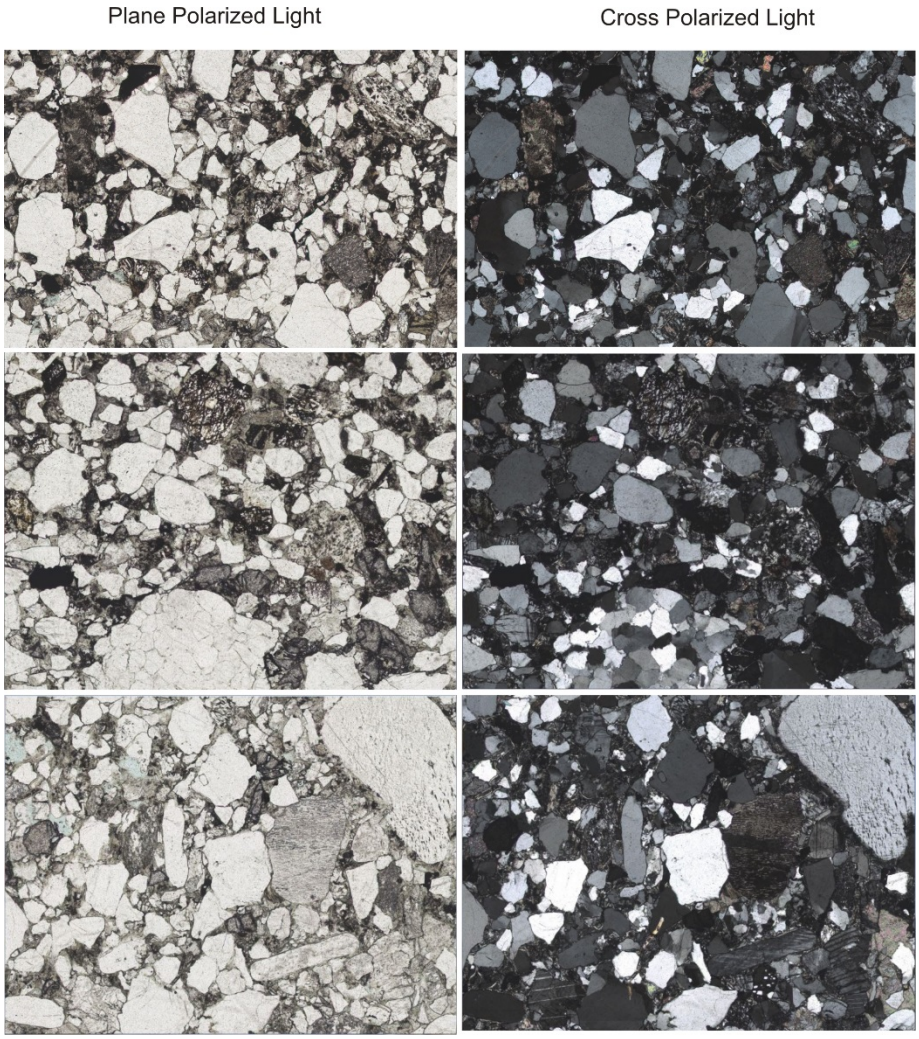

Figure 3-10 Micrographs of sample Whicher Range--6 under Plane Polarized Light (PPL) and Cross-Polarized Light (XPL). The grain size is coarse and the sorting is poor. The most abundant minerals are quartz and feldspar. Most of the quartz grains are clean and free of fractures.

As shown in Figure 3-11, fractures are widely spotted in the grains of quartz, the most abundant minerals in these samples. The distributions of fractures are dense and complex. The color of the cement turns into brown and fractures can also be spotted in the cements. All these changes indicate that there might be extra pore space created

during heating. However, the grains are less fractured in sample Whicher Range-12, compared with the other three samples, while the increase of porosity and permeability of Whicher Range-12 are higher. Therefore, the fractures in cements play a more important role in the improvement of reservoir quality than the fractures in grains.

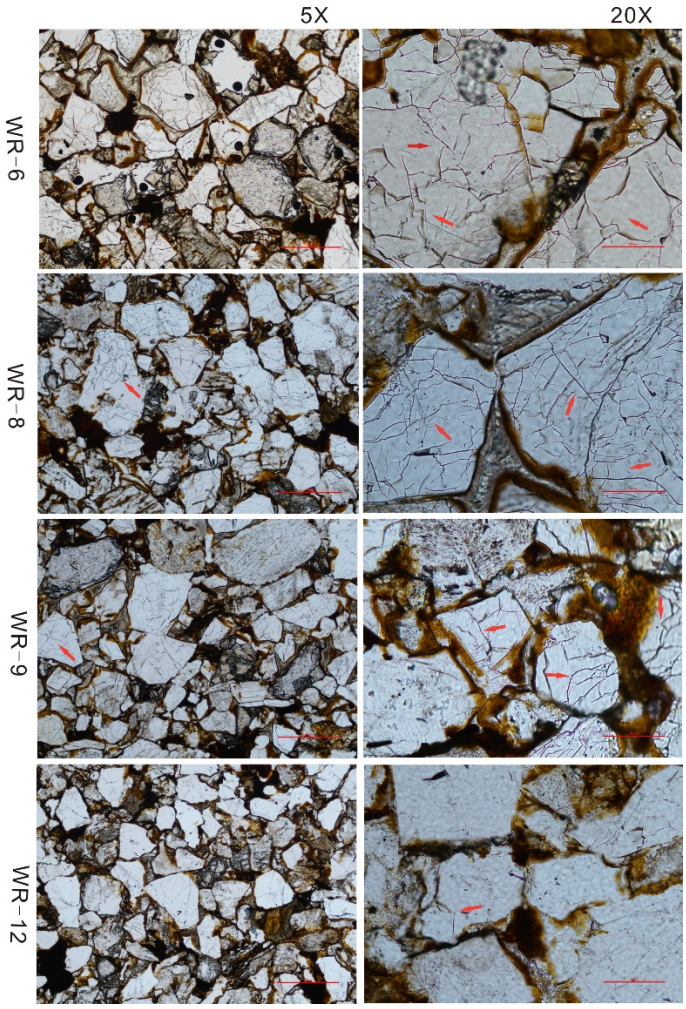

Figure 3-11 Thin section images of Whicher Range-6, Whicher Range-8, Whicher Range-9 and Whicher Range-12 after heating. The left column shows the thin section at low magnification (5X objective lens), the right column is at high magnification (20X objective lens). Fractures are widely observed in samples Whicher Range-6, Whicher Range-8 and Whicher Range-9, while the fractures are less in sample Whicher Range-12.

3.2.3 Changes of Compositions

The composition of samples has been investigated with XRD. By plotting the XRD spectrum of samples before and after heating together, the peak height, width and position are compared.

Quartz is the most abundant mineral in these tight sandstone samples and its peak height reduced after heating, as reflected in the XRD. In the sample before heating, calcite is found in the sample; however, after heating, the peak of calcite disappears. Calcite in the sandstone cements the grains and reduces the porosity and permeability. When treated with high temperature, the calcite decomposes to CaO, thus releasing some pore spaces and increasing the porosity and permeability (Figure 3-12). The peaks of kaolinite and dickite disappear after heating (Figure 3-13, Figure 3-14 and Figure 3-15). It is shown that the swelling clay mineral, montmorillonite, became amorphous during heating (Figure 3-14). This is positive to the reservoir quality because the swelling clays can block the pore throats when in contact with water of low salinity. It has been proven that the thermal method is effective in removing such swelling clays and the formation damages caused by them.

Based on the XRD spectra graphs in Figure 3-14 and Figure 3-15, it seems that illite has been formed after heating in sample Whicher Range-9 and Whicher Range-12. Illite can be transformed from dickite, smectite at high temperature; it can also be generated from K-feldspar and kaolinite reaction (Allen, P.A. and Allen, 2013).

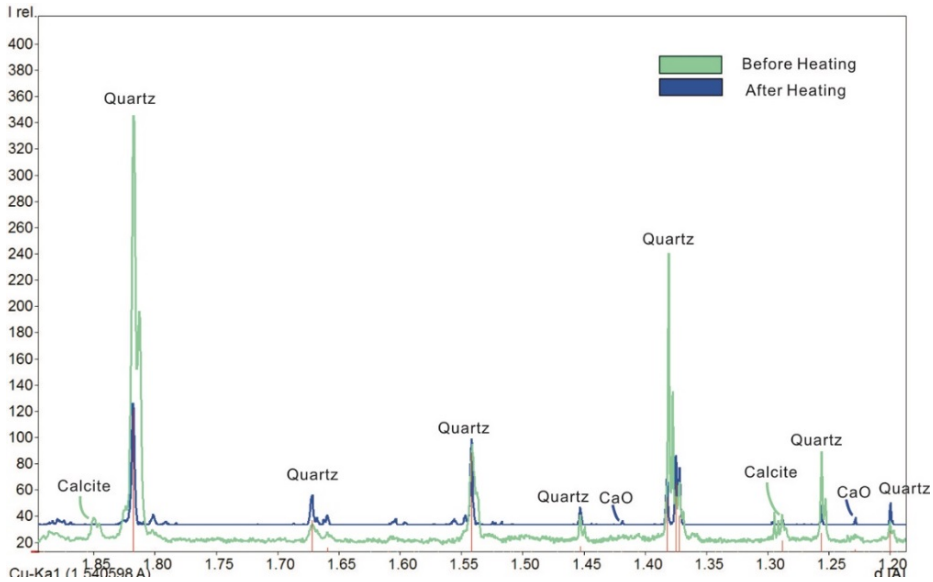

Figure 3-12 XRD pattern of Whicher Range-6 before and after heating at 600°C. Peak height of quartz in the sample decreased due to heating. Calcite has been found before heating, but its peak disappeared after heating. Instead, CaO, which is possibly the product of degradation of Calcite, appeared after heating.

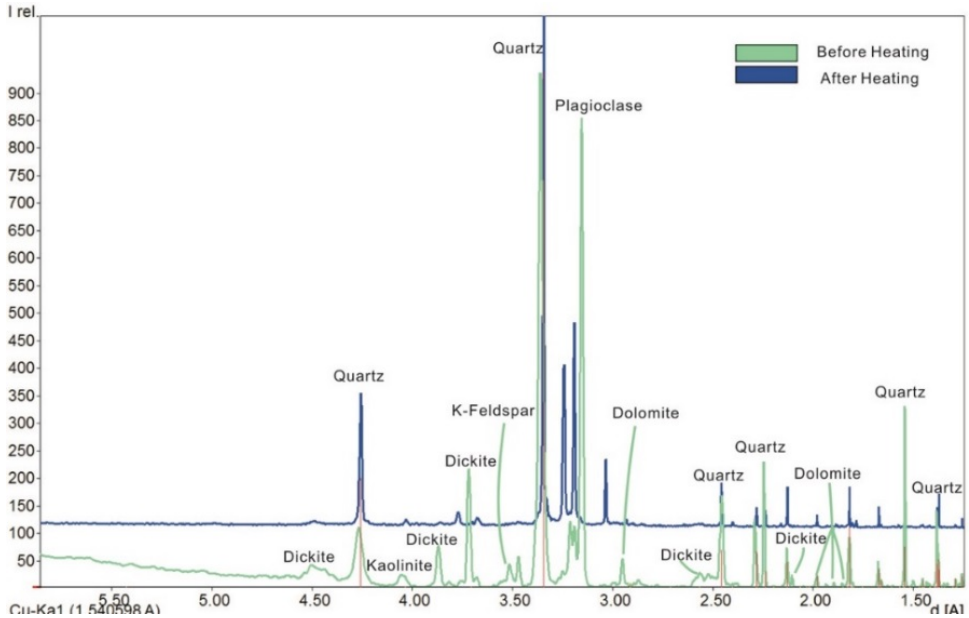

Figure 3-13 XRD pattern of Whicher Range-8 before and after heating at 600°C. Dolomite, dickite, plagioclase and K-feldspar disappeared after heating. The peak height of quartz decreased after heating.

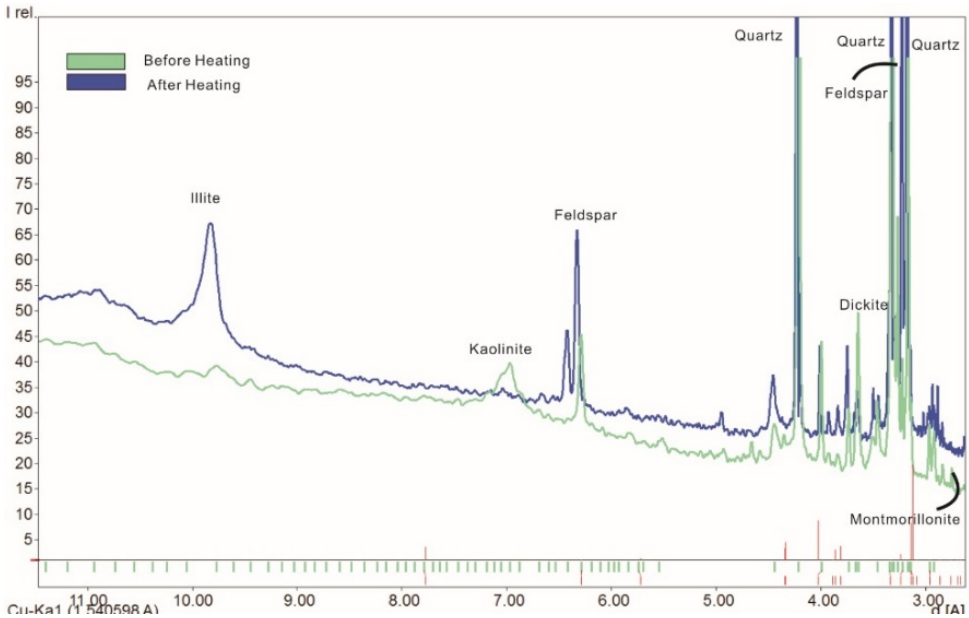

Figure 3-14 XRD pattern of Whicher Range-9 before and after heating at 600°C. The peaks of kaolinite, dickite and montmorillonite disappeared after heating while illite appeared after heating.

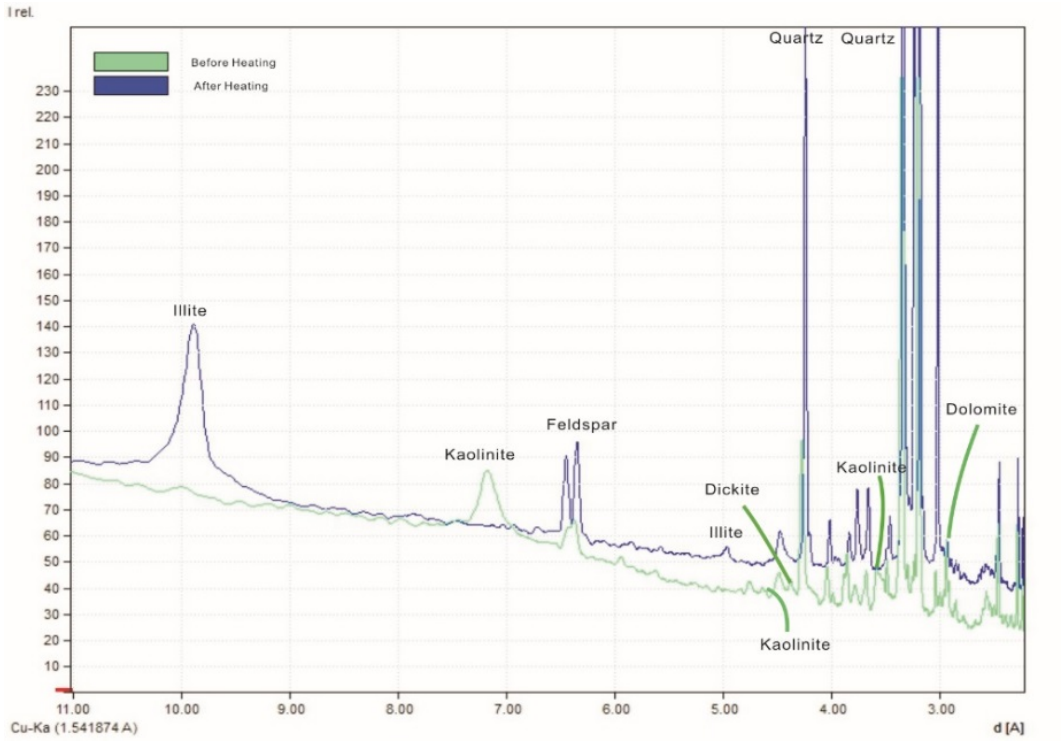

Figure 3-15 XRD pattern of Whicher Range-12 before and after heating at 600°C. The illite was found after heating in this sample, at the same time, peaks of kaolinite, dolomite and dickite disappeared. The peak height of feldspar was observed decreased.

3.3 Laboratory Microwave Heating

3.3.1 Reservoir Quality and Pore Size Distribution

The thermal method is effective in improving both porosity and permeability. The traditional Formation Heat Treatment (FHT) indicates that the porosity and permeability increased many folds in the near wellbore area and brought about great economical potential. Instead of utilizing electric heating or gas combustion, we used the microwave as the heat source. As shown in Figure 3-16, the reservoir quality of all-involved core plugs was enhanced. The porosity increased by 15.6%, 50.8%, 6.8% and 14.2% respectively for sample Erregulla-2, Whicher Range-1, Whicher Range-11 and Whicher Range-14, while the permeability had a greater growth of 238.5%, 728.6%, 315.2% and 464.0% respectively. Furthermore, the slight change in porosity leads to a large improvement in permeability, and the configuration of pore sizes is one factor that needs to be closely investigated.

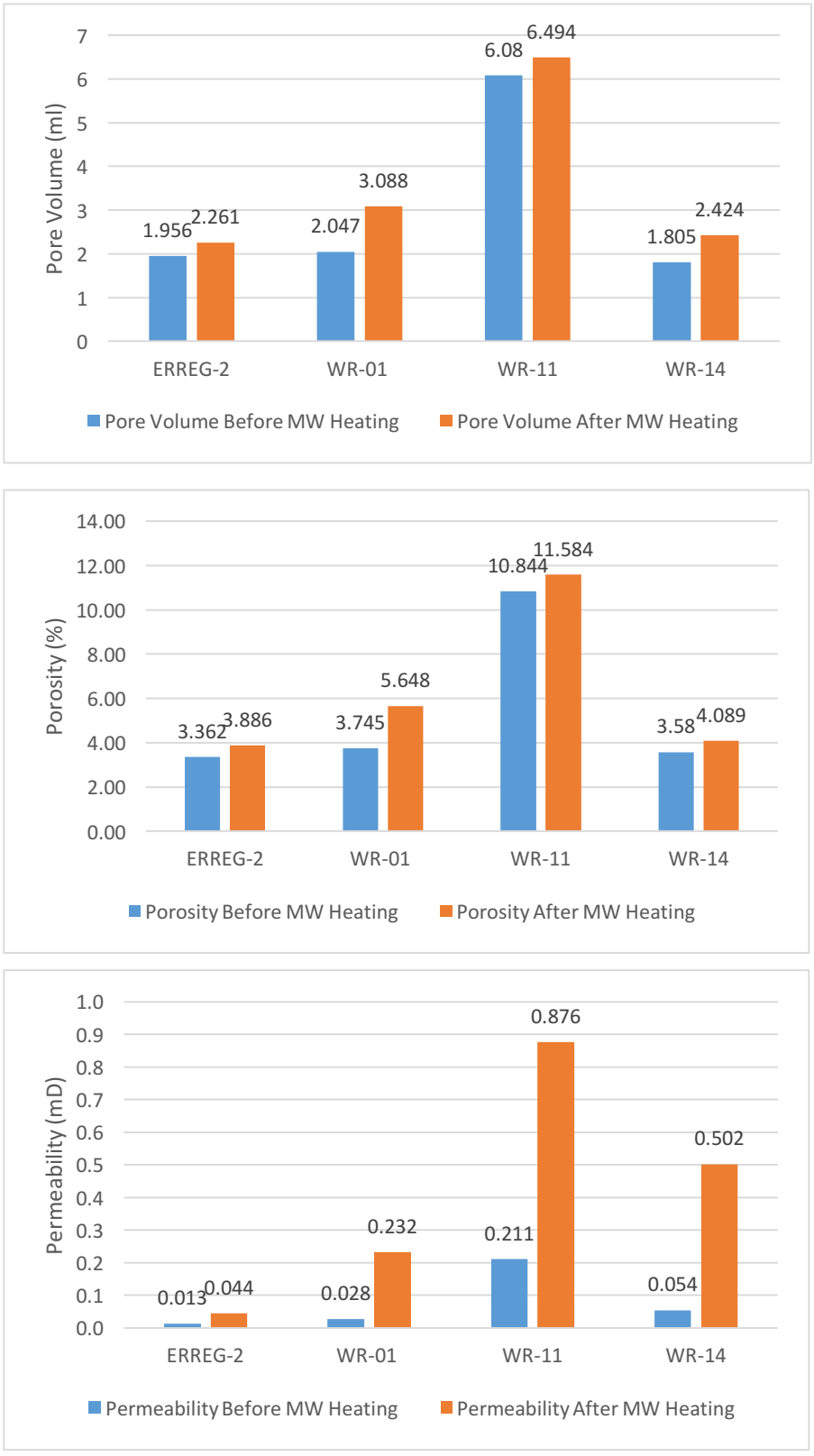

Figure 3-16 Comparison of pore volume, porosity and permeability before and after MW heating. The bulk volumes have no change while the pore volumes have a slight to moderate increase. As a result, the porosity and permeability have been improved after heating.

The encouraging findings are shown in Figure 3-17. As the tight sandstone samples have been 100% saturated before and after the NMR experiments, the area under the T2 curve from 1 to 100ms demonstrated an obvious increased porosity of the heated samples. In sample Erregulla-2, the population of medium and large pores had a slight growth after undergoing heating with the microwave; however, the amplitude decreased at around 0.1ms and between 1 and 10ms. Similarly, the population of pores, with T2 ranging from 0.1 to 0.3ms, decreased in sample Whicher Range-1, while it increased for medium and large pores, with T2 ranging from 0.6 to 30ms.

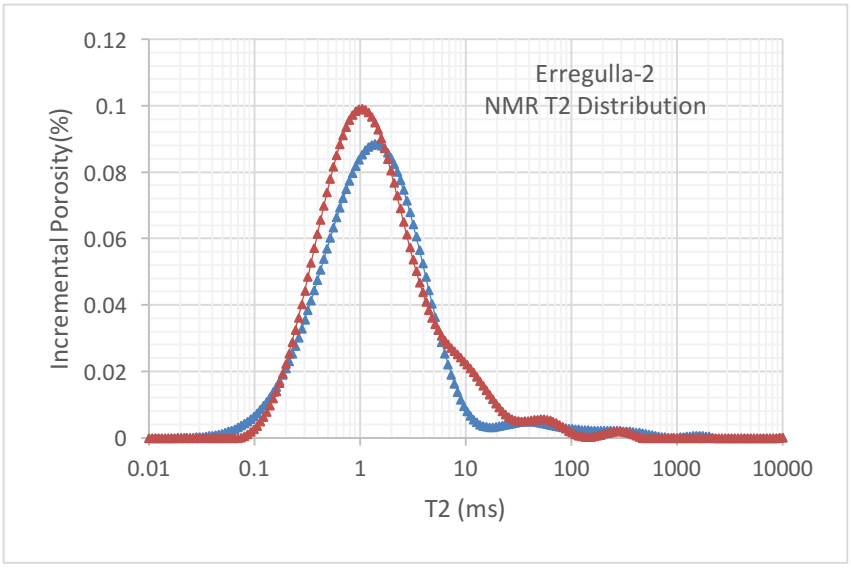

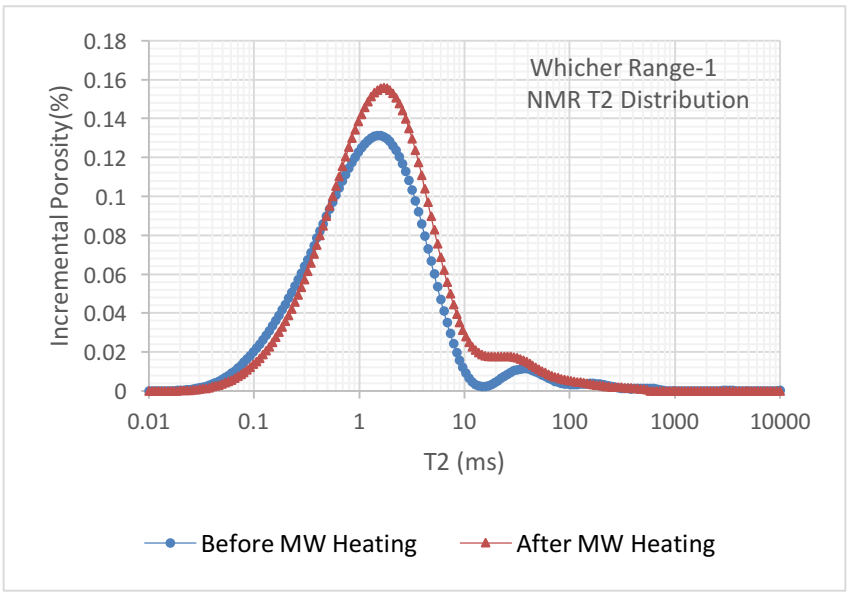

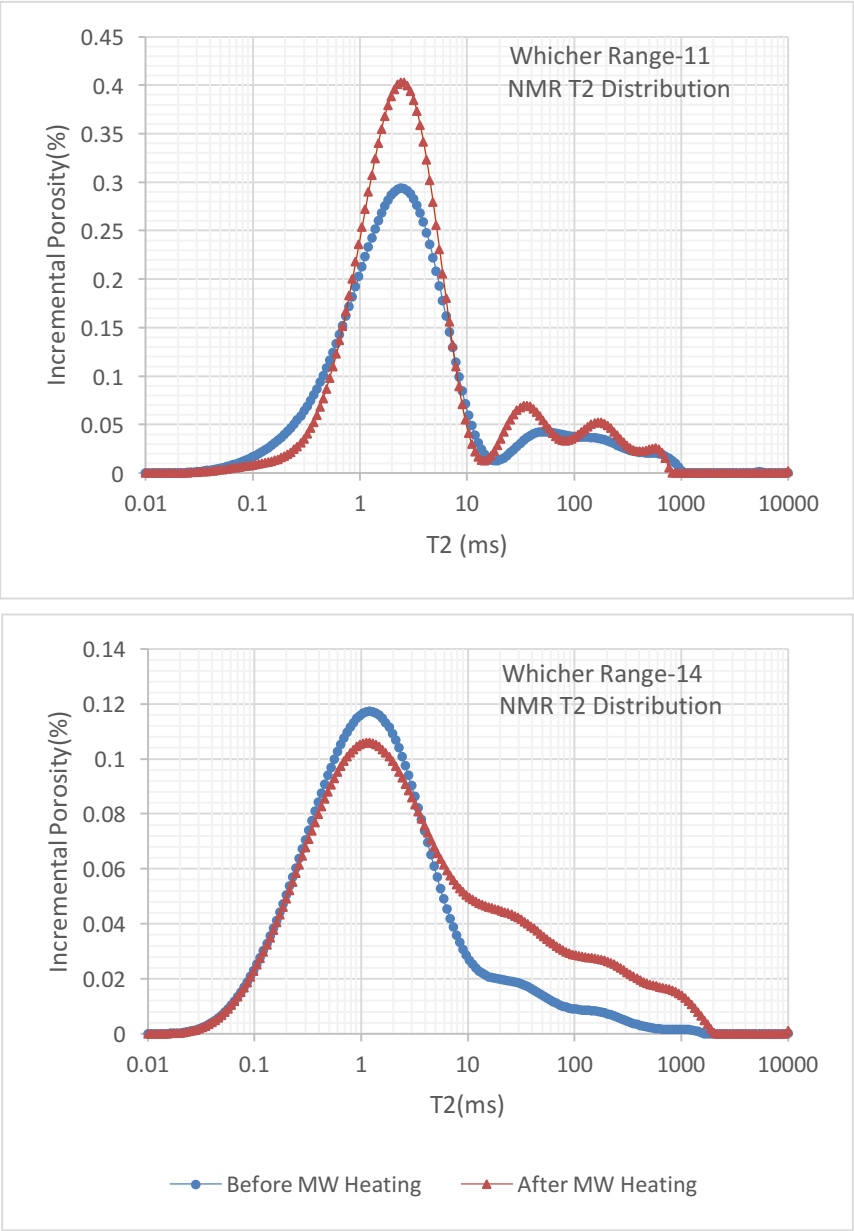

Figure 3-17 Comparisons of the NMR experimental results of 4 tight sandstone samples. The fraction of relative small pores of all samples decreased slightly. The fraction of medium pore size of sample Erregulla-2, Whicher Range-1 and Whicher Range-11 increased, while that of Whicher Range-14 decreased. However, the fraction of relative large pore size increased drastically.

3.3.2 The Effects of Microwave Heating on Tight Sandstone Structures

The presence of clay minerals affects the reservoir quality significantly. In this study, similar to conventional heating, the micro-fractures are generated due to thermal stress or differential thermal expansion. Differently, the electric properties of different

minerals will affect the temperature distribution thus the thermal stress in the samples heated by microwave.

As shown in Figure 3-18, in general, the CT numbers of four samples, Erregulla-2, Whicher Range-1, Whicher Range-11 and Whicher Range-14, dropped after heating, but the dropping degrees are different from sample to sample. In most of the samples, even the variations within the samples are not homogeneous throughout.

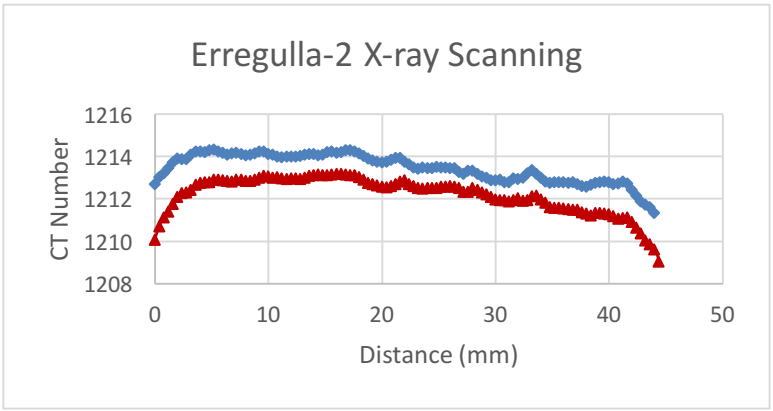

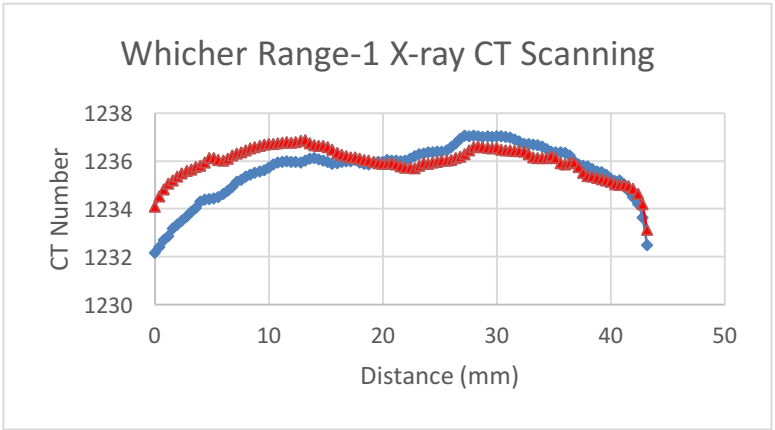

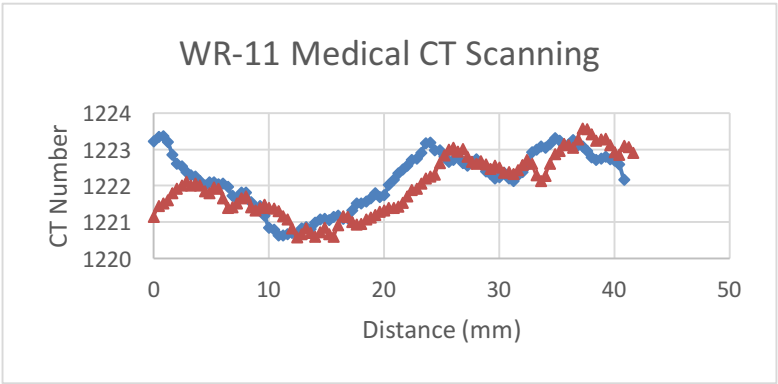

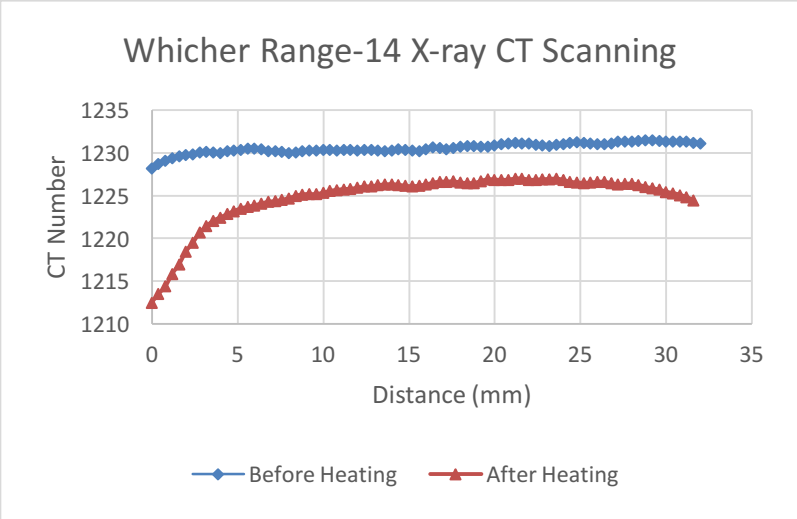

Figure 3-18 Comparisons of CT numbers before and after heating (High CT numbers represent low porosity, while low CT numbers represent high porosity. After MW heating, the CT numbers, which are calculated in the same software, are found decreased in all the samples).

It is obvious that the CT numbers reduced after microwave heating. In detail, for sample Erregulla-2, the porosity increases are homogeneous throughout the sample, because the X-ray CT profiles are parallel with each other and the CT number decreased. Similarly, overall porosity improvement is observed in sample Whicher Range-14, and there is greater porosity improvement (CT number decreases) at one end of the core plug. By investigating the X-ray CT images of Whicher Range-1 (Figure 3-19) and Whicher Range-14 (Figure 3-20), we found that the fractures generate inside the core plugs after heating. In sample Whicher Range 14, visible fracture from one end of the sample extended across the length within its internal body. In addition, the maximum fracture length is almost as long as the diameter, which accounts for the great enhancement of porosity.

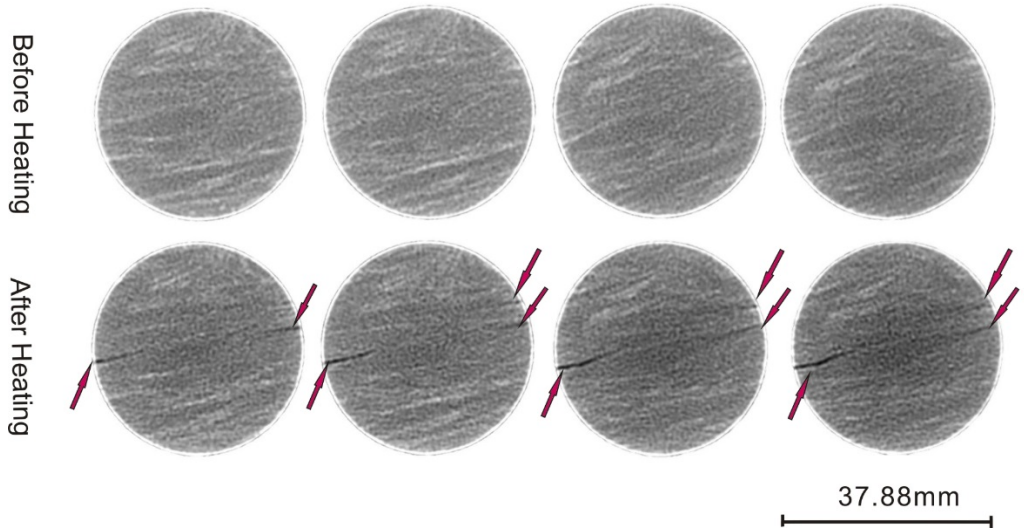

Figure 3-19 The X-ray CT scanning images of sample Whicher Range-1 before (Upper) and after (Lower) MW heating. These cross section images are taken from the same position of the core plug before and after heating to demonstrate the presence of fractures due to microwave heating. The red arrows indicate the positions of the fractures.

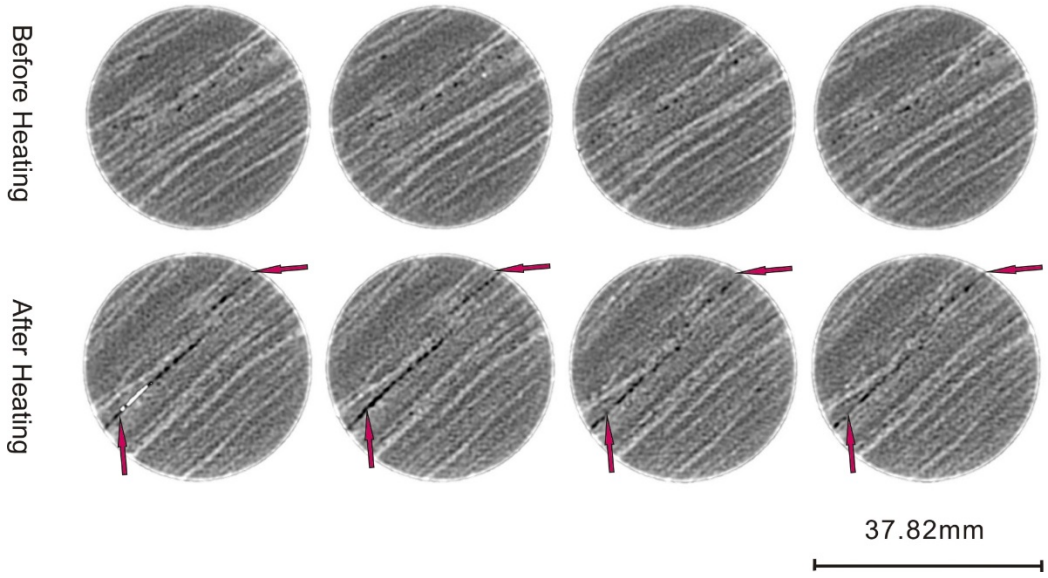

Figure 3-20 The X-ray CT scanning images of sample Whicher Range-14 before (Upper) and after (Lower) MW heating. These cross section images are taken from the same position of the core plug before and after heating to demonstrate the presence of fractures due to microwave heating. The red arrows indicate the positions of the fractures.

The microstructures have been investigated with the SEM technique at different magnifications in the samples before and after heating. The morphology of the fractures and mineralogy are closely examined to reveal the effects of microwave

heating on tight sandstones. The fractures in the sandstone are influenced by minerals, textures and microstructures of the samples, and the distribution of internal micro defect and nucleation. Based on different fracture morphology characteristics, the fracture mechanisms will include the inter-granular fracture, trans-granular fracture, clay cement fracture and the coupled inter granular- trans-granular fracture (Xie et al., 1989; Zuo et al., 2007).

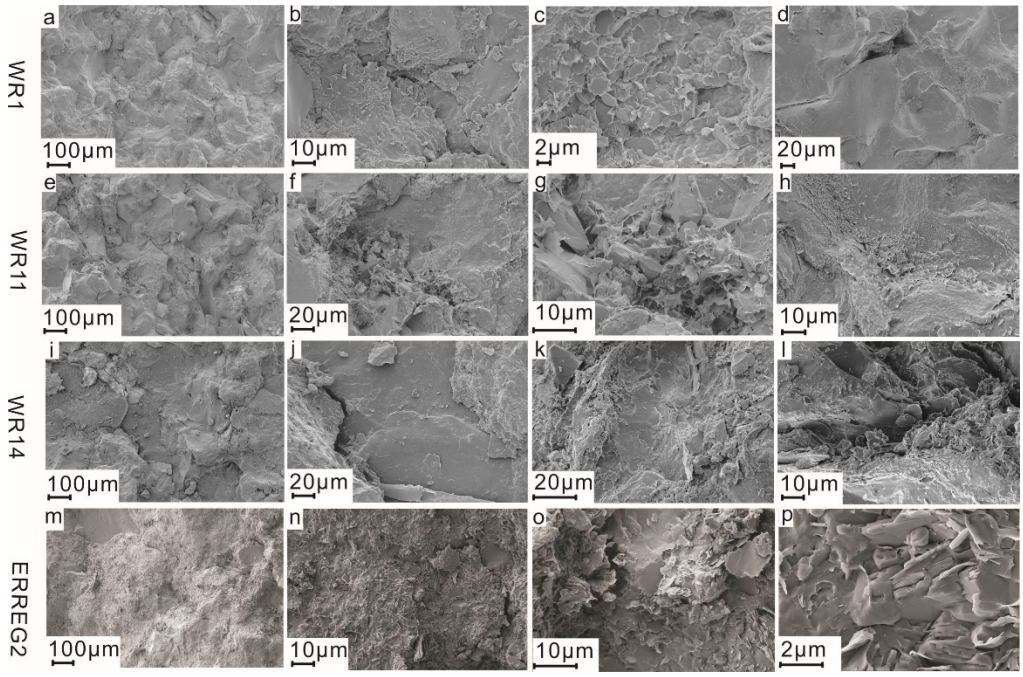

Figure 3-21 SEM images of samples before MW heating. Grains are attached to each other closely and fractures are hardly spotted in these images.

Before microwave heating, the tight sandstone samples, Whicher Range-1, Whicher Range-11, Whicher Range-14 and Erregulla-2, shown in Figure 3-21 are highly cemented and no fractures are observed in these samples with a magnification of 100. In terms of reservoir quality, all four samples are poor. Most of the samples contain quartz and some clay minerals can also be identified, as per the images (Figure 3-21-g, smectite; Figure 3-21-i, illite and Figure 3-21-p, kaolinite). After heating, fractures in all samples are widely observed in both low and high magnifications. In Figure 3-22, the fractures are visible at a relatively low magnification. Besides, the numbers and widths of the fractures are increased, compared with the respective samples before being heated. Fractures are observed along the boundaries of grains and in the

clay minerals. Combined with the NMR T2 distribution data (Figure 3-17), the presence of fractures accounted for the increased population of T2 larger than 10ms.

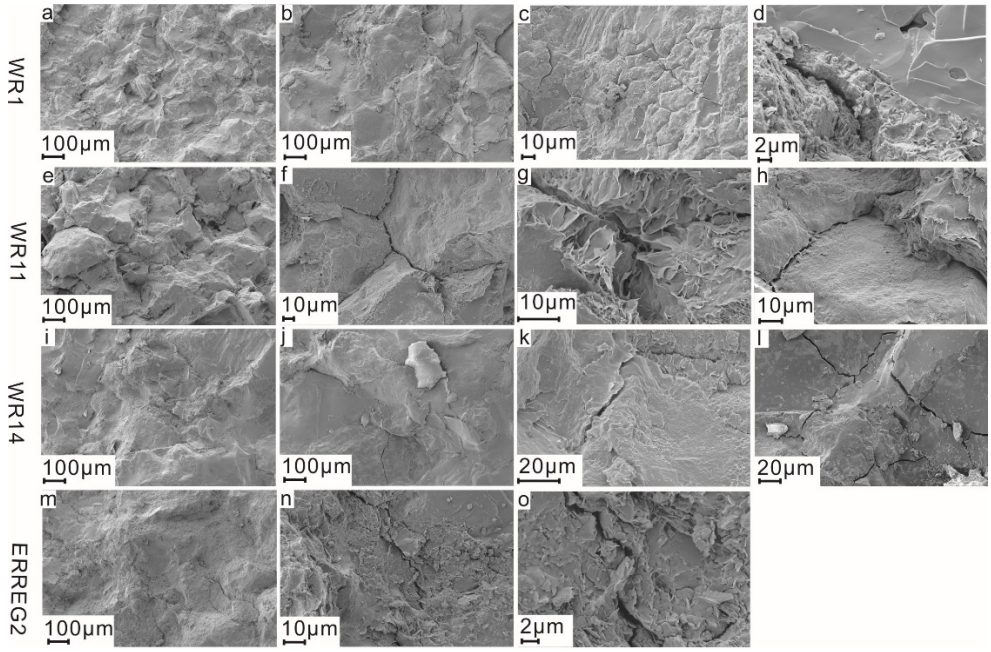

Figure 3-22 SEM images of the samples after MW heating. Fractures can be widely found in the samples after heating, f and h indicate the intergranular fractures, g indicates the fractures caused by clay shrinkage and l indicates the intergranular fractures.

The micrographs of sample Whicher Range-1 have been studied before and after heating. In Figure 3-23, the dominant minerals are quartz, feldspar and mica. The poor reservoir quality of the rock results from the poor sorting and good cementation. Few fractures can be found on the grains.

As indicated in Figure 3-24, there are fractures in the quartz grains, but the amount of fractures is less than that of samples which are heated by the traditional method. The color of cements is lighter than that in Figure 3-11. The fractures in the cements are difficult to recognize under low magnification, while some fractures can be identified in cements under higher magnification. In sample Whicher Range-1, there are some fractures in the cements but less fractures in the grains. It is demonstrated again that fractures in the cements are more important in improving permeability. This can also be used to explain that although the fractures in the grains after microwave heating are less widely observed than after traditional heating, both methods have similar effects on the permeability.

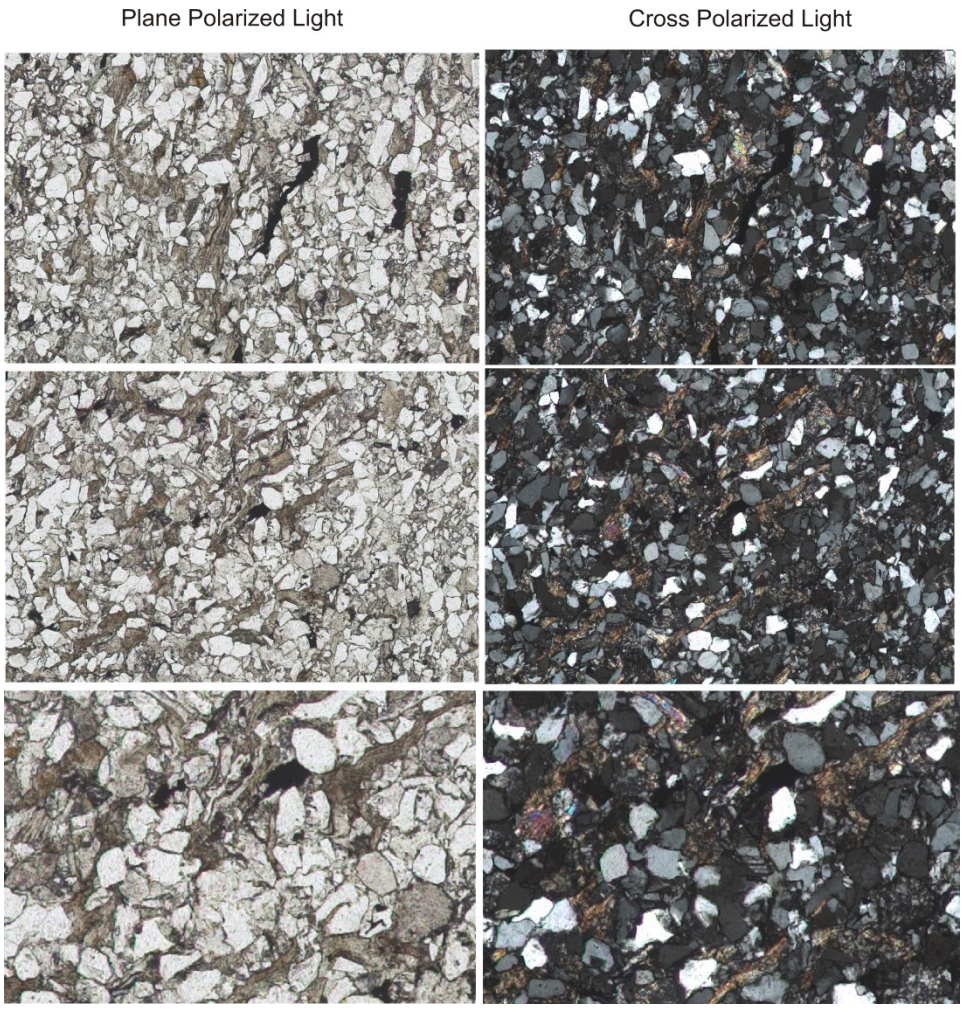

Figure 3-23 Micrographs of sample Whicher Range-01 before heating. Quartz, feldspar and mica are the dominant minerals. The roundness is sub-angular and the sorting is poor. Fractures are not observed in most of the grains.

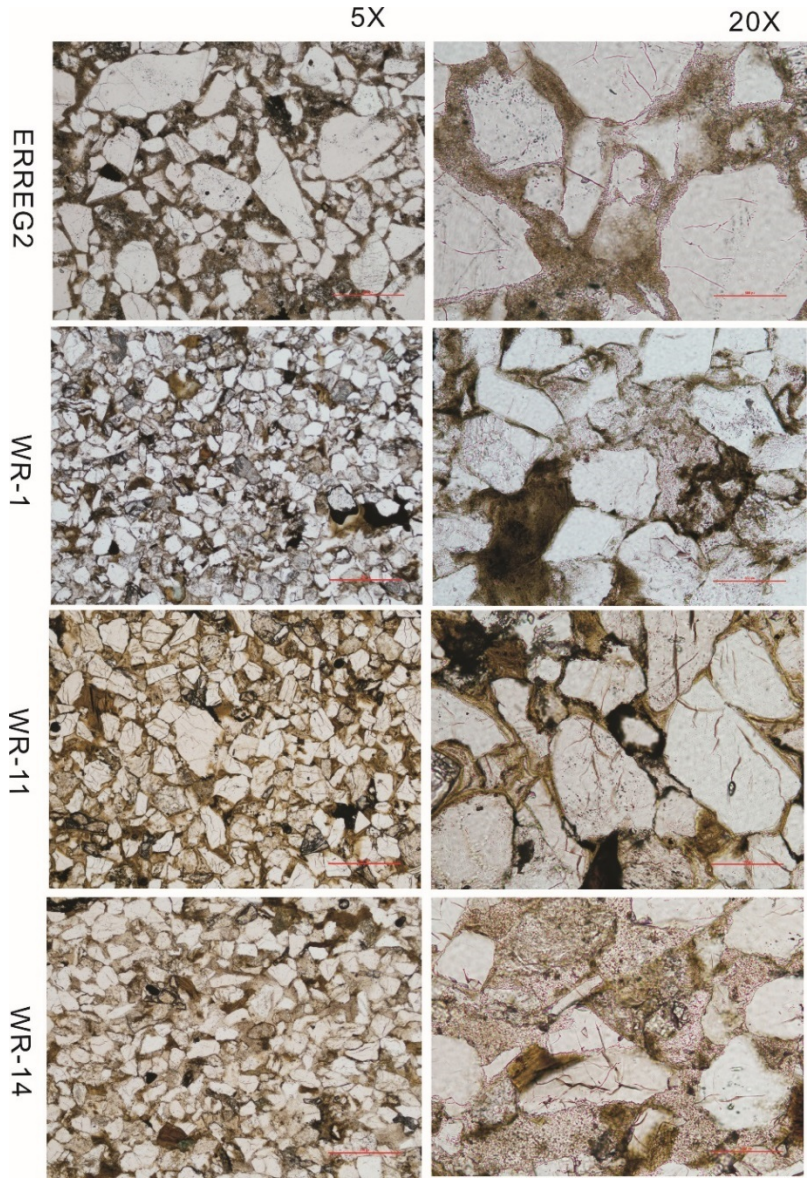

Figure 3-24 Thin section images of sample Erregulla-2, Whicher Range-1, Whicher Range-11 and Whicher Range-14 after MW heating. The left column shows the thin section at low magnification (5X objective lens), while the right column shows the thin section at high magnification (20X objective lens).

3.3.3 Changes of Tight Sandstone Compositions

Five tight sandstone plugs were heated with the microwave in the lab and XRD analysis was conducted on them. For the most abundant mineral, quartz, the microwave has no effect on it, because microwave is almost transparent in quartz and the temperature is not high enough to change quartz. As shown in Figure 3-25 (North Erregulla) and Figure 3-26 (West Erregulla), the peaks of kaolinite can be identified after heating (only a few peaks disappeared). By subjecting to microwave heating, the

crystalline of kaolinite is changed slightly. CaO is identified after the heating process in sample North Erregulla (Figure 3-25), Whicher Range-1 (Figure 3-27) and Whicher Range-11 (Figure 3-28), which indicates that the calcite or dolomite cements in the sample are degraded or decomposed by high temperatures. Since calcite may play a role of cementing grains in sandstone, the reservoir quality becomes poor when it is present in the sample. At the same time, the peaks of feldspar, which is another common cementing mineral, disappeared after heating. Finally, the structure changes in the montmorillonite group minerals, are shown by the decreased relative intensity in Figure 3-29.

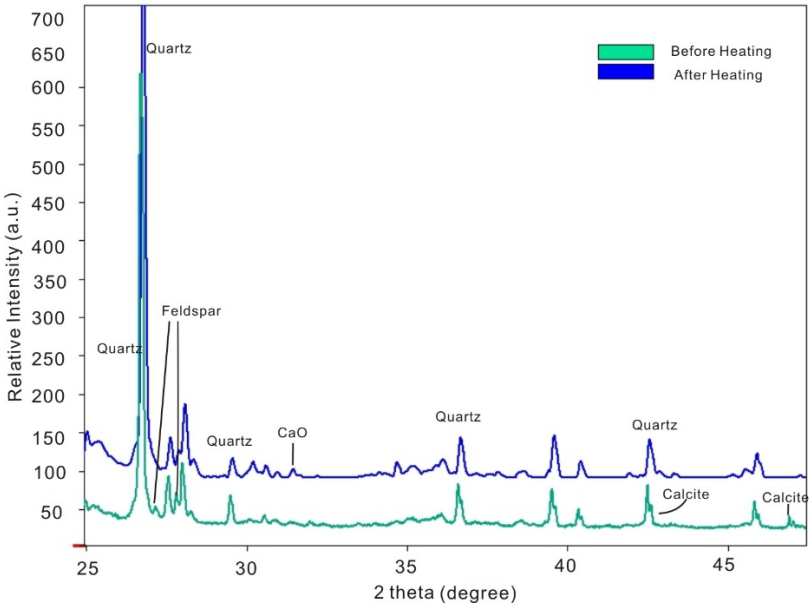

Figure 3-25 Comparison of XRD patterns of sample North Erregulla before and after MW heating. The degradation of Calcite to CaO is also found in this sample. The feldspar became amorphous after heating.

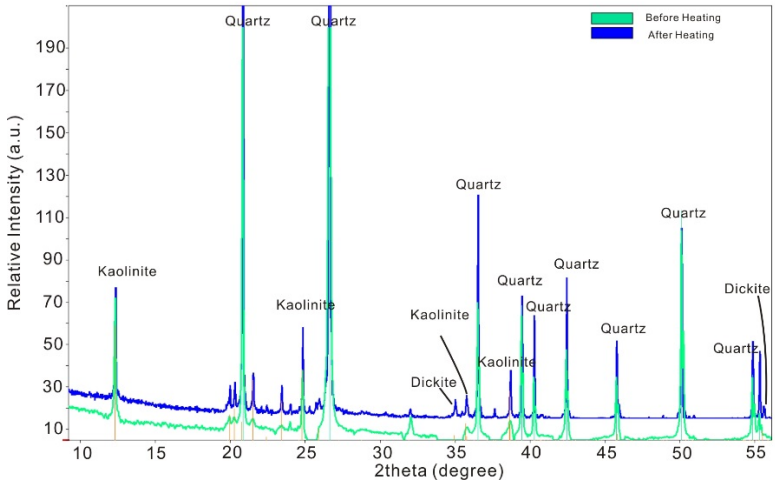

Figure 3-26 Comparison of XRD patterns of sample West Erregulla before and after MW heating. The minerals present in the sample are similar in pre-heating samples and post-heating samples. Quartz, kaolinite and dickite can be found in both samples, with only slight changes in some peaks.

The minerals, glauconite, mica, montmorillonite and feldspar, disappeared after heating (Figure 3-28 and Figure 3-29). Some of these minerals, like montmorillonite, can cause formation damages, and their disappearance is good for the reservoir quality.

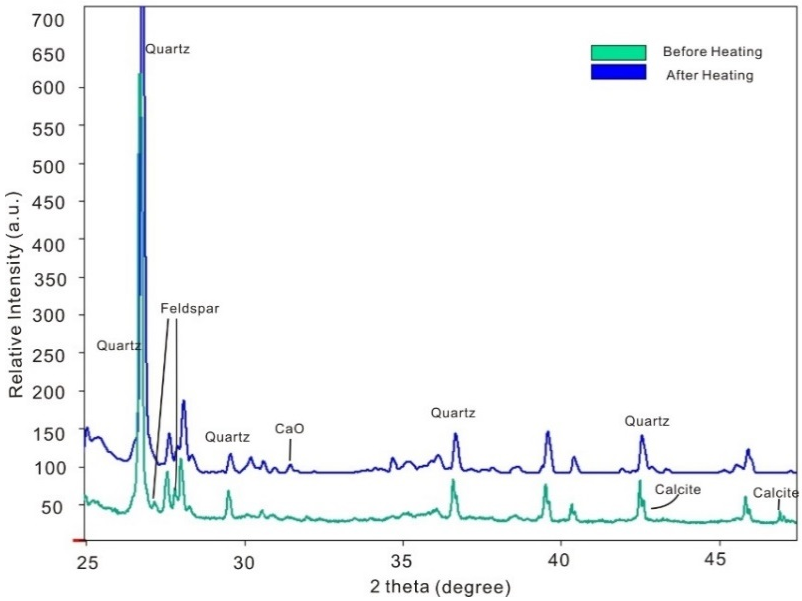

Figure 3-27 Comparison of XRD patterns of sample Whicher Range-1 before and after MW heating. It is found that the calcite degraded after heating, the possible product is CaO, which was only observed after heating.

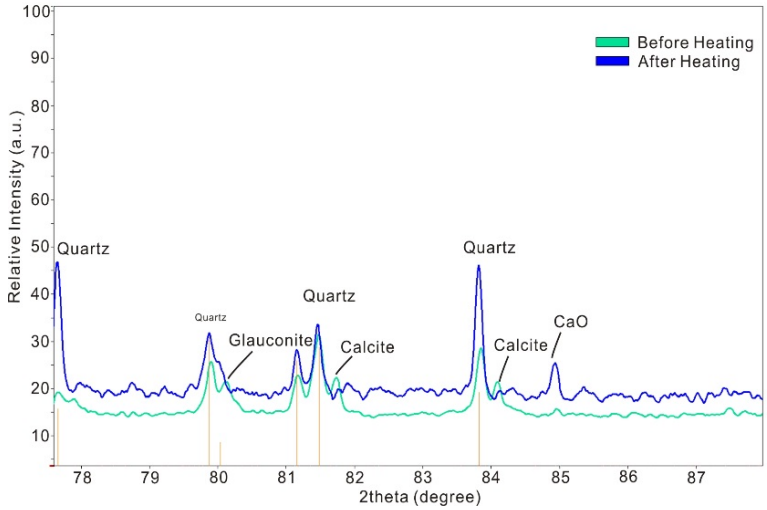

Figure 3-28 Comparison of XRD patterns of sample Whicher Range-11 before and after MW heating. The degradation of calcite to CaO is observed in this sample. Besides, the peak height of quartz increased after heating.

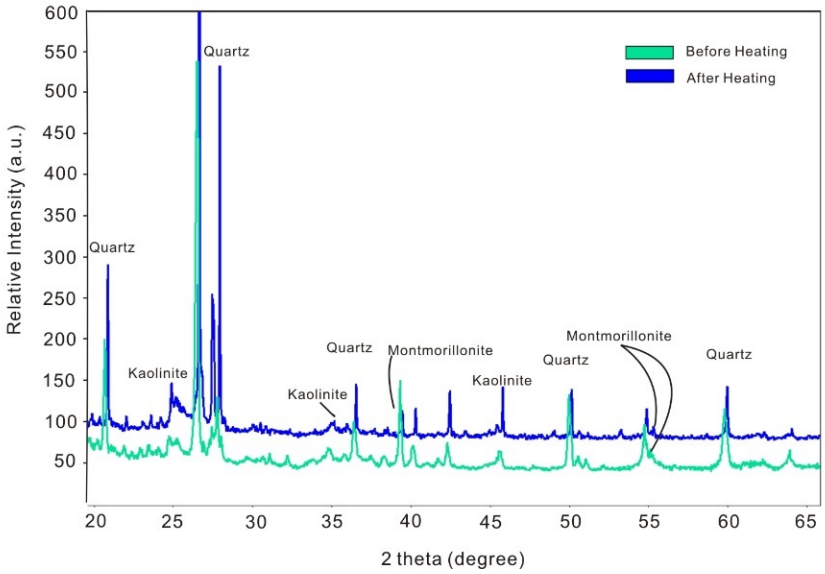

Figure 3-29 Comparison of XRD patterns of sample Whicher Range-14 before and after MW heating. The peak heights of quartz and montmorillonite decreased after heating. There was no change in kaolinite.

3.4 Numerical Simulation

3.4.1 Laboratory Microwave Heating

Electric field distributions are determined by the electrical properties of the sandstone samples. The relative permittivity and electrical conductivities of the tight sandstone core plugs have been measured at 2.45GHz in the lab and are used in numerical modeling. The electric field distributions for the sandstone plugs heated in the microwave oven are shown in Figure 3-30. The samples have the same properties, except for relative permittivity and electrical conductivity. The electric field in the oven distributes differently in all three cases.

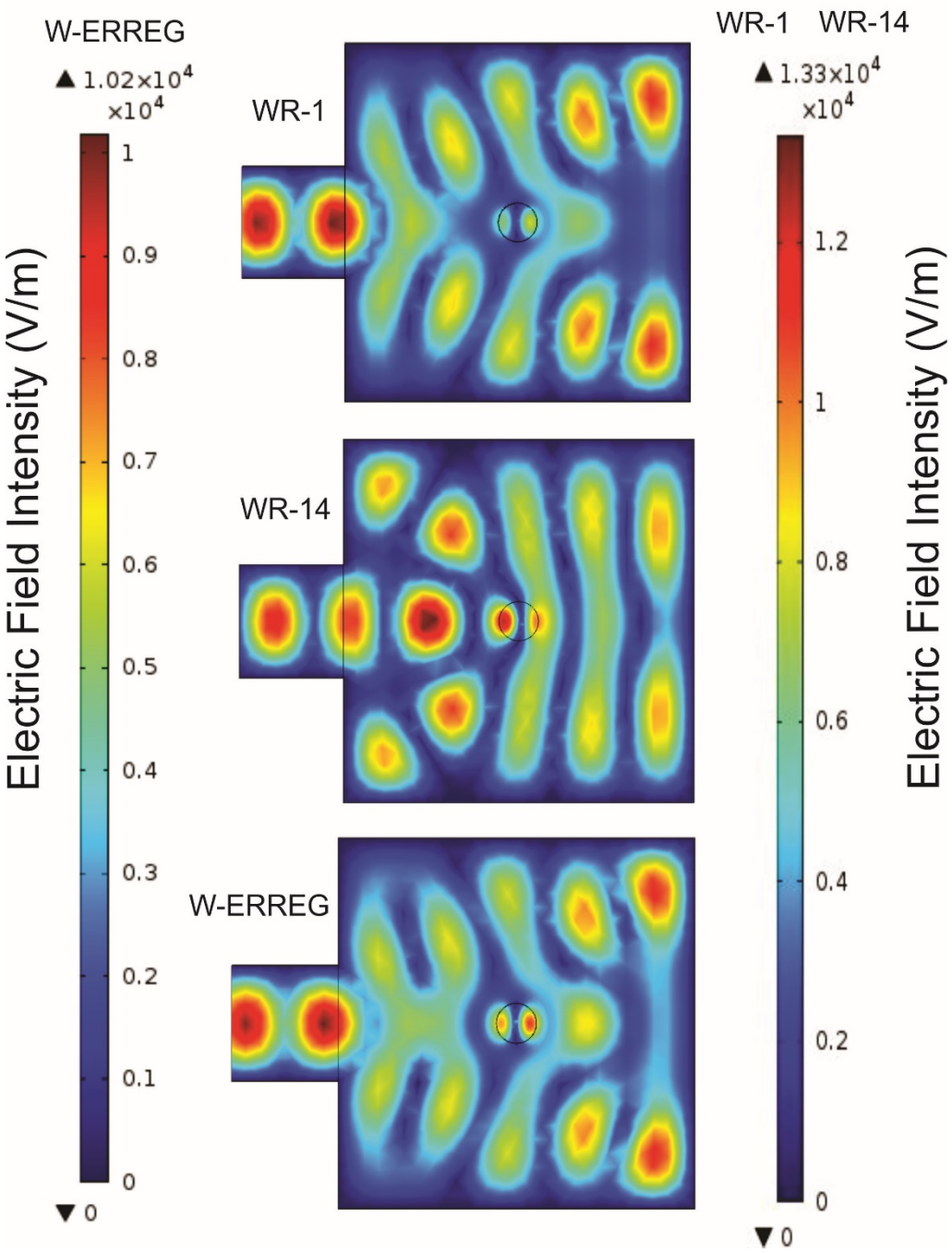

Figure 3-30 Electric field distribution in the numerical simulation (the unit is in V/m). It is observed that the intensity of electric field is greater in the waveguide (the smaller rectangular on the left). There are high intensity electric field in the core plugs which are of great significance to the heating rate.

More importantly, the electric field distributions in these core plugs vary from each other. Hence, temperature distributions show differences between them as well. In Figure 3-31, the differences in temperature distribution in the core plugs are in two points. First of all, the maximum temperatures are different in Whicher Range-1 (508°C), Whicher Range-11 (389°C) and West Erregulla (436°C). Secondly, the

positions of the maximum temperatures in the three samples vary with each other. The dielectric properties and electrical conductivity contribute to these differences by influencing the electric field distributions.

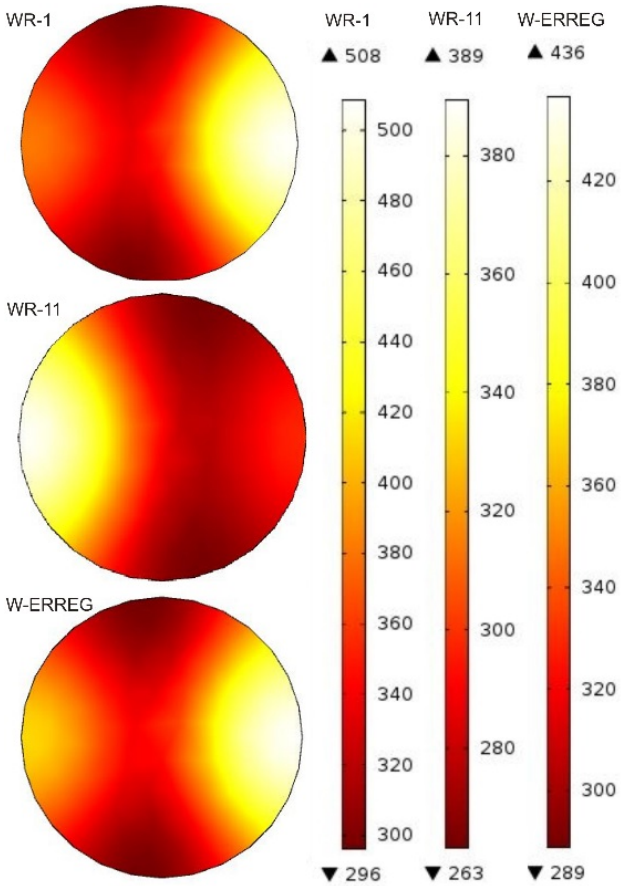

Figure 3-31 Temperature distribution in numerical modeling (the unit is in °C). Samples are put on the same position in the oven, and the parameters of the other parameters are the same except the properties of the core plugs. It is observed that the center of high temperature locates in different parts in three samples, and the value of the maximum temperatures are different either.

The tight sandstone plugs are heated with microwave in the lab and surface temperatures are recorded versus time. The simulated surface temperatures are plotted against time in the same coordinates. As indicated in Figure 3-32, the increase of surface temperature is nonlinear, both in simulation and in experiments, due to the complex mechanisms of microwave heating. The experimental data correlates well with the numerical modeling for the three tight sandstone samples WR-1, WR-11 and W-ERREG. The surface temperature reaches its maximum in 300s for WR-1 (500 °C), 480s for WR-11 (337 °C) and 360s for W-ERREG (409.8 °C).

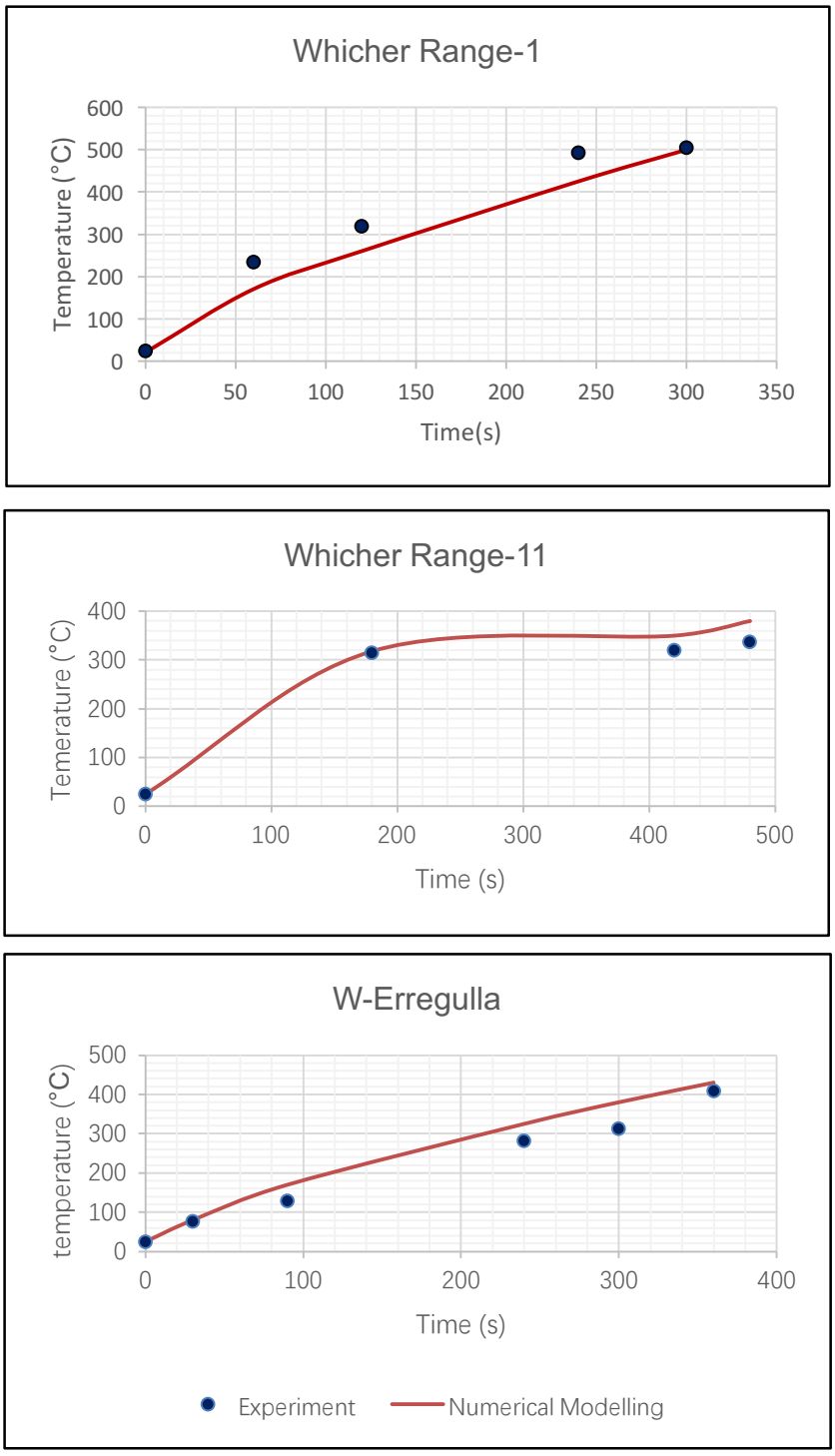

Figure 3-32 The temperature variations in sample Whicher Range-1, Whicher Range-11 and West Erregulla. Samples were heated for 300s to 480s, and their temperature changes were recorded against time. During this time, the temperatures increased with time, but the increasing rates are different from sample to sample.

3.4.2 Reservoir Microwave Heating

Reservoir simulations have been conducted to investigate the water invasion and FHT with microwave heating. In the ANSYS model, the electric field distribution and Joule heat generated in the reservoir are shown in Figure 3-33. The maximum electric field strength is 24692 V/m, and according to the engineering computation, the average dissipated power is 764 Watt and thus daily Joule heat generation is around 6.6×10^7 Joule. With increasing depth into the reservoir, the joule heat decreased. The maximum influenced depth reached about 10cm (Figure 3-34).

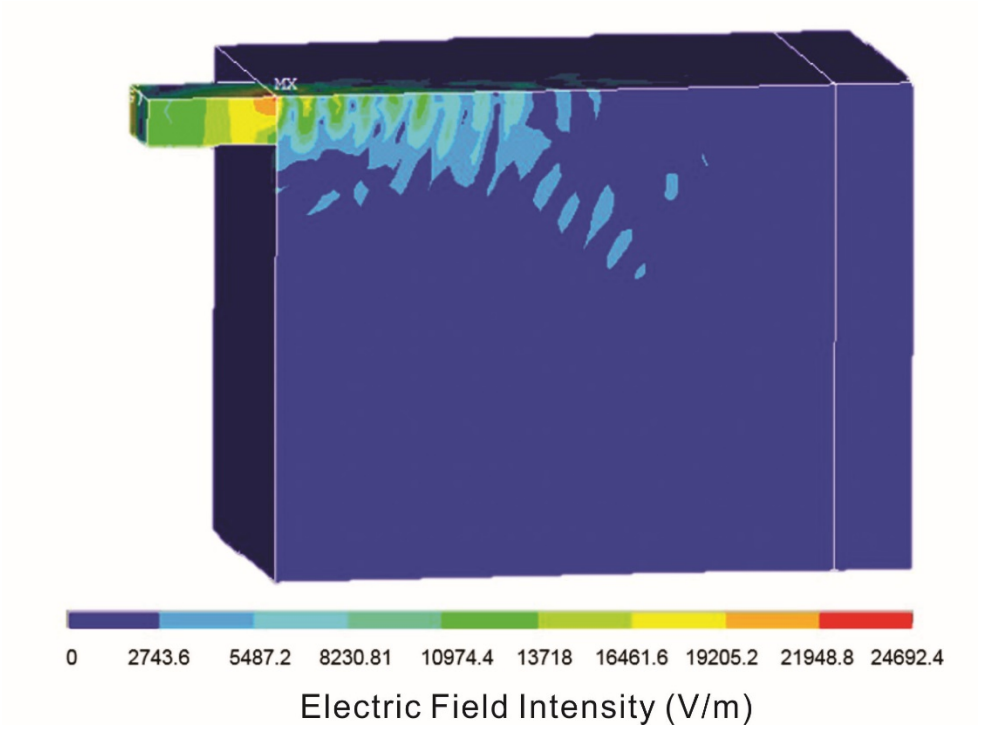

Figure 3-33 Electric Field Distribution (V/m) in the Reservoir (The maximum electric field is in the region where waveguide and the wall of wellbore contact and its value is 24692.4 V/m. The microwave penetrates over 10 cm in the reservoir with electric field decreasing to around 2743.6 V/m).

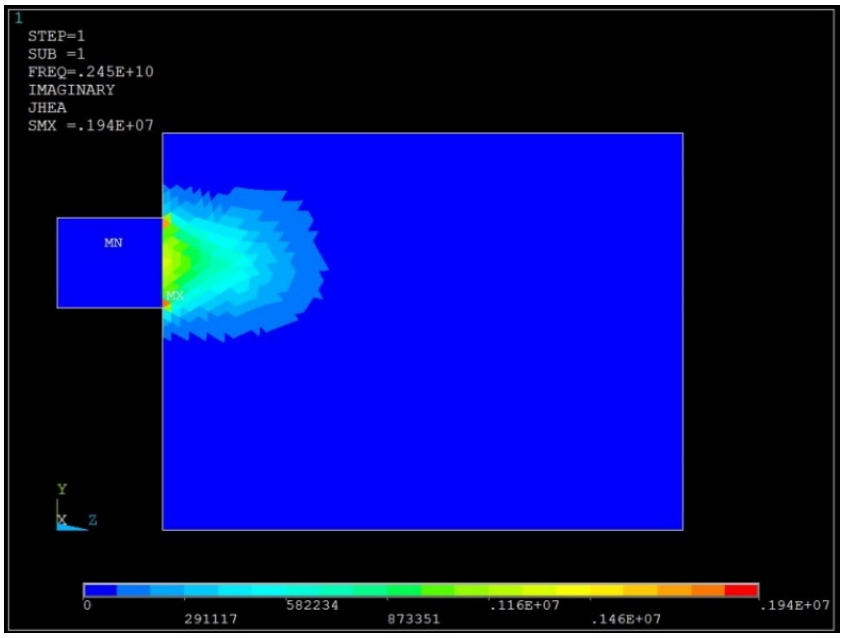

Figure 3-34 Joule heat distribution in the reservoir (the unit is in W/m^3).

In the CMG model, after injecting water for 3 days, the water saturation in the near wellbore area increased from 0.3 to around 0.8 and the invasion depth reached up to 0.7m (Figure 3-35 a). This agrees well with the approximate depth of invasion in an actual tight gas well, which is around 0.43 to 0.90m (Miesch and Albright, 1967; Rider, 1986). (Table 3-1)

Table 3-1 Depth of invasion (distance from borehole wall) versus porosity (Miesch and Albright, 1967 and Rider, 1986)

Hole Size (in)	17.5	12.25	8.5	Ratio invasion diameter: hole diameter
Porosity (%)	Depth of invasion (cm)			
1-8	200.0	140.0	97.0	10
8-20	90.0	62.0	43.0	5
20-30	22.5	15.5	11.0	2
30+	3.0	2.0	1.7	<2

Accordingly, the gas relative permeability decreased with an increase of water saturation to almost 0 after water injection (Figure 3-35, c) and the formation damage persisted even after the water injection stopped (Figure 3-35, d). To increase the relative permeability to gas, one method is to remove the water phase trapped in the near wellbore area by applying intensive heat to the target formation. In this case, a reservoir model without fractures was built and the two scenarios, applying microwave heating and without microwave heating, were considered. The simulation

used four downhole microwave devices, each with the same operation parameters as in the Finite Element Analysis (FEA) simulation abovementioned, to generate heat in four different directions in the wellbore. The reservoir size is 3.5m (length) × 3.5m (width) × 10m (thickness).

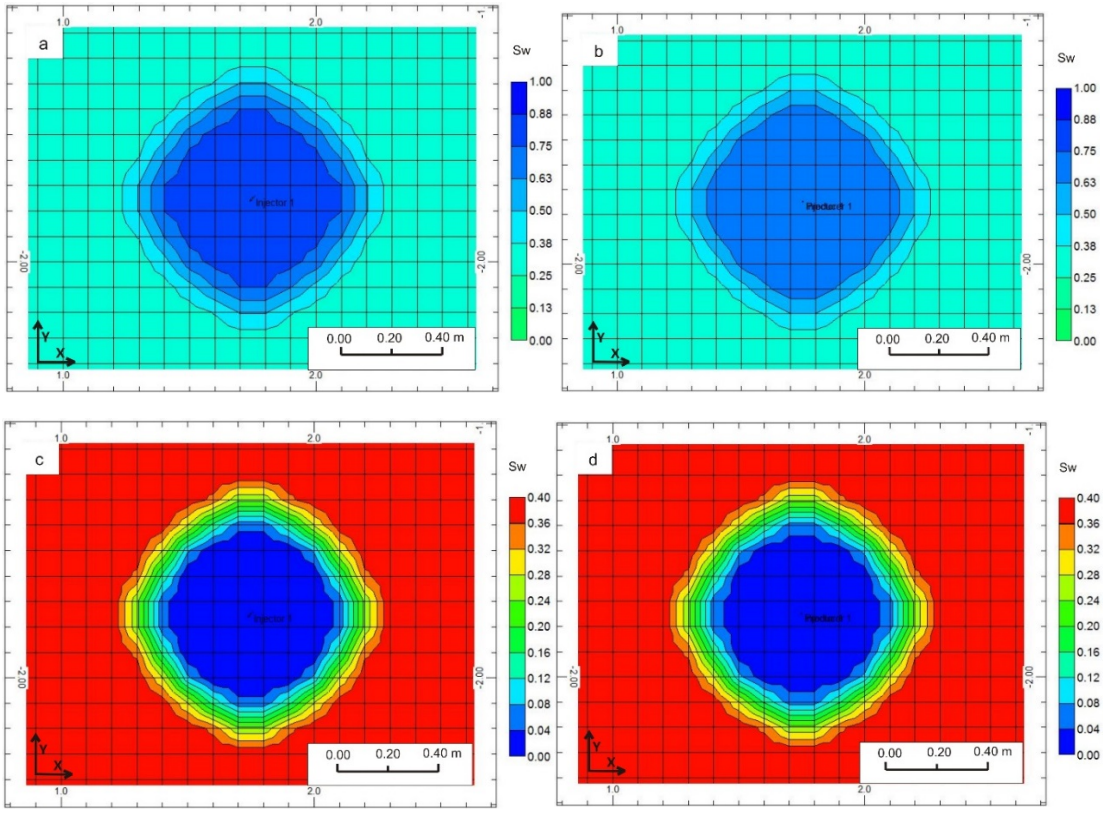

Figure 3-35 Water saturation distribution and relative permeability to gas in the well without heater in CMG-STARS. a- water saturation after 3-day water injection; b- water saturation after 3-day water injection and 1-day production; c- gas relative permeability after 3-day water injection; b- gas permeability after 3-day water injection and 1-day production.

Coupled with the ANSYS Multiphysics, the CMG can also be used to compute the temperature distribution as well as water saturation and relative permeability to gas in the heated formation. The temperature of the injected water was set the same as the reservoir temperature, so after water injection, the reservoir temperature is still around 139°C (Figure 3-36a). After microwave heating for a day, the maximum temperature in the near wellbore region reached to about 900°C and the depth influenced by the heat reached around 0.4 m. The water saturation in the near wellbore region was reduced significantly. As shown in Figure 3-37b, the water phase was completely

removed within about 25cm from the wellbore wall. Compared with Figure 3-37a, the moisture content in the further distance away from the wellbore dropped to a relative low level but not to zero. However, it can be confirmed that by increasing the microwave heating power and heating time, the penetration depth of treatment can be enlarged and water saturation can be further reduced.

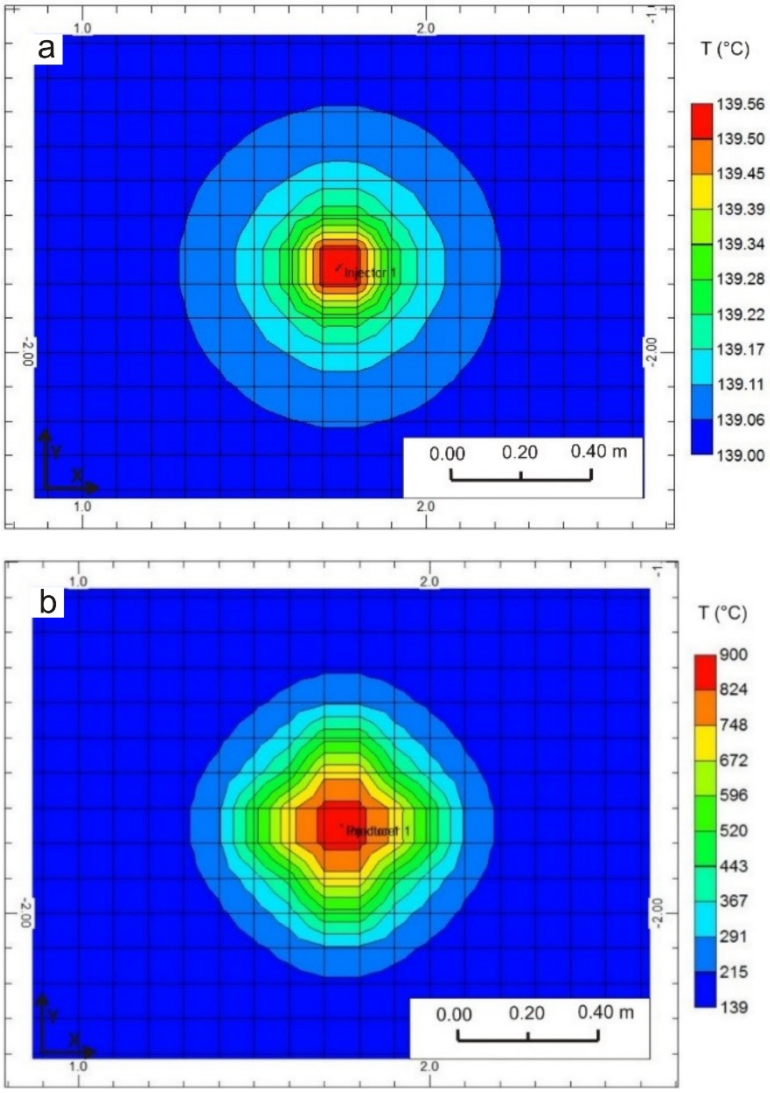

Figure 3-36 Temperature distribution in the formation at (a) the end of injection and (b) at the end of production in the well with the heater in CMG-STARS.

As shown in Figure 3-37a and c, water saturation increased from 0.3 to nearly 1 and the relative permeability to gas dropped to 0 after water invasion, which indicates that a severe formation damage has taken place. In other words, the well failed to produce gas after the water invasion since the pores are blocked by water. During the

production period, the downhole microwave heater was employed to generate heat. The heat generation rate is 2.94 × 10^7Joule/ day in one grid block (0.1m × 0.1m × 0.1m), which is within the penetration depth of microwave. The application of heat lowered the water saturation in the near wellbore area by evaporating the water in the formation. In Figure 3-37b, water saturation dropped to 0 within 25cm. Moreover, relative permeability improved near the wellbore (Figure 3-37d) to almost 1 because of the evaporation of trapped water. The cumulative gas production of the heated well is greater than the well without microwave heating. The gas production recovered quickly after applying microwave heating, while the gas production in the non-heating well needed more time to recover from the water invasion (Figure 3-38).

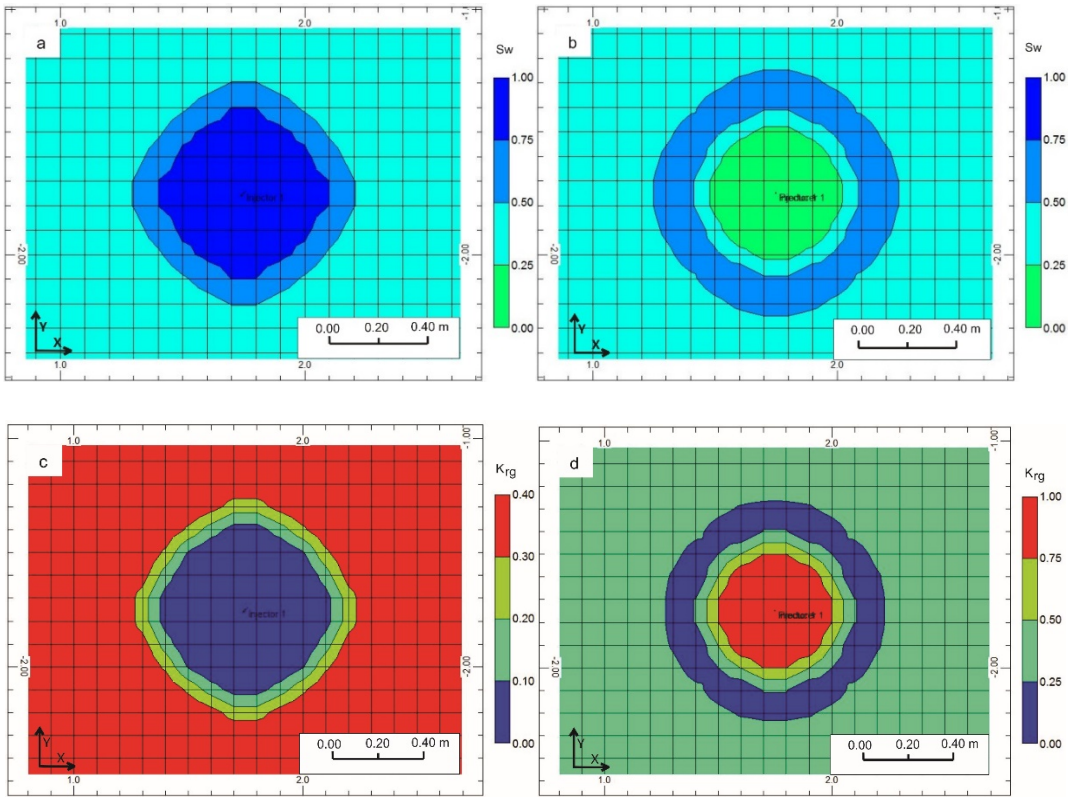

Figure 3-37 Water saturation distribution and relative permeability to gas in the well with heater. a- water saturation after 3-day water injection; b- water saturation after 3-day water injection and 1-day reservoir heating; c- gas relative permeability after 3-day water injection; b- gas permeability after 3-day water injection and 1-day reservoir heating.

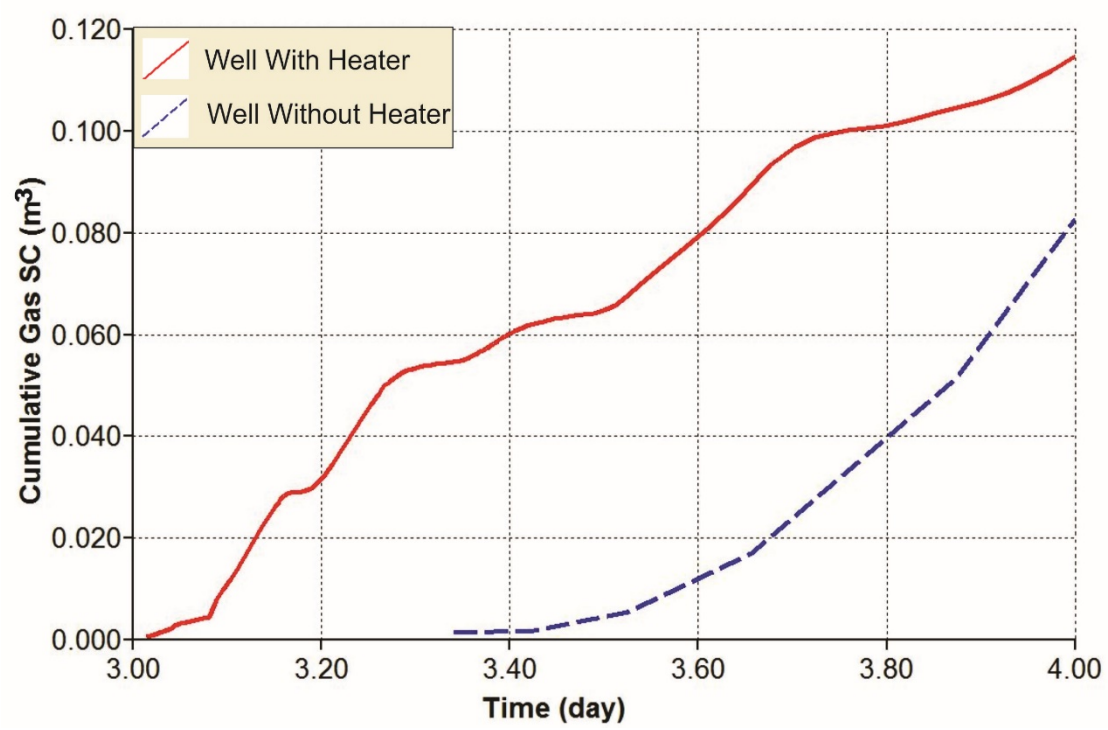

Figure 3-38 Comparison of cumulative gas between well with heater and well without heater after 3-day water injection.

4. Discussions

4.1 The Effects of High Temperature on Tight Sandstones

The effects of high temperature on reservoir quality have been studied through different experiments in the lab. The thermally induced fractures observed both in the CT and SEM images lead to the improvement of porosity and permeability. As shown in Figure 4-1, there are fractures generated (Figure 4-1-B) or expanded (Figure 4-1-C, D) in the image slices close to the core plug bottom. Accordingly, the NMR measurement results after heating show increase in the longer T2 components. Nevertheless, the fracture mentioned in Figure 4-1 is not the only factor contributing to the increase of porosity and permeability, the collapse of some minerals, which are reflected by XRD, is also important to the improvement of reservoir quality.

Microstructures have been investigated with SEM imaging at different magnifications in the samples before and after heating. The morphology of the fractures and mineralogy are closely examined to reveal the effects of high temperatures on tight sandstones. In terms of fractures generation, there are two main mechanisms: 1) the dehydration of clay minerals caused by high temperature heating brings about a shrinkage of minerals and creates fractures between the clay minerals (Li et al., 2006) (Figure 3-8f, Figure 3-9f and 7p); and 2) the degradation or decomposition of the cement creates intergranular fractures (Figure 3-8g and 6h). There are two possible reasons for the different NMR T2 distributions of 4 samples before and after heating. The combination of small pores or fractures (Figure 3-8f, Figure 3-9f and 7p) and the degradation or decomposition of minerals decreases the percentage of short T2 components in the NMR T2 distribution and creates larger pores, which have been reflected by the increase of amplitude at T2 from around 10 to 100ms in Figure 3-5. However, the kaolinite shown in Figure 3-9l could not be found after heating. Thus, the effects of high temperatures on kaolinite cannot be investigated in this study. The experiments on isolated kaolinite also revealed that the structure of kaolinite will be completely destroyed at 550℃ (Jamaluddin et al., 1998). In addition, D. Carroll

(1970) reported that the well-crystallized kaolinite will be replaced by amorphous meta-kaolinite when the temperature reaches 575 – 625℃ (Jamaluddin et al., 1998). The fractures in the sandstone are influenced by both the mineral components and microstructures, as well as the distribution of internal micro defect and nucleation. Based on different fracture morphology characteristics, the fracture mechanisms will include the inter-granular fracture, trans-granular fracture, clay cement fracture and the coupled inter granular- trans-granular fracture (Xie et al., 1989; Xie et al., 2007).

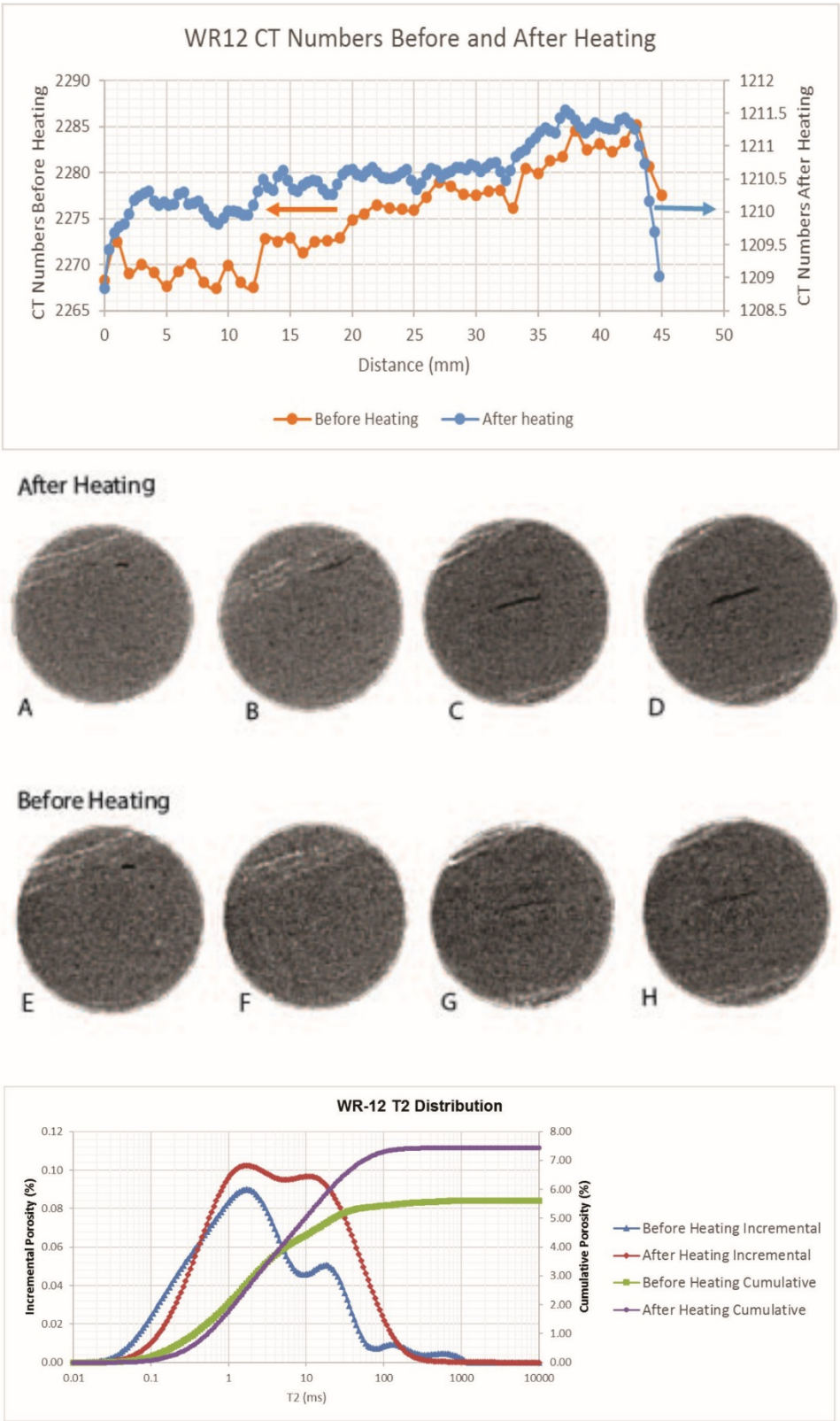

Figure 4-1 Sample Whicher Range-12 CT images showing fractures leading to an increase of porosity. The top graph shows the porosity enhancement by the decrease of CT number along the length of the core plugs; the bottom left diagram indicates the presence of fractures in the sample which may contribute to porosity enhancement; the bottom right graph shows the increase of the percentage of large pores (the amplitude of the longer T_2 increases after heating), which may be related to the fracture.

The XRD analysis shows the disappearance of calcite and kaolinite. Calcite is one of the common cements in sandstone. By decomposing calcite, pores can be created along the boundaries of the grains. Kaolinite is pore-filling mineral and causes micro-porosity and easy to migrate in the sample. After the collapse of the kaolinite crystalline structure, the spaces of micro-pores can be released and contribute to the porosity improvement. Furthermore, the collapse of kaolinite can reduce the sensitivity of reservoir to clay migration.

Among these studies, some factors affecting the results are worth discussing:

1. Due to the limitations of the experimental setup, the experiments are conducted at atmospheric condition, so the effects of confining pressure and reservoir temperature are not considered in this study. Therefore, the following will be influenced: firstly, the fractures of the sandstone may be wider due to a lack of confining pressure; secondly, the boiling point of water is related to the pressure, so in the reservoir condition, more heat will be needed for evaporating the same amount of moisture.
2. The CT scan images are used to analyze the increase of porosity. However, the resolution is one of the shortcomings of this technique, the minerals cannot be identified clearly. So in our study, we use it as a method to identify the fractures and compare the porosity profile. The data correlates well with porosity measurements.
3. SEM imaging focuses on a relatively small area in the sample, so it is not possible to investigate the whole sample. Hence, important information may be missing due to this limitation. In the future, increasing the sampling number is an effective way to solve this problem.

4.2 The Effects of Microwave Heating on Tight Sandstones

The laboratory works involved in this study are porosity and permeability measurement, NMR, X-ray CT scanning, XRD and SEM. In addition, numerical simulation concerning the heating of the reservoir with microwave has been conducted. Based on these data, the effects of microwave heating on the tight sandstone samples were understood.

After the tight sandstone samples were heated with the microwave, the samples' maximum surface temperature and heating time are 359.3℃ in 10 minutes for Erregulla-2, 504.1℃ in 5 minutes for Whicher Range-1, 337℃ in 8 minutes for Whicher Range-11 and 483.7℃ for Whicher Range-14 in 2 minutes. The internal temperature, which is believed to be higher than the surface temperature according to the power dissipation equation and penetration depth equation, was not accessible when we used microwave as the heating method. However, in terms of temperature, the higher is not necessarily the better, because some minerals have low melting point, which become high plastic deformation or start to melt when the temperature is high. As a result, these deformed or molten particles can block the other pores permanently.

The temperature distribution in core plug is mainly determined by the electrical conductivity, relative permittivity, thermal conductivity and specific heat capacity which rely on many factors such as porosity, water saturation, salinity and mineralogy. Instead of conducting a quantitative study on how these factors affect microwave heating, we put an emphasis on the effects of high temperature, which is generated by the interaction of microwave and sandstone, on the petrophysical properties. The factors affecting microwave heating will be discussed later.

The most important issues we are concerned about during the gas production are reservoir quality and pore size distribution. Microwave heating is able to recover the reservoir quality by evaporating the moisture phase or even further improve the reservoir quality by altering the mineralogy of sandstone and creating micro-fractures. The NMR T2 measurements on the dry sample after heating revealed that the NMR T_2 peaks became weaker after heating compared with the dry samples before heating. Most of the water, including the clay bound water, has been removed from the sample by microwave heating.

It is reckoned that the microwave heating altered the minerals thus pore size distributions by combining or expanding smaller pores into larger pores in the heated samples. In other words, the small pores contributed to the growth in the amounts of

larger pores. This can be clearly demonstrated in sample Whicher Range-11 (Figure 3-17). After heating, the incremental porosity at 0.2ms decreased from 0.05% to 0.02% while the incremental porosity at 2.5ms increased from 0.29% to 0.4%.

In sample Whicher Range-14, the change of pore size distributions is distinct from the other three samples: the population of medium pores decreased, but the large pores increased more significantly compared with the other samples. In fact, a part of sample Whicher Range-14 was observed to be melting during the experiment and the temperature in the sample was estimated to be higher than 700°C. Here, another possible reason for the change of pore size distribution is that some minerals have been molten in high temperature, which creates spaces and, at the same time, blocks other pore spaces.

The third reason is that the clay minerals with micro-pores are degraded and decomposed, thus creating large pore spaces. Hajpál and Török (2004) indicated that micro-fractures will develop at grain boundaries when the temperature is over 600℃ and a higher temperature of 750℃ is necessary for fractures within the crystals.

The Helium and NMR porosity for each sample were correlated to calibrate the NMR test results. As indicated in Figure 4-2, the trends of porosity changes are similar for all the involved samples. For example, the slope between “Erregulla-2 Before” and “Erregulla-2 After” of Helium porosity is the same as the slope of NMR porosity.

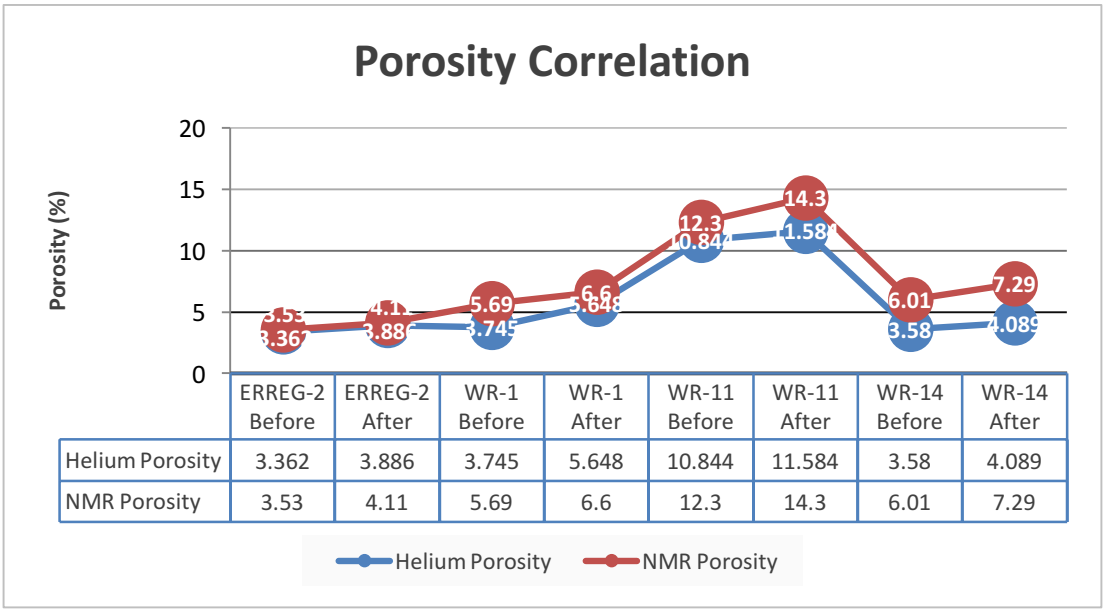

Figure 4-2 Porosity correlation of Helium and NMR porosity before and after MW heating. The NMR porosity is slightly higher than the Helium porosity for all the measurements. It is shown that both the Helium porosity and NMR porosity indicated the improvement of porosity.

Sample Whicher Range-1 and Whicher Range-14 showed fractures at one end of the core plug in Figure 3-19 and Figure 3-20. Figure 3-18 indicated an increase of porosity in the corresponding position in the CT number profiles. In comparison, sample Erregulla-2 has a homogeneous porosity improvement, which is because of the relative even temperature increase in this sample.

As the heating method is microwave radiation, according to its mechanism, the heating effect relies on the electric field distribution, which is not even in the target object. In addition, the thermal conductivity and heat capacity of minerals are different, so their temperatures will vary after exposing to the microwave. Moreover, these minerals have various thermal expansion properties, so the responses, for example, the temperature and thermal stress distribution, to microwave heating. These combined factors led to the presence of the fractures in the heated sample.

In sample Whicher Range-1 (Figure 3-19), which shows the fractures at one end of the sample. However, the dimensions of the fracture are much smaller than in Whicher Range-14. Besides the above three factors, we also should take into consideration the structure of the sample: compared with Whicher Range-1, Whicher Range-14 is more laminar. This laminar structure facilitates the generation and

development of fractures during microwave heating. The distributions of the porosity improvement are found heterogeneous in the other three samples. As a matter of fact, there are many reasons leading to a non-uniform temperature distribution:

1. The magnetic and electric field distributions are not even in the sandstones, so the intensities of different parts in the sample could vary from one to another.
2. The dielectric properties of the grains are different due to mineral types, water content and porosity. Based on Equation 8, the relative permittivity determines the efficiency of microwave heating. However, the heterogeneous heating effects brought about the differential thermal expansion and led to the generation of micro-fractures.
3. The texture and structure of the tight sandstones affects the temperature distributions because they are related to the distribution of minerals in the sample. For the aggregation of minerals with high dielectric loss, as it is more easily heated, its temperature is high; while for the aggregation of low loss minerals, its temperature is low.

In terms of the mechanisms of fractures creation, there are two main mechanisms:

1. Extra pore or micro-fractures are created among clay minerals because of their volume shrinkage induced by clay dehydration or degradation (Figure 3-22-g and Figure 3-22-o) (Li, et al., 2006).
2. Intergranular fractures are generated between the grains due to differential thermal expansion and decomposition of cement between the grains (Figure 3-22-f and Figure 3-22-h). Intragranular fractures are formed in the grains because of thermal expansion and surrounding thermal stress (Figure 3-22-i).

Compared with conventional heating, microwave heating is not as effective in decomposing the kaolinite. It is possibly because the heating time is short and the temperature is not high enough. Due to the same reason, the generation of illite can be found only in the samples heated by high temperature muffle but not the samples heated by microwave. The presence of illite will increase the risk of clay migration, which should be taken into consideration. By heating the reservoir rock with the

microwave, the calcite cement within may decompose as well. This leads to the improvement of porosity and permeability of sandstones. The disappearance of feldspar further contributes to the reservoir quality enhancement.

4.3 The Effects of Salinity on Microwave Heating

The quantitative study on factors affecting microwave heating of tight sandstones is of great significance in developing the application of microwave heating in Formation Heat Treatment (FHT).

Salinity is one of the crucial factors that control the temperature rise in the sample during microwave heating. From the chemistry viewpoint, as a result of the introduction of ions into a solution, the dielectric heating rates increase. The structure of water is influenced when ionic salts are dissolved in it (Gabriel et al., 1998). However, in higher salinity brine the water molecules get around the ions and the ability of them to adjust in the applied electric field is weakened. Thus, permittivity and heat generation are reduced (Anwar et al., 2015; Hasted, 1973).

In Figure 4-3a, the samples saturated with 20000ppm and 30000ppm brine reached a higher temperature, of approximately 140°C in 2 minutes; while the samples saturated with 40000ppm and fresh water reached a lower temperature, about 110°C in 2 minutes. Similarly, in Figure 4-3b, the samples saturated with 20000ppm and 30000ppm brine reached a higher temperature, of approximately 140°C in 2 minutes; while the samples saturated with 40000ppm and fresh water reached a lower temperature, about 130°C in the same amount of time. Due to the high salinity, the sample saturated with 40000ppm brine has a low microwave heating rate, which is the same as fresh water (distilled water). In contrast, the sodium chloride solution (with a lower concentration of salt) enhances the microwave heating. The presence of ions fixes the rotation of the water molecules which are coordinated to the ions. In higher salinity brine, more water molecules are in a fixed state due to the presence of more ions (Craig, 1995; Gabriel et al., 1998).

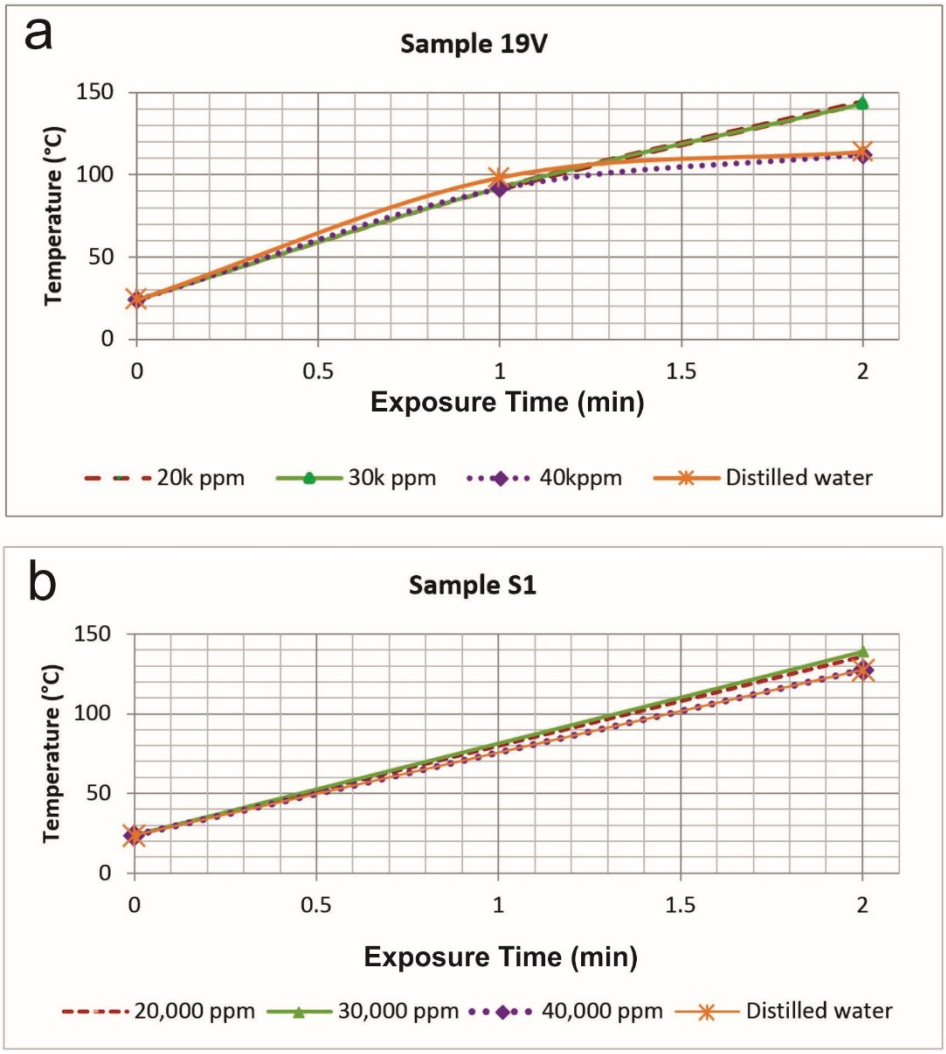

Figure 4-3 The effects of salinity on MW heating. During the same exposure time to microwave, the sample saturated with lower salinity brine (20k ppm and 30k ppm) has got a higher temperature than sample saturated with higher salinity brine (40k ppm) and freshwater.

4.4The Effects of Water Saturation on Microwave Heating

Water saturation varies in the actual formation. The increasing water saturation leads to negative effects on microwave heating due to the energy loss in the phase change (from water to vapor), although water is a good microwave absorber. After determining the water saturation in the reservoir, the temperature and downhole heating time can be estimated.

The water saturation that we selected (20%, 40%, 60%, 80% and 100%) in this study is solely for the purpose of finding out the relationship between temperature variations and water saturations.

In this study, air and brine are two substances that fill the pore space. The Mixing Law can be written as:

$$\sqrt{\epsilon^*} = S_w \emptyset \sqrt{\epsilon_w^*} + S_G \emptyset \sqrt{\epsilon_G^*}$$

Equation 13

Where ϵ is the relative permittivity, $\emptyset$ is the porosity, S is the saturation, W represents water and G represents gas.

According to the Equation 13, the porosity is constant for a specific sample, the relative permittivity of water and gas (air) is constant as well, since the salinity of brine water is constant, the relative permittivity of brine can be considered as constant. The variables are water and gas (air) saturation. Any change of S_w and S_G will lead to a variation of relative permittivity of the sandstone sample (minerals and interstitial fluids as a whole).

In Figure 4-4, after 1-minute microwave heating, the differences between them are evident: the experiment with the lowest water saturation (20%) got the highest temperature (144°C), while the fully saturated sample got the lowest temperature (96°C). It is shown that the higher the water saturation of the sample, the lower the temperature it obtained. Although relative permittivity plays an important role in microwave heating, it is not the only factor affecting the microwave heating in this study. The amount of water plays a more critical role in this case, as evaporating water helps to bring the temperatures down.

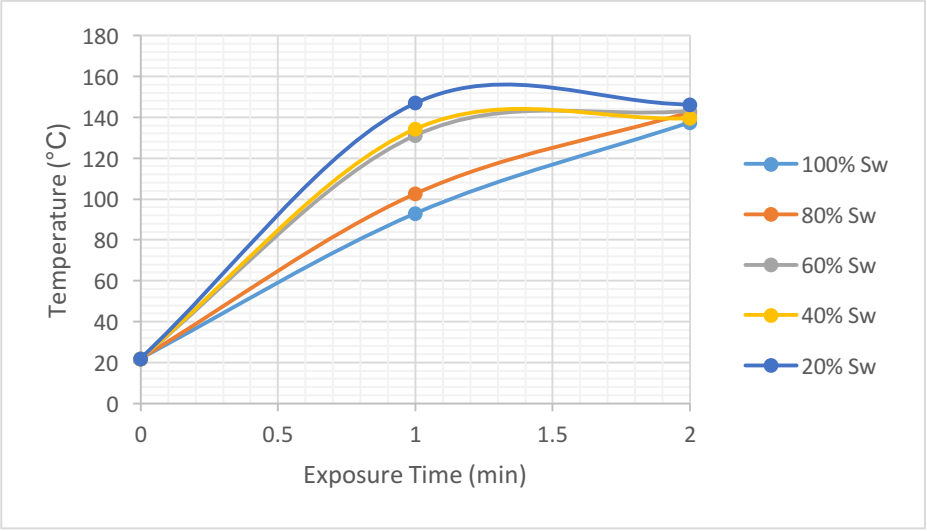

Figure 4-4 The effects of water saturation on MW heating. After heating for 1 minute, the higher water saturation, the lower temperature it reached; after heating 2 minute, all the sample reached approximately 140 °C.

4.5The Effects of Salt Types on Microwave Heating

To understand how the salt type affects microwave heating, solutions of 4 different salts, NaCl, $MgCl_2$, $CaCl_2$ and KCl, were prepared separately in the lab and the samples were saturated in these solutions. All of these solutions have the same salinity of 20000ppm. After 1 minute of heating, $CaCl_2$ reached the highest temperature at around 124°C, NaCl reached 102°C, while the other two samples reached a temperature between the above temperature range. However, in 2 minutes, three samples reached a similar temperature at around 156°C, while the sample saturated with NaCl reached 144°C. But at the end of the microwave heating, after 3 minutes, all the samples reached a similar temperature of around 160°C.

Although the salinities of the samples are the same (20000ppm), the concentrations of the ions are different. The weight percentage of the salts are 2%, but the concentrations of Na^+, K^-, $Ca^{2+}$and Mg^{2+} are 0.0215mol/L, 0.018mol/L, 0.0111mol/L and 0.0122mol/L respectively. In Figure 4-5, it is found that a presence of high concentration ions lead to a low temperature rise. For example, the sample saturated with NaCl had the lowest temperature in 1 minute, while the sample saturated with $CaCl_2$ reached the highest temperature in the same time frame. Anwar et al. (2015)

conducted studies on different saline solutions of different concentrations. By plotting the converted salinity (20000 ppm) into concentrations (Na^+, 0.0215mol/L; K^-, 0.018mol/L; Ca^{2+}, 0.0111mol/L; and Mg^{2+}, 0.0122mol/L), the temperatures of the 4 samples were obtained as 40.1°C, 40.1°C, 40.6°C and 40.6°C respectively. The same trend has been found - the solution with a higher ion concentration leads to a low heating rate. Furthermore, in Anwar et al. (2015)'s study, due to the effect of the larger ion radius, the temperatures of the samples with the same ion concentrations are in the following order: $MgCl_2$> $CaCl_2$> NaCl> KCl. However, in our work, the effect of ion concentrations overwhelmed the effect of ion radii. In other words, compared with the ion radius, the concentrations of ions are more important when heating brine-saturated sandstone with microwave radiation.

Although it has been reported that the larger the ion radius, the lower the temperature after microwave heating (Anwar et al., 2015), the effect of ion concentration dominates in influencing microwave heating in our laboratory study.

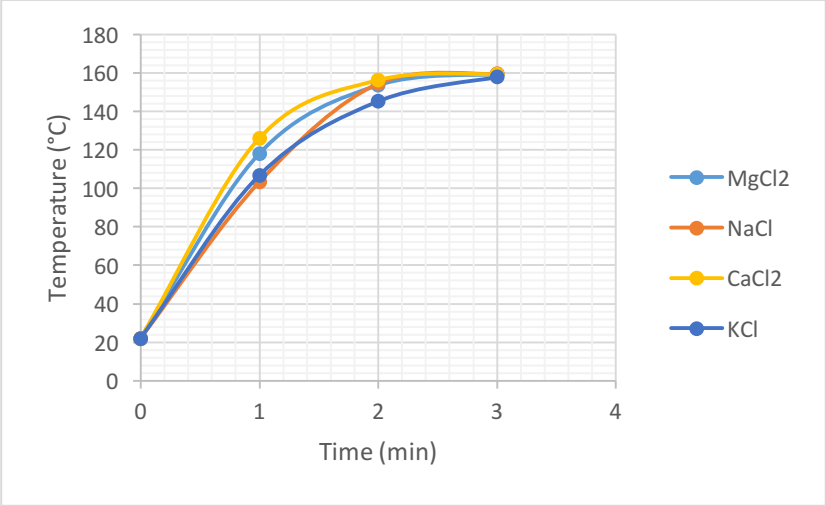

Figure 4-5 The effects of salts on MW heating. The differences of temperatures of samples saturated with different salts solution are minimal. In the first minute, the sample saturated with $CaCl_2$ solution reached 124°C, which is higher than the other samples. After 2 minutes, the sample saturated with KCl reached 145 °C, which is lower than the other three samples. All of them reached about 160°C in three minutes.

4.6Numerical Simulation

Microwave heating of tight sandstone is a complex process which needs the coupling of multiple physics fields including the electromagnetic, thermal and fluid flow fields. Among the properties of sandstones, the dielectric properties and electrical conductivity are of great importance. These properties are temperature-dependent. Generally, relative permittivity increases with temperature for most minerals. A more complex model is needed to include the temperature dependence on microwave heating. However, in this feasibility study, temperature-dependence was not considered. In order to study the effects of heating on water saturation and relative permeability, we coupled the ANSYS and CMG-STARS software suites. Based on the results, we have the following conclusions: 1) the dielectric properties have a dramatic effect on both electric field and temperature distributions. For microwave volumetric heating in the lab, the suitable penetration depth is the key to achieve a satisfying heating result; 2) the electrical conductivity had more influences on the temperature distribution than on the electric field distribution; 3) by applying heat to the formation, water saturation in the formation decreased, leading to an increase of the relative permeability to gas. It is suggested that microwave heating is a promising method for Enhanced Gas Recovery.

The temperature distributions in the reservoir are computed in the ANSYS and CMG-STARS software. These two results are compared against each other in order to verify the microwave heating method of the reservoir.

According to Figure 4-6 and Figure 4-7, after 30 minutes of microwave heating, the highest temperature in the target formation reached to over 300°C in both computation methods. The influence depth of microwave heating reached about 10cm in 30 minutes. A comparison of the results from CMG and ANSYS are illustrated in Figure 4-8.

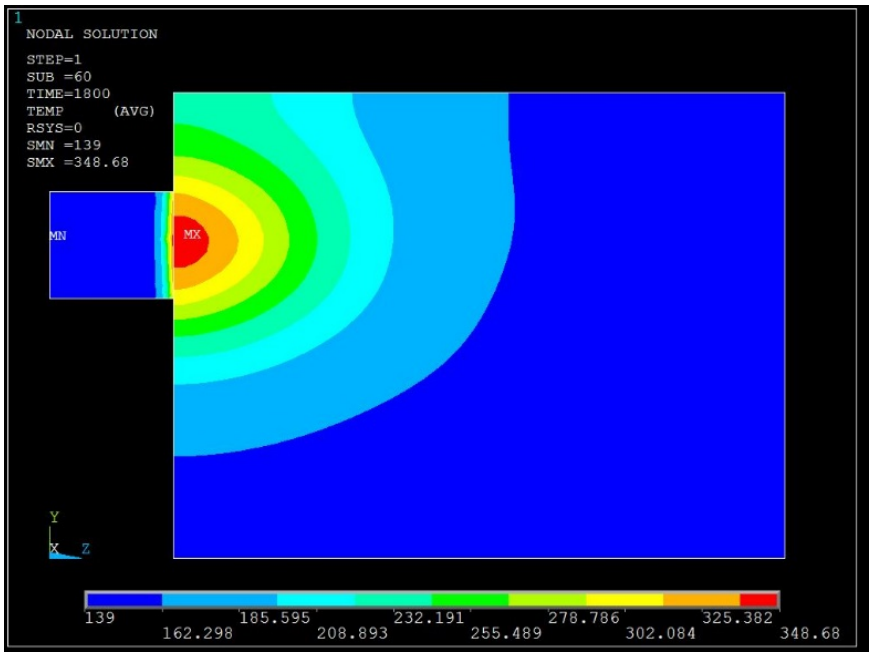

Figure 4-6 Temperature distribution after heating with the MW for 30 minutes (the unit is in °C). The maximum temperature reached 348.68 °C after 30 minutes and depth being influenced is around 10 cm.

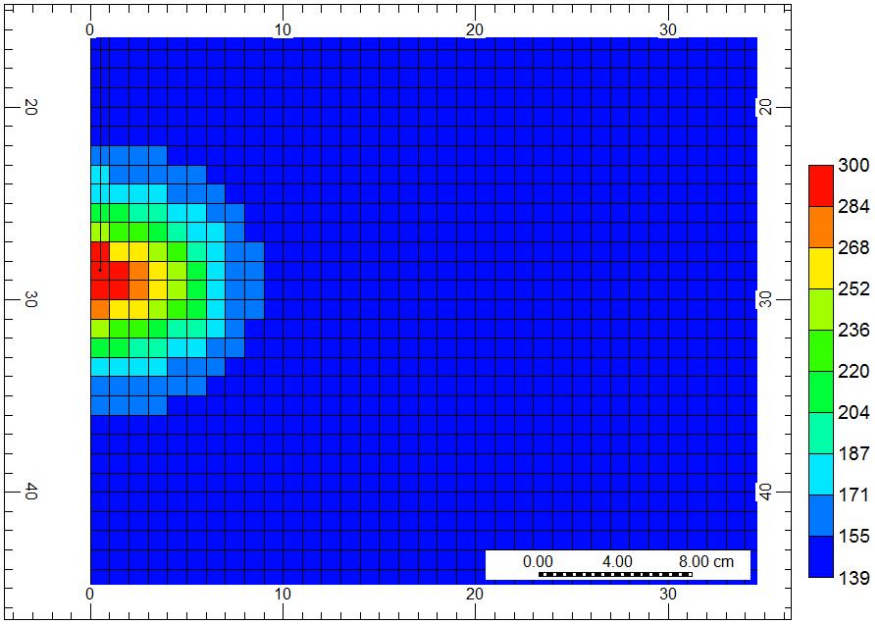

Figure 4-7 Temperature distribution after heating with the MW for 30 minutes (the unit is in °C). The maximum temperature reached to 300 °C in area close to the well. In the depth 10cm, the temperature reached to only around 150°C.

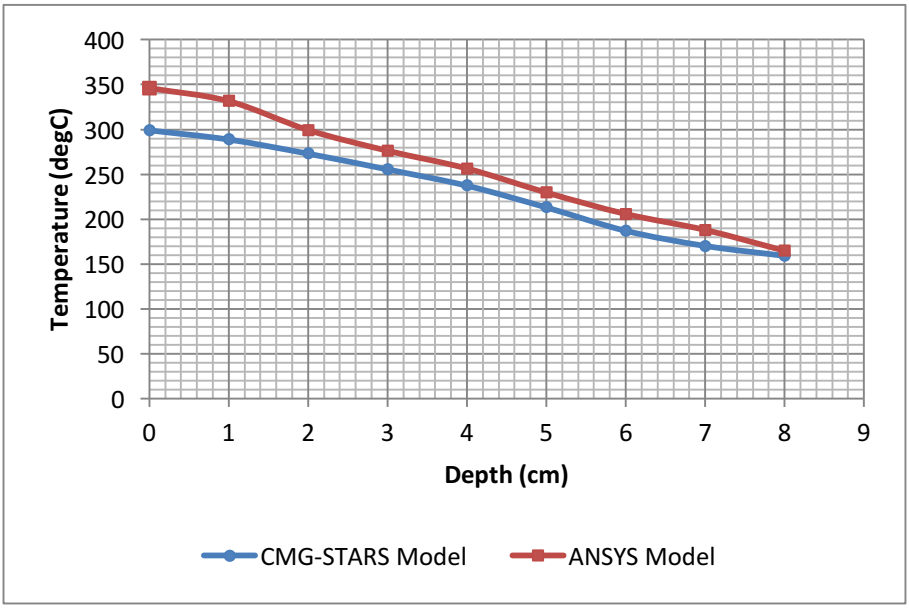

Figure 4-8 Temperature versus depth in CMG and ANSYS models. With the depth increases, the temperature of reservoir rock decreased in both models. The temperature decreased to 160°C in the depth of 8cm.

5. Conclusions

The formation damages in tight gas reservoir cause various problems for gas production. This study utilizes the thermal method, especially the microwave heating, as a major technique to remove formation skin damage in the near wellbore region. Petrographic and petrophysical properties of tight sandstone samples are investigated with multiple lab techniques before and after conducting the heating experiments. These properties are then analyzed and compared to understand the effects of heating on samples. Furthermore, they are included in the numerical simulation works in the lab scale and in the reservoir scale. Based on the experimental and numerical simulation works, this study comes to the following conclusions.

5.1 Effects of High Temperature on Tight Sandstone Samples

- The porosity and permeability of all the samples, as measured by helium porositmeter/permeameter, increased after conventional heating. As such, the heating treatment is effective in improving reservoir quality.
- The combinations of small fractures or pores in the sample create larger fractures or pores. This can be reflected from the change of T2 distribution of fully saturated samples. Moreover, the data of SEM (presence of intergranular fractures after heating) and X-ray CT scanning (decrease of CT numbers after heating and generation of fractures) agree well with the NMR result at this point.
- The comparison of XRD patterns reveals that high temperature is effective in removing kaolinite, which has micro-porosity and easily migrates, as well as montmorillonite, which is sensitive to low salinity formation water and easily swells. The decomposition of these clay minerals will then lead to the alleviation or removal of formation damages caused by them.
- By conducting the NMR test on samples after heating, it is found that the signal from water became extremely weak, which means that water content has been removed when being exposed to high temperatures of up to 600°C.

Compared with samples before heating, the irreducible water of heated samples reduced significantly to nearly zero. Furthermore, the shrinkage of smectite promoted the generation of fractures in the sample and thus enhanced the reservoir quality. Undeniably, the conventional heating is effective in eliminating water blocking and clay swelling in tight gas reservoirs.

5.2 The Effects of Microwave Heating on Tight Sandstones

- By subjecting the tight sandstone samples to the microwave, the surface temperature of sandstone can be raised to around 400℃ or more (depending on the dielectric properties of the sample), while the internal temperature is usually higher than that.
- The shrinkage of the clay minerals due to the loss of water during microwave heating has been observed in this study. The differential thermal expansion and dehydration of clay minerals created fractures leading to an increase in the porosity and permeability values. More importantly, the enhancement of permeability is higher than the porosity for all studied samples, which shows a great economical potential.
- Similar to conventional heating, the micro-fractures grew into larger fractures/pores when the sandstones were heated by microwave. In the NMR T2 distribution of fully saturated samples: the area under the short components of the T2 curve decreased, while the long T2 increased. The analysis of SEM images and X-ray CT scanning images supports the NMR analysis well.
- Some minerals were changed due to microwave heating. By using the technique of XRD, calcite and feldspar were found to have disappeared after heating. Since they are common cement minerals in sandstone, reservoir quality can benefit from the decomposition of these minerals.

5.3 Controlling Factors of Microwave Heating

- The experiments on the sample saturated with lower salinity brine, 20000ppm and 30000ppm, tend to be more easily heated and more likely to end with a

higher surface temperature, while the sample saturated with higher salinity brine (40000ppm) and fresh water reached a lower surface temperature. The salinity of the formation water has positive effects on microwave heating when the salinity is in the lower ranges. As the salinity increased beyond this range, the positive effects are weakened.

- In terms of water saturation, the increasing water saturation brings negative effects on microwave heating due to the energy loss in the phase change (from liquid water to vapor), even though water is a good microwave absorber. After determining the level of water saturation in the reservoir, the temperature and downhole heating time can be estimated.
- In microwave heating, the concentration of the ions plays a more important role than the ion radius.

5.4 Numerical Simulation of Microwave Heating Treatment

- The simulated depth of phase invasion was around 0.7m and the temperature reached up to 900°C within a day. The water phase was completely removed within 25cm, although the water saturation reduced a depth slightly beyond that. Thus, it is promising for microwave heating to bring down water saturation in the near wellbore region.
- The increase of water saturation in the near wellbore area causes a drop in the relative permeability of gas and production. However, by heating the reservoir, the gas relative permeability, as well as the cumulative gas production saw an increase.
- When suitable electrical conductivity and relative permittivity are provided, the Finite Element Method (FEM) simulation agrees well with the experimental data in terms of the surface temperature of the sandstone plugs.
- Two simulation methods have a good correlation in computing the reservoir temperature distribution. Therefore, the FEM method can be an effective and reliable way of predicting the temperature distribution in an actual well.

5.5Other Conclusions

- Comparison of heating time between conventional heating and microwave heating shows that the microwave is more time efficient than the conventional heating.
- The sample heated by conventional method has a greater porosity improvement than those heated by microwave. However, both of them have a similar positive effect on permeability.
- Traditional heating may cause more fractures in the quartz grains, while microwave heating causes less fractures. However, these fractures are not as important as those along the grain boundaries.
- The optimization of microwave heating in the field may be achieved by improving the design of the downhole microwave heating device, as well as increasing the operation power and heating time. Research and development on the design of the downhole microwave device is also necessary.

Nomenclature

a: coefficient dependent on the formation type

A: Cross section area

B: Intensity of magnetic field

BVI: Bound water volume

C: Variable dependent on the formation

CT: Computed Tomography

D: Penetration depth

E: Intensity of electric field

f: Frequency

f_0: Resonant frequency

FFI: Free fluid volume

h: Height

J: Current density

K: Permeability

k: Thermal conductivity

k_{rnw}: Non-wetting phase relative permeability

k_{rw}: Wetting phase relative permeability

K_{rg}: Gas relative permeability

M: Factor related to the aspect ratio

M_o: Fluid volumetric heat capacity

M_T: Total volumetric heat capacity

mD: Milidarcy

NMR: Nuclear Magnetic Resonance

P: Absorbed power per unit volume

P: Fluid pressure

Q: Quality factor of the cavity

q: Local heat flux density

r: Capillary radius

S: Mass rate of liquid absorption per unit volume of porous medium

S_G: Gas saturation

S_O: Oil saturation

SEM: Scanning Electron Microscope

S_t: Total specific heat

S_w: Water saturation

T: Temperature

t: Time

T_{2gm}: Geometric mean of the T2 distribution

T_1: Longitudinal relaxation time

T_2: Transverse relaxation time

XRD: X-ray Diffraction

α_e: Electric field absorption coefficient

γ: Complex propagating factor of electromagnetic wave

δ: Shift of resonance frequency of material

∅: Porosity

∇: Nabla symbol (∇· is divergence operator, ∇× is a curl operator)

ε": Loss factor

ε': Dielectric constant

ε: Permittivity

ε_0: Permittivity of free space ($8.854\,187\,817\times 10^{-12}$ F/m)

θ: Contact angle

λ_{cutoff}: Cutoff wavelength

μ: Magnetic permeability

μ0: Permeability of free space ($1.2566370614\times10^{-6}$ H/m)

ρ_l: Density of the incompressible liquid

ρ_P: Mass concentration of the fine particles

ρ_t: Total density

σ: Electrical conductivity

σ_{lg}: Liquid gas surface tension

σ_{gw}: Gas water surface tension

σ_{SW}: Change of pore volume per unit bulk volume due to swelling expressed as equivalent particle mass

ω: Angular frequency

References

1. Abdulagatova, Z., Abdulagatov, I. M., & Emirov, V. N. (2009). Effect of temperature and pressure on the thermal conductivity of sandstone. International Journal of Rock Mechanics and Mining Sciences, 46(6), 1055-1071.

2. Abdulsattar, Z. R., Agim, K., Lane, R. H., & Hascakir, B. (2015, April). Physicochemical Interactions of Source Rocks with Injected Water-Based Fluids. In SPE International Symposium on Oilfield Chemistry. Society of Petroleum Engineers.

3. Abernethy, E. R. (1976). Production increase of heavy oils by electromagnetic heating. Journal of Canadian Petroleum Technology, 15(03).

4. Abramovitch, R. A., ChangQing, L., Hicks, E., & Sinard, J. (2003). In situ remediation of soils contaminated with toxic metal ions using microwave energy. Chemosphere, 53(9), 1077-1085.

5. Agca, C., & Yortsos, Y. C. (1985, January). Steady-State Analysis of In-Situ Combustion. In SPE California Regional Meeting. Society of Petroleum Engineers.

6. Ahmed, T. (2006). Reservoir engineering handbook. Gulf Professional Publishing.

7. Akin, S., & Kovscek, A. R. (2003). Computed tomography in petroleum engineering research. Geological Society, London, Special Publications, 215(1), 23-38.

8. Ali, M., & Hascakir, B. (2016). Water/Rock Interaction for Eagle Ford, Marcellus, Green River, and Barnett Shale Samples and Implications for Hydraulic-Fracturing-Fluid Engineering. SPE Journal.

9. Allen, P.A. and Allen, J. R. (2013). Basin Analysis, Principles and Application to Petroleum Play Assessment. Wiley-Blackwell. http://doi.org/10.1007/s13398-014-0173-7.2

10. Amaerule, J. O., Kersey, D. G., Norman, D. K., & Shannon, P. M. (1988, January). Advances in formation damage assessment and control strategies. In Annual Technical Meeting. Petroleum Society of Canada.

11. Anders, M. H., Laubach, S. E., & Scholz, C. H. (2014). Microfractures: A review. Journal of Structural Geology, 69, 377-394.

12. Anderson, W. G. (1987). Wettability literature survey-part 4: Effects of wettability on capillary pressure. Journal of Petroleum Technology, 39(10), 1-283.

13. Anwar, J., Shafique, U., Waheed-uz-Zaman, Rehman, R., et al. (2015). Microwave chemistry: Effect of ions on dielectric heating in microwave ovens. Arabian Journal of Chemistry, 8(1), 100–104.

14. Asghari, K., & Sheidaei, M. (2011). Application of Microwave for Reservoir Heating and Preventing Wax Precipitation in Production Wells. Petroleum Science and Technology, 29(15), 1555-1564.

15. Atomic Energy of Canada Limited Research Company and Voss Associates Engineering Ltd., 1990. Microwaves and Minerals. Industrial Mineral Background Paper#14.

16. Bahrami, H., Rezaee, M. R., Ostojic, J., Nazhat, D. H., & Clennell, M. B. (2011, January). Evaluation of damage mechanisms and skin factor in tight gas reservoirs. In SPE European Formation Damage Conference. Society of Petroleum Engineers.

17. Bahrami, H., Rezaee, R., & Clennell, B. (2012). Water blocking damage in hydraulically fractured tight sand gas reservoirs: An example from Perth Basin, Western Australia. Journal of Petroleum Science and Engineering, 88, 100-106.

18. Bartnikas, R. (1983). Dielectric loss in solids. In Engineering Dielectrics Volume IIA Electrical Properties of Solid Insulating Materials: Molecular Structure and Electrical Behavior. ASTM International.

19. Bennion, D. B. (2002). An overview of formation damage mechanisms causing a reduction in the productivity and injectivity of oil and gas producing formations. Journal of Canadian Petroleum Technology, 41(11).

20. Bennion, D. B., Thomas, F. B., Schulmeister, B. E., & Rushing, J. (2002, January). Laboratory and field validation of the mechanism of establishment of very low initial water saturations in ultra-low permeability porous media. In Canadian International Petroleum Conference. Petroleum Society of Canada.

21. Bennion, D. B., & Thomas, F. B. (2005). Formation damage issues impacting the productivity of low permeability, low initial water saturation gas producing formations. Journal of energy resources technology, 127(3), 240-247.

22. Bennion, D. B., Thomas, F. B., & Bietz, R. F. (1996A, January). Low permeability gas reservoirs: problems, opportunities and solutions for drilling, completion, stimulation and production. In SPE Gas Technology Symposium. Society of Petroleum Engineers.

23. Bennion, D. B., Thomas, F. B., Bietz, R. F., & Bennion, D. W. (1996B). Water and hydrocarbon phase trapping in porous media-diagnosis, prevention and treatment. Journal of Canadian Petroleum Technology, 35(10).

24. Bennion, D. B., Thomas, F. B., Schulmeister, B., & Romanova, U. G. (2006, January). Water and Oil Base Fluid Retention in Low Permeability Porous Media-an Update. In Canadian International Petroleum Conference. Petroleum Society of Canada.

25. Birchak, J. R., Gardner, C. G., Hipp, J. E., & Victor, J. M. (1974). High dielectric constant microwave probes for sensing soil moisture. Proceedings of the IEEE, 62(1), 93-98.

26. Borg, I., Friedman, M., Handin, J., & Higgs, D. V. (1960). Experimental deformation of St. Peter sand: a study of cataclastic flow. Geological Society of America Memoirs, 79, 133-192.

27. Bowers, M. C., Ehrlich, R., Howard, J. J., & Kenyon, W. E. (1995). Determination of porosity types from NMR data and their relationship to porosity types derived from thin section. Journal of Petroleum Science and Engineering, 13(1), 1-14.

28. Brooks, R. H., & Corey, A. T. (1966). Properties of porous media affecting fluid flow. Journal of the Irrigation and Drainage Division, 92(2), 61-90.

29. Bykov, Y. V., Rybakov, K. I., & Semenov, V. E. (2001). High-temperature microwave processing of materials. Journal of Physics D: Applied Physics,34(13), R55.

30. Carrizales, M. A., Lake, L. W., & Johns, R. T. (2008, January). Production improvement of heavy-oil recovery by using electromagnetic heating. In SPE Annual Technical Conference and Exhibition. Society of Petroleum Engineers.

31. Carrizales, M. A., Lake, L. W., & Johns, R. T. (2010, January). Multiphase fluid flow simulation of heavy oil recovery by electromagnetic heating. InSPE Improved Oil Recovery Symposium. Society of Petroleum Engineers.

32. Carrizales, M.A. (2010). Recovery of stranded heavy oil by electromagnetic heating. Thesis.

33. Carroll, D. (1970). Clay minerals: a guide to their X-ray identification (Vol. 126). Geological society of America.

34. Chandrasekaran, S., Ramanathan, S., & Basak, T. (2013). Microwave food processing—A review. Food Research International, 52(1), 243-261.

35. Chekhonin, E., Parshin, A., Pissarenko, D., Popov, Y., Romushkevich, R., Safonov, S., & Stenin, V. P. (2012). When rocks get hot: thermal properties of reservoir rocks. Oilfield Review, 24(3), 20-37.

36. Chen, T. T., Dutrizac, J. E., Haque, K. E., Wyslouzil, W., & Kashyap, S. (1984). The relative transparency of minerals to microwave radiation.Canadian Metallurgical Quarterly, 23(3), 349-351.

37. Civan, F. (1996, January). A multi-purpose formation damage model. In SPE Formation Damage Control Symposium. Society of Petroleum Engineers.

38. Civan, F. (2011). Reservoir formation damage. Gulf Professional Publishing.

39. Civan, F., & Knapp, R. M. (1987, January). Effect of clay swelling and fines migration on formation permeability. In SPE Production Operations Symposium. Society of Petroleum Engineers.

40. Clark, D. E., & Sutton, W. H. (1996). Microwave processing of materials.Annual Review of Materials Science, 26(1), 299-331.

41. Coates, G. R., Xiao, L., & Prammer, M. G. (1999). NMR logging: principles and applications. Gulf Professional Publishing.

42. Cole, K. S., & Cole, R. H. (1941). Dispersion and absorption in dielectrics I. Alternating current characteristics. The Journal of Chemical Physics, 9(4), 341-351.

43. Craig, D.Q.M. (1995). Dielectric Analysis of Pharmaceucitical Systems. London, UK: Taylor and Francis.

44. Davletbaev, A., Kovaleva, L., Babadagli, T., & Minnigalimov, R. (2010, January). Heavy oil and bitumen recovery using radiofrequency electromagnetic irradiation and electrical heating: Theoretical analysis and field scale observations. In Canadian Unconventional Resources and International Petroleum Conference. Society of Petroleum Engineers.

45. De Loor, G. P. (1968). Dielectric Properties of Heterogeneous Mixtures Containing Water*. Journal of Microwave Power, 3(2), 67-73.

46. Dodd, C. G., Conley, F. R., & Barnes, P. M. (1955). Clay minerals in petroleum reservoir sands and water sensitivity effects. Clays and Clay Minerals, 221-38.

47. Doscher, T. M. (1981). Enhanced Recovery of Crude Oil. American Scientist, 69: 193-200.

48. Ehrlich, R., & Crane, F. E. (1969). A model for two-phase flow in consolidated materials. Society of Petroleum Engineers Journal, 9(02), 221-231.

49. El-Dairy, M., Perez, J. M., & Poston, J. M. (1993). Petrophysical analysis of sandstones using CT scanning and conventional methods. AAPG Bulletin (American Association of Petroleum Geologists) ;(United States), 77(CONF-9310237).

50. Evans, C. E., & Guerrero, E. T. (1979, January). Theory and application of capillary pressure. In SPWLA 20th Annual Logging Symposium. Society of Petrophysicists and Well-Log Analysts.

51. Fadele, O., Zhu, D., & Hill, A. D. (2000, January). Matrix acidizing in gas wells. In SPE/CERI Gas Technology Symposium. Society of Petroleum Engineers.

52. Flock, D. L., & Dranchuk, P. M. (1971). A Current Review of Forward Combustion. Journal of Canadian Petroleum Technology, 10(02).

53. Ford, J. D., & Pei, D. C. T. (1967). High temperature chemical processing via microwave absorption. Red, 6, 1000.

54. George R. Coates, L. X., Manfred G. Prammer. (1999). NMR Logging Principles and Applications: Halliburton Energy Services.

55. Ghaffari, A. (1980). Model for predicting thermal conductivity of rock-fluid systems (No. LBL-11384). California Univ., Berkeley (USA). Coll. of Engineering.

56. Godard, A., & Rey-Bethbeder, F. (2011, January). Radio Frequency Heating, Oil Sand Recovery Improvement. In SPE Heavy Oil Conference and Exhibition. Society of Petroleum Engineers.

57. Grant, E., and Halstead, B. J. (1998). Dielectric parameters relevant to microwave dielectric heating. Chemical Society Reviews, 27(3), 213-224.

58. Grim, R.E. and Bradley, W.F. (1940). Investigation of the Effect of Heat On The Clay Minerals Illite And Montmorillonite. Journal of the American Ceramic Society, 23(8), 242-248.

59. Henry Greenside. (2011). Phase Transitions As A Metaphor for the Genesis of Complexity. Retrieved from http://www.phy.duke.edu/~hsg/363/table-images/water-phase-diagram.html.

60. Hajpál, M. and Török, A. (2004). Mineralogical and colour changes of quartz sandstones by heat. Environmental Geology, 46(3-4), 311-322.

61. Hale, A., Sandberg, C., & Kovscek, A. (2013, April). History and Application of Resistance Electrical Heating in Downhole Oil Field Applications. In SPE Western Regional & AAPG Pacific Section Meeting 2013 Joint Technical Conference. Society of Petroleum Engineers.

62. Harvey, A. H., Arnold, M. D., & El-Feky, S. A. (1979). Selective electric reservoir heating. Journal of Canadian Petroleum Technology, 18(03).

63. Hascakir, B., Acar, C., & Akin, S. (2009). Microwave-assisted heavy oil production: an experimental approach. Energy & Fuels, 23(12), 6033-6039.

64. Hascakir, B., & Akin, S. (2009). Recovery of Turkish oil shales by electromagnetic heating and determination of the dielectric properties of oil shales by an analytical method. Energy & Fuels, 24(1), 503-509.

65. Hasted, J. B. (1973). Aqueous dielectrics. London: Chapman and Hall.

66. Ho, W., & Hall, W. F. (1973). Measurements of the dielectric properties of seawater and NaCl solutions at 2.65 GHz. Journal of Geophysical Research,78(27), 6301-6315.

67. Hoekstra, P. (1976). Rock, Frozen Soil and Ice Breakage by High Frequency Electromagnetic Radiation: A Review (No. CRREL-76-36). Cold Regions Research and Engineering Lab Hanover NH.

68. Holditch, S. A. (2006). Tight gas sands. Journal of Petroleum Technology,58(06), 86-93.

69. Israelachvili, J. N. (2011). Intermolecular and surface forces: revised third edition. Academic press.

70. Jabbour, C., Quintard, M., Bertin, H., & Robin, M. (1996). Oil recovery by steam injection: three-phase flow effects. Journal of Petroleum Science and Engineering, 16(1), 109-130.

71. Jamaluddin, A. K. M., Bowen, C. T. and Hasan, M. (1997). Mathematical modeling of formation heat treatment process. The Canadian Journal of Chemical Engineering, 75.

72. Jamaluddin, A.K.M., Hamelin, M., Harke, K., McCaskill, H. and Mehta, S.A. (1999). Field testing of the formation heat treatment process. Journal of Canadian Petroleum Technology, 38(03).

73. Jamaluddin, A.K.M., Vandamme, L.M., Nazarko, T.W. and Bennion, D.B. (1998). Heat treatment for clay-related near wellbore formation damage. Journal of Canadian Petroleum Technology, 37(01).

74. Jamaluddin, A.K.M., Vandamme, M. and Mann, B.K. (1995), January. Formation heat treatment (FHT): a state-of-the-art technology for near-wellbore formation damage treatment. In Annual Technical Meeting. Petroleum Society of Canada.

75. Jennings Jr, A. R., & Stowe, L. R. (1990). U.S. Patent No. 4,892,147. Washington, DC: U.S. Patent and Trademark Office.

76. Jha, K. N., & Chakma, A. (1999). Heavy-oil recovery from thin pay zones by electromagnetic heating. Energy Sources, 21(1-2), 63-73.

77. Jones, D. A., Lelyveld, T. P., Mavrofidis, S. D., Kingman, S. W., & Miles, N. J. (2002). Microwave heating applications in environmental engineering—a review. Resources, conservation and recycling, 34(2), 75-90.

78. Jones, F. O., & Owens, W. W. (1980). A laboratory study of low-permeability gas sands. Journal of Petroleum Technology, 32(09), 1-631.

79. Kappelmeyer, O., & Haenel, R. (1974). Geothermics with special reference to application. Berlin Gebrueder Borntraeger Geoexploration Monographs Series, 4, 31.

80. Kar, T., & Hascakir, B. (2015). The Role of Resins, Asphaltenes, and Water in Water–Oil Emulsion Breaking with Microwave Heating. Energy & Fuels, 29(6), 3684-3690.

81. Katz, A. J., & Thompson, A. H. (1986). Quantitative prediction of permeability in porous rock. Physical review B, 34(11), 8179.

82. Kawala, Z., & Atamanczuk, T. (1998). Microwave-enhanced thermal decontamination of soil. Environmental science & technology, 32(17), 2602-2607.

83. Kenyon, W. E., Howard, J. J., Sezginer, A., Straley, C., Matteson, A., Horkowitz, K., & Ehrlich, R. (1989, January). Pore-size distribution and NMR in microporous cherty sandstones. In SPWLA 30th Annual Logging Symposium. Society of Petrophysicists and Well-Log Analysts.

84. Kersey, D. G. (1986, January). The Role of Petrographic Analyses in the Design of Nondamaging Drilling, Completion, and Stimulation Programs. In International Meeting on Petroleum Engineering. Society of Petroleum Engineers.

85. Klein, L. A., & Swift, C. T. (1977). An improved model for the dielectric constant of sea water at microwave frequencies. Antennas and Propagation, IEEE Transactions on, 25(1), 104-111.

86. Kranz, R.L. (1983). Microcracks in rocks: a review. Tectonophysics, 100(1), pp.449-480.

87. Kraszewski, A., Kulinski, S., & Stosio, Z. (1977). A preliminary study on microwave monitoring of moisture content in wheat. Journal of Microwave Power, 12(3), 241-252.

88. Krueger, R. F. (1988, January). An overview of formation damage and well productivity in oilfield operations: An update. In SPE California Regional Meeting. Society of Petroleum Engineers.

89. Li, G., Meng, Y. and Tang, H. (2006, January). Clean up water blocking in gas reservoirs by microwave heating: laboratory studies. In International Oil & Gas Conference and Exhibition in China. Society of Petroleum Engineers.

90. Liu, M., & Zhao, G. (2013, June). A Performance Comparison Study of Electromagnetic Heating and SAGD Process. In SPE Heavy Oil Conference-Canada. Society of Petroleum Engineers.

91. Liu, M.Y. and Zhao, G. (2012). Parametric study of heavy oil recovery by electromagnetic heating. COMSOL Conference 2012, Boston.

92. M. J. Jamin (1860). Sull'equilibrio e sul movimento dei liquidi nei corpi porosi Comptes Rendus.

93. Madsen, F. T., & Müller-Vonmoos, M. (1989). The swelling behaviour of clays. Applied Clay Science, 4(2), 143-156.

94. McGill, S.L., Walkiewicz, J.W. and Clark, A.E. (1995). Microwave Heating of Chemicals and Minerals. US Department of the Interior, Bureau of Mines.

95. Meredith, R. J. (1998). Engineers' handbook of industrial microwave heating (No. 25). IET.

96. Messer, E. S. (1951). Interstitial water determination by an evaporation method. Journal of Petroleum Technology, 3(10), 269-274.

97. Metaxas, A. A., & Meredith, R. J. (1983). Industrial microwave heating (No. 4). IET.

98. Miesch, E.P. and Albright, J.C. (1967, January). A Study of Invasion Diameter. In SPWLA 8th Annual Logging Symposium. Society of Petrophysicists and Well-Log Analysts.

99. Mohan, K. K., Vaidya, R. N., Reed, M. G., & Fogler, H. S. (1993). Water sensitivity of sandstones containing swelling and non-swelling clays.Colloids and surfaces A: Physicochemical and engineering aspects, 73, 237-254.

100. Moore, T. F., & Slobod, R. L. (1955, January). Displacement of oil by water-effect of wettability, rate, and viscosity on recovery. In Fall Meeting of the Petroleum Branch of AIME. Society of Petroleum Engineers.

101. Mubiayi, M.P. (2013). Characterisation of sandstones: mineralogy and physical properties. Proceedings of the World Congress on Engineering.

102. Mutyala, S., Fairbridge, C., Paré, J. J., Bélanger, J. M., Ng, S., & Hawkins, R. (2010). Microwave applications to oil sands and petroleum: A review. Fuel Processing Technology, 91(2), 127-135.

103. Naufel, R., De Sa, C. H. M., Panisset, C. M. D. V., Martins, A. L., Ataide, C. H., Pereira, M., & Barrozo, M. (2013, October). Microwave Drying of Drilled Cuttings. In OTC Brasil. Offshore Technology Conference.

104. Nelson, P. H. (2009). Pore-throat sizes in sandstones, tight sandstones, and shales. AAPG bulletin, 93(3), 329-340.

105. Newsham, K. E., Rushing, J. A., Chaouche, A., & Bennion, D. B. (2002). Laboratory and Field Observations of an Apparent Sub Capillary-Equilibrium Water Saturation Distribution in a Tight Gas Sand Reservoir. paper SPE, 75710, 5-8.

106. Newsham, K. E., Rushing, J. A., Lasswell, P. M., Cox, J. C., & Blasingame, T. A. (2004, January). A comparative study of laboratory techniques for measuring capillary pressures in tight gas sands. In SPE Annual Technical Conference and Exhibition. Society of Petroleum Engineers.

107. Ni, H., Datta, A. K., & Torrance, K. E. (1999). Moisture transport in intensive microwave heating of biomaterials: a multiphase porous media model.International Journal of Heat and Mass Transfer, 42(8), 1501-1512.

108. Osborne III, K. L. (2009). Temperature-dependence of the contact angle of water on graphite, silicon, and gold (Doctoral dissertation, Worcester Polytechnic Institute).

109. Osman, M. K., Ghodke, N. T., & Al-Dogail, F. S. (2011, January). Gas Well Deliquificatin Using Microwave Heating. In SPE Production and Operations Symposium. Society of Petroleum Engineers.

110. Ovalles, C., Fonseca, A., Lara, A., Alvarado, V., Urrecheaga, K., Ranson, A., & Mendoza, H. (2002, January). Opportunities of downhole dielectric heating in venezuela: three case studies involving medium, heavy and extra-heavy crude oil reservoirs. In SPE International Thermal Operations and Heavy Oil Symposium and International Horizontal Well Technology Conference. Society of Petroleum Engineers.

111. Perez, J.M. (1993). Petrophysical Analysis of Sandstones Using CT Scanning and Conventional Methods.

112. Petrov, E. I. et al. (1977). The Possibilities of Using Electromagnetic Fields to Improve Ore Concentrates. Electrochemistry in Industry Processing and Biology (6), 46-49.

113. Pigott, M. J., Parker, M. H., Mazzanti, D. V., Dalrymple, L. V., Cox, D. C., & Coyle, R. A. (2002, January). Wellbore heating to prevent liquid loading. In SPE Annual Technical Conference and Exhibition. Society of Petroleum Engineers.

114. Pittman, E. D. (1992). Relationship of porosity and permeability to various parameters derived from mercury injection-capillary pressure curves for sandstone (1). AAPG bulletin, 76(2), 191-198.

115. Poelchau, H. S., Baker, D. R., Hantschel, T., Horsfield, B., & Wygrala, B. (1997). Basin simulation and the design of the conceptual basin model. InPetroleum and basin evolution (pp. 3-70). Springer Berlin Heidelberg.

116. Purcell, W. R. (1949). Capillary pressures-their measurement using mercury and the calculation of permeability therefrom. Journal of Petroleum Technology, 1(02), 39-48.

117. Ramey, H. J. (1971, January). In Situ Combustion. In 8th World Petroleum Congress. World Petroleum Congress.

118. Randolph, P. L., Soeder, D. J., & Chowdiah, P. (1984, January). Porosity and permeability of tight sands. In SPE Unconventional Gas Recovery Symposium. Society of Petroleum Engineers.

119. Rezaee, M. R., Jafari, A., & Kazemzadeh, E. (2006). Relationships between permeability, porosity and pore throat size in carbonate rocks using regression analysis and neural networks. Journal of Geophysics and Engineering, 3(4), 370.

120. Rezaee, R., Saeedi, A., & Clennell, B. (2012). Tight gas sands permeability estimation from mercury injection capillary pressure and nuclear magnetic resonance data. Journal of Petroleum Science and Engineering, 88, 92-99.

121. Rider, M. H. (2002). The Geological Interpretation of Well Logs: Rider-French Consulting Ltd.

122. Robertson, E. C. (1988). Thermal properties of rocks (No. 88-441). US Geological Survey.

123. Robinson, J. P., Kingman, S. W., & Onobrakpeya, O. (2008). Microwave-assisted stripping of oil contaminated drill cuttings. Journal of environmental management, 88(2), 211-218.

124. Rodriguez, A., & Abreu, R. (1990, January). A mixing law to model the dielectric properties of porous media. In SPE Latin America Petroleum Engineering Conference. Society of Petroleum Engineers.

125. Rose, W. and Witherspoon, P. A. (1956). Trapping Oil in a Pore Doublet, Producers Monthly 21, No. 2, 32-38.

126. Sahni, A., Kumar, M., & Knapp, R. B. (2000, January). Electromagnetic heating methods for heavy oil reservoirs. In SPE/AAPG Western Regional Meeting. Society of Petroleum Engineers.

127. Sanmiguel, J. E., Mallory, D. G., Mehta, S. A., & Moore, R. G. (2001, January). Formation heat treatment process by combustion of gases around the wellbore. In Canadian International Petroleum Conference. Petroleum Society of Canada.

128. Sanmiguel, J. E., Mehta, S. R., & Moore, R. G. (2003). An experimental study of controlled gas-phase combustion in porous media for enhanced recovery of oil and gas. Journal of energy resources technology, 125(1), 64-71.

129. Schlumberger.http://www.glossary.oilfield.slb.com/en/Terms.aspx?LookIn=term%20name&filter=steamflood.

130. Schmidt, J. H. (2015). U.S. Patent Application No. 14/613,717.

131. Seleznev, N. V., Habashy, T. M., Boyd, A. J., & Hizem, M. (2006, January). Formation properties derived from a multi-frequency dielectric measurement. In SPWLA 47th Annual Logging Symposium. Society of Petrophysicists and Well-Log Analysts.

132. Seleznev, N., Boyd, A., Habashy, T., & Luthi, S. M. (2004, January). Dielectric mixing laws for fully and partially saturated carbonate rocks. InSPWLA 45th Annual Logging Symposium. Society of Petrophysicists and Well-Log Analysts.

133. Sharon Mitchell and Javier Pérez-Ramíre. (2012). X-ray diffraction. Course material of Surface Science and Methods in Catalysis.

134. Sheen, J. (2005). Study of microwave dielectric properties measurements by various resonance techniques. Measurement, 37(2), 123-130.

135. Sheng, J. J. (2013). Chapter 15 - Steam Flooding. In J. J. Sheng (Ed.), Enhanced Oil Recovery Field Case Studies (pp. 361-388). Boston: Gulf Professional Publishing.

136. Shokri, N., Lehmann, P., & Or, D. (2010). Evaporation from layered porous media. Journal of Geophysical Research: Solid Earth, 115(B6).

137. Showalter, W. E. (1963). Combustion-drive tests. Society of Petroleum Engineers Journal, 3(01), 53-58.

138. Sierra, R., Tripathy, B., Bridges, J. E., & Ali, S. M. (2001, January). Promising progress in field application of reservoir electrical heating methods. In SPE International Thermal Operations and Heavy Oil Symposium. Society of Petroleum Engineers.

139. Sinnokrot, A. A., Ramey Jr, H. J., & Marsden Jr, S. S. (1971). Effect of temperature level upon capillary pressure curves. Society of Petroleum Engineers Journal, 11(01), 13-22.

140. Soeder, D. J., & Randolph, P. L. (1987). Porosity, permeability, and pore structure of the tight Mesaverde Sandstone, Piceance Basin, Colorado. SPE Formation Evaluation, 2(02), 129-136.

141. Somerton, W. H. (1992). Thermal properties and temperature-related behavior of rock/fluid systems (Vol. 37). Elsevier.

142. Somerton, W. H., Janah, A. H., & Ashqar, P. I. (1981, January). Thermal expansion of fluid saturated rocks under stress. In SPWLA 22nd Annual Logging Symposium. Society of Petrophysicists and Well-Log Analysts.

143. Sresty, G. C., Dev, H., Snow, R. H., & Bridges, J. E. (1986). Recovery of bitumen from tar sand deposits with the radio frequency process. SPE Reservoir Engineering, 1(01), 85-94.

144. Stuchly, S. S., Mladek, J., Stuchly, M.A., and Parisien, B. (1979). A method for measurement of the permittivity of thin samples. Journal of Microwave Power, 14(1): 7.

145. Sutton, W. H. (1989). Microwave Processing of Ceramic Materials. Ceramic Bulletin, 68(2): 376-386.

146. Sutton, W. H. (1992). Microwave processing of ceramics-an overview. MRS Proceedings (Vol. 269, p. 3). Cambridge University Press.

147. Thostenson, E. T., & Chou, T. W. (1999). Microwave processing: fundamentals and applications. Composites Part A: Applied Science and Manufacturing, 30(9), 1055-1071.

148. Tinga, W. (1969). Multiphase dielectric theory applied to cellulose mixtures. PhD Thesis, University of Alverta, Edmonton, Canada.

149. Toumelin, E., Torres-Verdín, C., & Bona, N. (2008). Improving petrophysical interpretation with wide-band electromagnetic measurements. SPE Journal,13(02), 205-215.

150. Ulaby, F. T., Bengal, T. H., Dobson, M. C., East, J. R., Garvin, J. B., & Evans, D. L. (1990). Microwave dielectric properties of dry rocks. Geoscience and Remote Sensing, IEEE Transactions on, 28(3), 325-336.

151. Van, J., Jiang, G., & Wu, X. (1997). Evaluation of formation damage caused by drilling and completion fluids in horizontal wells. Journal of Canadian Petroleum Technology, 36(05).

152. Venkatesh, M. S., & Raghavan, G. S. V. (2005). An overview of dielectric properties measuring techniques. Canadian Biosystems Engineering, 47(7), 15-30.

153. Vermeulen, F.E. and Chute, F.S. (1983). Electromagnetic techniques in the in-situ recovery of heavy oils. Journal of Microwave Power, 18(1), 15-29.

154. Wacker, B., Karmeileopardus, D., Trautmann, B., Helget, A. and Torlak, M. (2011, January). Electromagnetic Heating for In-situ Production of heavy oil and bitumen Reservoirs. In Canadian Unconventional Resources Conference. Society of Petroleum Engineers.

155. Wang, H., Rezaee, R. and Saeedi, A. (2015, November). Evaluation of Microwave Heating on Fluid Invasion and Phase Trapping in Tight Gas Reservoirs. In SPE Asia

Pacific Unconventional Resources Conference and Exhibition. Society of Petroleum Engineers.

156. Wang, H., Rezaee, R., & Saeedi, A. (2016). Preliminary study of improving reservoir quality of tight gas sands in the near wellbore region by microwave heating. Journal of Natural Gas Science and Engineering, 32, 395-406.

157. Washburn, E. W. (1921). The dynamics of capillary flow. Physical review,17(3), 273.

158. Wattenbarger, R. A., & McDougal, F. W. (1988). Oil production response to in situ electrical resistance heating (ERH). Journal of Canadian Petroleum Technology, 27(06).

159. Wellington, S.L. and Vinegar, H.J. (1987). X-ray computerized tomography. Journal of Petroleum Technology, 39(08), 885-898.

160. Wells, J. D., & Amaefule, J. O. (1985, January). Capillary pressure and permeability relationships in tight gas sands. In SPE/DOE Low Permeability Gas Reservoirs Symposium. Society of Petroleum Engineers.

161. Welton, J.E. (1984). SEM petrology atlas (p. 237). Tulsa Oklahoma: American Association of Petroleum Geologists.

162. Western Australian Energy Research Alliance & Geological Survey of Western Australia & Western Australia. Dept. of Mines and Petroleum (2012). Whicher Range tight gas sands study. Geological Survey of Western Australia, East Perth, W.A

163. White, P. D., & Moss, J. T. (1965). High-temperature thermal techniques for stimulating oil recovery. Journal of Petroleum Technology, 17(09), 1-007.

164. Wu, G., Wang, Y., Swift, G. and Chen, J. (2011). Physico-mechanical and thermo-mechanical characterisation of sandstone. Artificial Neural Networks in Biological and Environmental Analysis, p.386.

165. Wyckoff, R. W. (1968). Crystal structures. Vol. 4, Miscellaneous inorganic compounds, silicates, and basic structural information.

166. Xie, H.P et, al. (1989). Analysis of rock fracture micro-mechanism (In Chinese). J China Coal Soc, 2, 57–67.

167. Yale, D. P., Nabor, G. W., Russell, J. A., Pham, H. D., & Yousef, M. (1993, January). Application of variable formation compressibility for improved reservoir analysis. In SPE Annual Technical Conference and Exhibition. Society of Petroleum Engineers.

168. Yao, Y., Liu, D., Che, Y., Tang, D., Tang, S., and Huang, W. (2009). Non-destructive characterization of coal samples from China using microfocus X-ray computed tomography. International Journal of Coal Geology, 80(2), 113-123.

169. Zhang, Y., Zhang, X., & ZHAO, Y. S. (2005). Process of sandstone thermal cracking. Chinese Journal of Geophysics, 48(3), 722-726.

170. Zhou, Z., & Law, H. S. (1998). Swelling clays in hydrocarbon reservoirs: the bad, the less bad, and the useful. In 7th UNITAR Conference on Heavy Crude and Tar Sands, Beijing, China, October (pp. 27-30).

171. Zimmerman, R. W. (1989). Thermal conductivity of fluid-saturated rocks. Journal of Petroleum Science and Engineering, 3(3), 219-227.

172. Zuo, J., Xie, H., Zhou, H., & Peng, S. (2007). Thermal-mechanical coupled effect on fracture mechanism and plastic characteristics of sandstone. Science in China Series E: Technological Sciences, 50(6), 833-843.